

SKI Report 98:41

---

# **Statistical Patterns of Geochemistry in Crystalline Rock and Effect of Sorption Kinetics on Radionuclide Migration**

Shulan Xu  
Anders Wörman

September 1998

ISSN 1104-1374  
ISRN SKI-R--98/41--SE

---

The logo for SKI, consisting of the letters 'S', 'K', and 'i' in a bold, black, sans-serif font. The letter 'i' has a red dot above it.

SKI Report 98:41

# **Statistical Patterns of Geochemistry in Crystalline Rock and Effect of Sorption Kinetics on Radionuclide Migration**

Shulan Xu  
Anders Wörman

Department of Earth Sciences, Uppsala University,  
Villavägen 16, SE-752 36 Uppsala, Sweden

September 1998

SKI Project Number 96076, 98112

This report concerns a study which has been conducted for the Swedish Nuclear Power Inspectorate (SKI). The conclusions and viewpoints presented in the report are those of the authors and do not necessarily coincide with those of the SKI.

## Contents

Summary	4
Sammanfattning	6
1. General Introduction	8
Part A:	
2 Statistical Patterns of Geochemistry in Crystalline rock	9
2.1 Introduction	9
2.2 Materials and Experimental Methods	10
2.2.1 Materials	10
2.2.2 Geostatistical analysis and sampling strategy	10
2.2.3 Method for porosity measurements	11
2.2.4 Method for effective diffusivity measurements	12
2.2.5 Method for surface adsorption selectivity analysis	13
2.3 Results and Discussion	13
2.3.1 Results from porosity measurements	13
2.3.2 Results from effective diffusivity measurements	16
2.3.3 Results from surface adsorption selectivity experiment	18
2.4 Conclusions	19
Part B:	
3 Effect of Sorption Kinetics on Radionuclide Migration	21
3.1 Introduction	21
3.2 Models and Criteria of the Effect of Sorption Kinetics	22
3.2.1 Models of migration process	22
3.2.2 Semi-empirical equation for adsorption kinetics	25
3.2.3 Analytical solution to the temporal moments	

of the breakthrough curves	27
3.2.4 Effect of adsorption kinetics, dispersion and matrix diffusion on solute migration	29
3.2.5 Simulation of the effect of adsorption kinetics	30
3.3 Materials and Experimental Methods	31
3.3.1 Materials	31
3.3.2 Method for determining adsorption kinetics on crushed rock particles	31
3.3.3 Method for determining adsorption kinetics on intact rock	32
3.4 Results and Discussions	33
3.4.1 Results from measurements of adsorption kinetics on crushed rock particles	33
3.4.2 Results from measurements of adsorption kinetics on intact rock	37
3.4.3 Effect of adsorption kinetics on migration of radionuclides in fractures	42
3.5 Conclusions	46
4 General Conclusions	48
5 Acknowledgements	48
6 References	50
Appendix I: Solution to the first two temporal moments of the probability density function for the residence time	53
Appendix II: Diffusivity data from 4 mm $\text{ÄD}$ slabs	57
Appendix III: Diffusivity data from 6 mm $\text{ÄD}$ slabs	64
Appendix IV: Notation	70

## Summary

The overall objective of the current project is to develop a quantitative understanding of the effects of spatial variability in physical and geochemical properties of the rock on the migration of radionuclides along a single fracture in crystalline rock. The strategy is first to deduce the basic geostatistics of the main model parameters by means of detailed laboratory (batch) experiments on a large number of rock samples taken from Swedish crystalline basement. The results are then analysed by geostatistical methods and used for stochastic interpretations of a series of laboratory migration experiments to be conducted in a later phase of the project.

In an earlier phase of the project, a new mathematical model was developed as a basis for the interpretation of experimental results and the generalisation to performance assessment (PA) analyses (Wörman and Xu, 1996). The model describes migration of radionuclides along a two-dimensional fracture and includes the transversal diffusion into the rock matrix and surface. To be able to discriminate between the effects of parameter heterogeneity and potential effects of kinetics, a model description has also been developed for first-order sorption kinetics. The main model parameters are represented as spatially random.

This report contains results from the batch tests and the geostatistical analysis (Part A) and the progress of the model formulation for transport of radionuclides (Part B).

Geostatistics of the main parameters was experimentally determined for two rock types, Äspö diorite, and Småland granite. Drill cores were collected at the Äspö Hard Rock Laboratory and sawn into a large number of slabs. The porosity, the effective diffusivity and the adsorption characteristics were determined using various experimental methods on the individual pieces. Semi-variograms show that both porosity and effective diffusivity are correlated over a separation distance of 30 to 40 cm. The coefficients of variation of the porosity of rock samples with a size of 20x20 mm and varying thickness in the range 6- 15 mm are ~10% for both Äspö diorite and Smålands granite. The corresponding variation in effective diffusivity is ~100%.

In order to be able to differentiate the effects of adsorption kinetics on the migration of radionuclides from the effects of other mechanisms (e.g. effect of heterogeneity), efforts have been made to improve the understanding of adsorption processes in rock. Two approaches were applied to estimate the adsorption rate of Cs on crystalline rock, one being focused on adsorption on mineral surfaces and the other on adsorption occurring in the pore system of intact rock. In order to provide an acceptable explanation of the experimental data from in-diffusion tests with intact rock slabs the model framework had to include the effects of both surface diffusion (diffusion in a weakly sorbed state) and adsorption kinetics. A traditional way to evaluate the in-diffusion tests based on the assumption of equilibrium adsorption gives a significant deviation between the theory and the measured data. The results indicate that the adsorption rate of Cs on intact rock is 2 or 3 orders of magnitude lower than the adsorption rate obtained for the crushed rock. This is probably

because the kinetics of adsorption on intact rock is dominated by the diffusion into dead-end pores. Independent investigations reported in the literature indicate that about 40% of the pore volume in crystalline rock is not active in matrix diffusion.

The degree of importance of adsorption kinetics for radionuclide migration in fractured rock was quantified by deriving analytical expressions for the residence time of the nuclides in the fracture. Interpretations of these expressions and results from a numerical study indicate that adsorption kinetics has negligible effect on the transport of radionuclides in fractured rock for sufficiently weakly adsorbing ( $\rho/\varepsilon K_D < \sim 2.5 \cdot 10^3 \text{ m}^3/\text{kg}$ ) and strongly adsorbing ( $\rho/\varepsilon K_D > \sim 2.5 \cdot 10^6 \text{ m}^3/\text{kg}$ ) nuclides. In the intermediate cases, sorption kinetics might be important depending on the combination of other parameters.

## Sammanfattning

Föreliggande rapport behandlar ett forskningsprojekt kring radionuklidens migration i sprickigt berg. Projektets övergripande målsättning är att förbättra kunskapen om hur den rumsliga variabiliteten i bergets geokemiska och fysikaliska egenskaper påverkar migrationen av radionuklider i enskilda sprickor. Strategin är att ta fram geostatistik för de viktigaste fysiska och geokemiska parametrarna i kristallint berg i Sverige och att använda denna information i stokastiska tolkningar av ett flertal migrationsförsök som kommer att genomföras med klyvna borrhärlor. Heterogeneiteten i borrhärlornas mineralogi och porositet kommer att ha en viss betydelse för transporten av radionuklider (caesium och jodid kommer att användas) och denna betydelse skall kvantifieras. Den föreslagna tolkningsmetoden innebär en deterministisk processbeskrivning och en stokastisk representation av olika parametrar som porositet, diffusivitet och sorption.

Under ett tidigare skede av projektet har en matematisk modell utvecklats som underlag för utvärdering av planerade migrationsförsök. Ett datorbaserat beräkningspaket har utarbetats i en blandad programmeringsmiljö, FORTRAN och MATLAB (Wörman and Xu, 1996). Modellen beskriver migration av radionuklider i ett tvådimensionellt sprickplan med rumsligt varierande geokemiska och fysikaliska transportegenskaper samt tar hänsyn till diffusion in i bergmatrisen och första ordningens sorptionskinetik. Modellparametrarna kan ansättas som rumsligt stokastiska fält för att representera heterogenitet i geokemi. För att kunna särskilja effekten av parameterheterogenitet från andra effekter på transporten av radionuklider i sprickor, har tolkningsmodellen utvecklats med avseende på vissa effekter av sorptionskinetik.

Denna rapporten innehåller resultat från geostatistiska undersökningar av kristallint berg i Sverige (Part A) samt utveckling av modellbeskrivningen (Part B).

Ett stort antal experiment har genomförts för att bestämma geostatistiken för modellens parameterar och sorptionskinetiken för Cs i kristallint berg. Två borrhärlor med olika bergarter hämtades från Äspö berglaboratorium, en Smålandsgranit och en Äspödiorit. Borrhärlorna sågades i ett stort antal provbitar med ett tvärsnitt av 20x20 mm och en tjocklek som varierade mellan 6- 15 mm. Olika experimentella metoder användes för att bestämma porositet, effektiv diffusivitet och sorptionsegenskaper för de individuella bitarna.

Resultaten visar att samtliga undersökta egenskaper i Äspödiorit uppvisar en kovarians upp till ett separationsavstånd av omkring 40 cm. I Småland granit är kovariansen periodisk med ett intervall av omkring 34 cm. För båda bergarterna är variationskoefficienten 10% för porositet och 100% för effektiv diffusivitet (med den valda storleken av provbitarna).

För att kunna särskilja effekten av parameterheterogenitet från andra effekter på radionuklidmigration är det viktigt att förstå bland annat sorptionskinetik i intakt berg. I detta syfte genomfördes två typer av experiment där ytsorptionskinetiken studerades med hjälp av krossat berg och sorptionskinetiken i intakt berg studerades

genom sk indiffusionsförsök. En teori för sorptionskinetiken på mineralytor har utvecklats på en form som är konsistent med en Langmuir adsorptionsisoterm. Obekanta koefficienter i modellen bestämdes med experimentella resultat från batchtester med krossat berg. Cesium-137 ( $^{137}\text{Cs}$ ) användes som spårämne. Ytkinetiken utvärderades för korn som är tillräckligt små för att den yta som är tillgänglig för sorption skall domineras av kornets yttre, veckade yta.

För att erhålla en acceptabel anpassning av modell och resultat från indiffusionsförsöken var det nödvändigt att inkludera både sorptionskinetik och ytdiffusion (diffusion i ett svagt adsorberat tillstånd). En traditionell utvärdering baserad på antagandet om jämviktssorption ger markanta avvikelser mellan teori och data. Resultaten med Cs visar att sorptionsintensiteten (kinetiken) i intakt berg är två eller tre storleksordningar lägre än för krossat berg. Detta beror på att kinetiken i intakt berg i hög grad styrs av diffusion i icke-ledande mikrosprickor ("dead-end-pores"). Oberoende undersökningar har visat att ungefär 40% av porvolymen i kristallint berg inte deltar aktivt i matrisdiffusionen.

Effekten av sorptionskinetik på migrationen av Cs i ett enskilt sprickplan har analyserats dels genom numeriska experiment och dels genom att härleda ett teoretiskt samband för uppehållstiden av Cs i sprickan. Sambanden kan användas för att bestämma det relativa felet som uppkommer genom att anta jämviktssorption istället för en kinetisk beskrivning av sorptionen. Dessa samband och numeriska analysresultat visar att adsorptionskinetiken kan försummas för svagt ( $\rho/\varepsilon K_D < \sim 2.5 \cdot 10^3 \text{ m}^3/\text{kg}$ ) adsorberande nuklider och för kraftigt adsorberande ( $\rho/\varepsilon K_D > \sim 2.5 \cdot 10^6 \text{ m}^3/\text{kg}$ ) nuklider. I mellanliggande fall kan kinetiken ha betydelse beroende på övriga parameterkombinationer.

## 1. General Introduction

The preferred method disposal of spent nuclear fuel in Sweden is based on isolation in a deep bedrock repository. As part of its research programme for the safety of the final disposal, the Swedish Nuclear Power Inspectorate (SKI) initiated a project to examine how spatial variability in geochemistry and physical parameters of the rock in combination with spatial variability in matrix diffusion affects the radionuclide migration along single fractures in crystalline rock. The project has been proceeding for three years and will continue for another two years.

The overall purpose of the project is to deduce basic geostatistics of physical and chemical parameters in crystalline rock in Sweden and to use this information in the interpretation of a series of laboratory migration experiments with nuclides migrating in fractured drill cores. The heterogeneity in the properties of the rock, such as porosity, diffusivity and sorption characteristics, will have a certain impact on the migration. The combination of a deterministic description of processes and a stochastic representation of the model parameters should be used as a basis for interpretation of the experimental results. The purpose of the present study is to determine the geostatistical pattern of some of the most important geochemical parameters in crystalline rock in Sweden, such as adsorption characteristics, effective diffusivity and porosity. Further, the report includes a critically review the concurrent methods used to describe the combination of matrix diffusion and sorption phenomena in environmental science (in sediments and in rock). Based on a number of decisive experimental methods and theoretical developments, formulations for migration of radionuclides in fractured rock will be proposed.

In order to differentiate the effects of various mechanisms on the migration of radionuclides, one needs a thorough understanding of the parameter variability in rock, shear dispersion and adsorption kinetics. We have therefore included a study of the variation of the dispersion coefficient with the aspect ratio of a rectangular flow section (Wörman and Xu, 1998). Other critical issues are the statistical patterns of physical and geochemical properties in crystalline rock as well as the effect of adsorption kinetics on migration. The latter two issues are covered in part A (geostatistics of parameters) and part B (sorption kinetics).

The geochemical properties to be determined are adsorption characteristics, effective diffusivity and porosity. This is done on samples from a typical Swedish crystalline rock collected at the Äspö Hard Rock Laboratory. The spatial variability in parameters is determined using a number of experimental methods and a large set of rock samples. Another purpose is to estimate the effect of sorption kinetics on the migration of radionuclide migration for the specific rock types found at Äspö. The isotope specifically used in these investigations is  $^{137}\text{Cs}$ . An important issue is to delimit cases for which sorption kinetics can be omitted. The mathematical description can then be based on equilibrium chemistry.

The geochemical and physical parameters of the Äspö rock types will be analysed and presented in a form that facilitates incorporation of the data in stochastic transport analyses.

## Part A:

### 2 Statistical Patterns of Geochemistry in Crystalline Rock

#### 2.1 Introduction

As mentioned in the general introduction, the overall purpose of the project is to improve the understanding of the effect of heterogeneity in properties of crystalline rock on the migration of radionuclides. As a basis for analyses, a transport model describing the migration of radionuclides in fractured rock has been developed and implemented in a numerical simulation package (Wörman and Xu, 1996). The model formulation is two-dimensional along the fracture plane and the main model parameters are conceived as spatially random. The purpose of Part A of this study is to deduce basic geostatistics of the main model parameters. This will be done by conducting a large number of batch tests with samples taken in two-dimensional patterns in a selected rocks. The parameters to be measured and analysed statistically are porosity and effective diffusivity. Sorption characteristics are reported in part B but without a geostatistical analysis.

A specific objective was that the experimental material should be produced from drill cores collected from two rock types at the Äspö Hard Rock Laboratory located in south-eastern Sweden, Äspö-diorite (ÄD) and Småland granite (SG). The Äspö hard rock laboratory is placed in a typical Swedish crystalline bedrock and has been appointed as a suitable location for testing of the Swedish concept of final disposal of nuclear wastes. One of several drill cores from each rock type will be sawn into a large number of slabs in order to facilitate examination of the individual pieces and evaluation of adsorption characteristics, porosity and effective diffusivity. Despite the fact that the variance of the properties depends

Table 1 List of experiments included in the study

Experiments	Äspö diorite slab thickness	Småland granite slab thickness
Porosity (leaching method, NaI)	4 mm, > 50 samples* 6 mm, > 50 samples* 10 mm, > 50 samples* 15 mm, 10 samples*	6 mm, > 50 samples*  10 mm, > 50 samples*
$D_e$ , effective diffusivity (through-diffusion, NaI)	4 mm, > 50 samples*	4 or 6 mm, > 50 samples
(through-diffusion, NaI)	6 mm, > 50 samples*	
$k_d$ , partition coefficient (in-diffusion method) (crushed particles)	10 mm, > 50 samples** particle size: 0.0065, 0.011, 0.0154, 0.0227, 0.104, 0.65, 1.198 and 2.397 mm*	10 mm, > 50 samples**
Migration experiment	3 sets	3 sets

\* Experiments are completed. \*\* Experiments still in progress.

Table 2 Composition of minerals in Äspö diorite and Småland granite

Minerals	Äspö diorite (%)	Småland granite (%)
Quartz	20.73	40.99
Potassium feldspar	16.34	22.96
Plagioclase	21.71	17.04
Muscovite	0.24	0.25
Biotite	13.17	2.72
Hornblende	6.34	-
Fe-Ti oxides	0.98	0.25
Titanite	1.95	1.48
Saussuritized feldspar	15.85	12.84
Others*	2.68	1.48
Total number of grains counted	411	406

\*Others include zircon, calcite, epidote and chlorite.

on the size of the slabs, the correlation length can be determined based on the arbitrary slab size used in this study. Remaining cores should be stored for future laboratory migration experiments. The experimental methods to be used in the study are in- and through-diffusion experiments and leaching experiments. Table 1 summarises the experiments included in the project.

## 2.2 Materials and Experimental Methods

### 2.2.1 Materials

Two drill cores with a diameter of 20 cm and a length of 50 to 60 cm were taken from the Äspö hard rock laboratory, Kalmar County in Sweden, and used to investigate parameter variabilities. One drill core was Äspö diorite and the other one was Småland granite. Two thin sections from each of the drill cores were prepared and studied in transmissive light. The average mineral compositions were determined by point counting on the thin sections (Table 2). The dominating minerals of Äspö diorite are plagioclase, potassium feldspar, quartz and biotite. The main minerals of Småland granite are quartz, potassium feldspar, muscovite and saussuritized feldspar. There are a few scattered macropores that presumably have resulted from the dissolution of Fe-Ti oxides.

### 2.2.2 Geostatistical analysis and sampling strategy

As mentioned earlier, one of the four drill cores in each series was used to determine the adsorption characteristics, the porosity and the effective diffusivity. Rock slabs were taken in a certain pattern (see Fig. 1) which facilitated a reliable

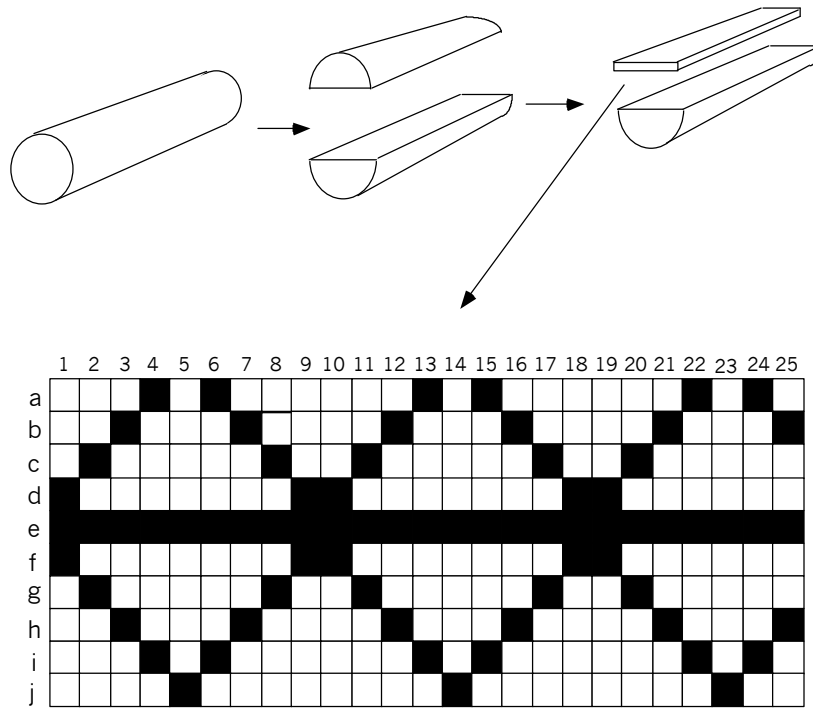


Fig. 1 Schematic of disintegration of drill core and pattern of rock slab sampling. Black squares represent slabs to be investigated with regard to a specific parameter.

geostatistical analysis of the data in two dimensions. The size of each slab face was 20x20 mm and the thickness varied in the range 6- 15 mm.

The spatial covariance of the data can be represented in terms of the semi-variogram. If the mean is constant, the data pairs are grouped according to their separation distances, lag distances and the semi-variogram  $r(w)$  is expressed as a function of the lag distance (Isaaks and Srivastava, 1989; ASCE, 1990)

$$r(w) = \frac{1}{2n(w)} \sum_{i=1}^{n(w)} [b(x_i + |w|) - b(x_i)]^2 \tag{1}$$

in which  $n$  is number of observation pairs,  $b(x_i)$  is an arbitrary parameter value (data) at point  $x_i$ ,  $b(x_i + |w|)$  is the corresponding parameter value separated from point  $x_i$  by the space vector  $w$ ,  $|w|$  is lag distance.

2.2.3 Method for porosity measurements

The porosity of the samples was measured by the leaching method (Skagius, 1986). The rock slabs were placed in a vacuum chamber to remove gas trapped in pores and then saturated with a solution of iodide with a concentration of 1.25 M for at least three weeks. The amount of iodide contained by each slab in the saturated condition was determined by placing the iodide-saturated sample in distilled water and measuring the leaching of iodide from the slabs. The leaching was performed

until the iodide concentration of each solution became practically constant with time. The experiments show that the equilibrium stage is reached after a period of at least three weeks. The pore volume and the porosity of the slab were then calculated by means of a formulation of the mass balance of iodide.

#### 2.2.4 Method for effective diffusivity measurements

The effective diffusivity was determined with the through-diffusion technique described by e.g. Johansson *et al.* (1997). The apparatus for a through-diffusion experiment is shown schematically in Fig. 2. The rock slab was placed in a quadratic hole being fixed to a PVC plate with silicone rubber. The plate with the rock slab was then kept in a vacuum chamber for air removal and saturated with distilled water in the same way as in the porosity measurements. After saturation, the plate was mounted between two water containers and sealed with o-rings on both sides. The volume of the containers was 20 ml. One side of the diffusion cell was filled with 0.1 M sodium iodide solution as a tracer substance. The other cell was filled with 0.1 M sodium nitrate solution in order to avoid osmotic effects (Skagius, 1986). Samples (1 ml) were repeatedly taken from the cell with sodium nitrate. Each time a sample was withdrawn, 1 ml of sodium nitrate solution was added to the cell to maintain a constant liquid volume in the cell. The sodium iodide concentration in the samples was measured by an iodide selective electrode (AST Orion Model 9653).

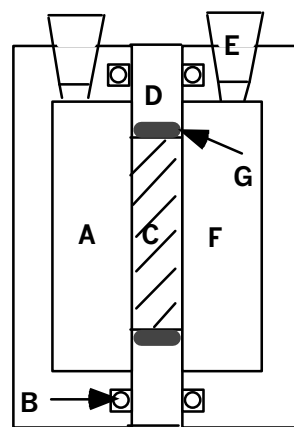


Fig. 2 Schematic of the diffusion cell (design after Johansson *et al.* 1997). A tracer container, B o-ring, C rock sample, D PVC plate, E sampling hole and rubber plug, F measurement container, G silicone rubber.

The measured sodium iodide concentrations were evaluated by means of the diffusion theory described by Skagius and Neretnieks (1986). The total amount of diffusing substance,  $Q$ , passing through the slab during the time  $t$  can be obtained by solving the diffusion equation for the following boundary conditions: the concentration,  $C_1$ , on the upper side of the slab, at  $x=0$ , is constant for  $t \geq 0$  and the concentration,  $C_2$ , on the downward side of the slab, at  $x=l$ , is much less than  $C_1$  for  $t \geq Q$ , where  $l$  is the thickness of the slab. If  $C_2 = 0$ , the solution to the diffusion equation with constant parameters becomes

$$Q = \frac{C_1 D_e}{l} t - \frac{C_1 \kappa l}{6} - \frac{2 \kappa C_1 l}{\pi^2} \sum_{n=1}^{\infty} \frac{(-n)^n}{n^2} \exp \left\{ -\frac{D_e n^2 \pi t}{l^2 \kappa} \right\} \quad (2)$$

where  $\kappa$  is the adsorption capacity of the rock in the form of  $\varepsilon + K_D \rho$ ,  $\varepsilon$  is the porosity of the rock,  $K_D$  is the adsorption partition coefficient with the unit of  $[m^3/kg]$ , effective diffusivity  $D_e = \varepsilon_t D_p$ ,  $\rho$  is the density of the rock and  $\varepsilon_t$  is the porosity available to transport. As  $t$  tends to  $\infty$ , (2) takes the form of

$$Q = \frac{C_1 D_e}{l} t - \frac{C_1 \kappa l}{6} \quad (3)$$

The assumptions underlying (3) are that  $D_e$  is constant, the concentration in the injection cell  $C_1$  is constant with time, the concentration in the measuring cell  $C_2$  is negligible compared to  $C_1$  for all times, and the slab is homogeneous in its thickness and quasi-steady state is reached (time derivatives tend to zero as time tends to infinity). These assumptions should be reasonable for the through-diffusion experiments. The effective diffusivity  $D_e$  will be obtained by fitting the measured data to (3).

## 2.2.5 Method for surface adsorption selectivity analysis

Rock surface adsorption selectivity was analysed with an electron microprobe analysis technique as part of a MSc thesis (Hoffstedt, 1997). In the electron microprobe analysis, electron bombardment generates the X-rays emitted from the sample surface. From the wavelength and intensity of lines in the X-ray spectrum emitted from the surface, the elements present on the bombarded surface can be identified and their concentrations estimated. An Åspö diorite slab (2 x 2 cm) was used in these experiments. The surface of the slab was first polished and then the slab was placed in 100 ml of the synthetic ground water with an initial Cs concentration of 1000 ppm for 4 months. A surface area of  $1 \text{ mm}^2$  was analysed with an electron microprobe analysis technique, using the instrument CAMECA SX50. The three elements caesium, sodium and iron were analysed. Minerals were determined based on the assumptions that all the Na is hosted in the plagioclase and all the Fe is hosted in the biotite. A blank test was performed with a slab placed in the synthetic ground water without Cs.

## 2.3 Results and Discussion

### 2.3.1 Results from porosity measurements

As mentioned, ÅD slabs of several thicknesses were used to determine the porosities, namely 4 mm, 6 mm, 10 mm and 15 mm. The SG slabs was prepared with thicknesses 6 and 10 mm. The fact that porosity decreases with increasing

Table 3 Summary of porosity values from different experiments

Samples	Mean value %	Median value %	Variance	Coefficient of skewness
4 mm ÄD	0.84	0.83	0.01	+0.54
6 mm ÄD	0.70	0.70	0.005	+0.51
10 mm ÄD	0.55	0.55	0.003	+0.24
15 mm ÄD	0.40	0.39	0.003	+0.48
6 mm SG	0.39	0.38	0.0025	+0.82
10 mm SG	0.36	0.35	0.001	+1.03

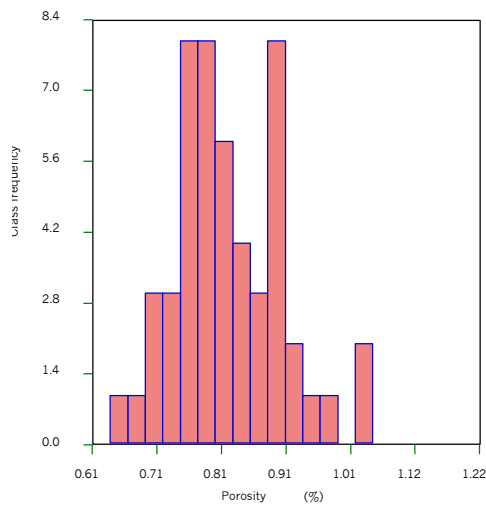


Fig. 3 Histogram of porosity for 4 mm ÄD slabs.

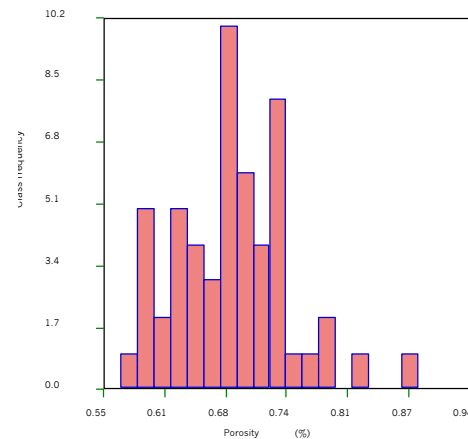


Fig. 4 Histogram of porosity for 6 mm ÄD slabs.

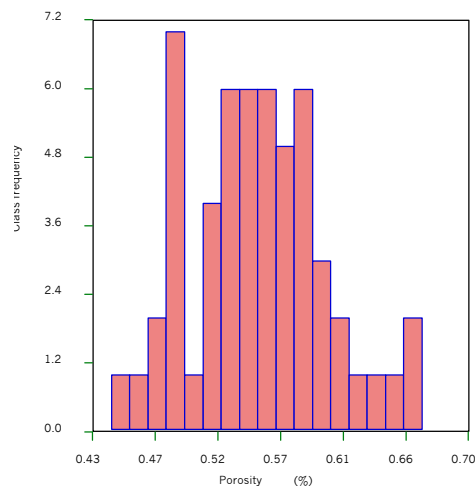


Fig. 5 Histogram of porosity for 10 mm ÄD slabs.

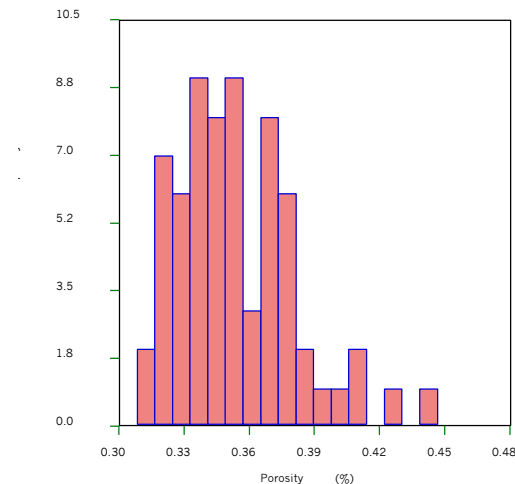


Fig. 6 Histogram of porosity for 10 mm SG slabs.

slab thickness is probably an effect of the sawing. Histograms show the distribution of the porosity for the slabs of different thicknesses and different rock types (Figs. 3 to 6). As can be seen in these figures, the histogram is positively

skewed. Mean porosity for the 15 mm slab of ÄD is 0.40% and for the 10 mm slabs of SG is 0.36%. The measured porosity data are summarised in Table 3

One rock core of each of ÄD and SG having a diameter of 24 mm and a length of 40 mm was sent to the Laboratory of Radiochemistry at the University of Helsinki for complementary porosity measurements. These complementary porosity measurements employed impregnation of rocks by  $^{14}\text{C}$  labelled polymethylmethacrylate ( $^{14}\text{C}$ -PMMA), autoradiography and optical densitometry applying digital image processing (Siitari-Kauppi, 1997). The porosity values obtained in this way were  $0.33 \pm 0.05\%$  and  $0.22 \pm 0.03\%$  in ÄD and SG, respectively. The median porosity value measured on 15 mm ÄD slabs by the leaching method is close to that measured by the  $^{14}\text{C}$ -PMMA method.

From the semi-variogram shown in Fig. 7, the semi-variance for the porosity of ÄD approaches the sill (variance for completely uncorrelated pairs) at a lag distance of about 30 cm, the correlation length is  $\sim 30$  cm. The directional variograms with different angles (not included in the report) indicate that the degree of anisotropy is insignificant. Fig. 8 shows that the variogram of measured porosity data for Småland granite has a clear cyclical form. This cyclic characteristic, often referred to as a hole effect, suggests that the porosities of the samples separated by 17 cm is generally most dissimilar and results from samples separated by 34 cm have the highest covariance. In spite of the sawing effect, the variograms of the porosity for different slab thicknesses can be represented by similar correlation lengths.

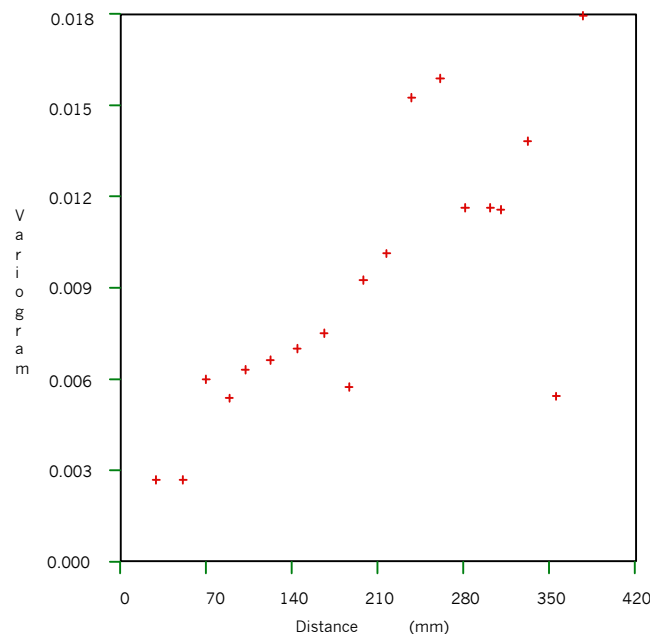


Fig. 7 Semi-variogram of porosity for 4 mm ÄD slabs.

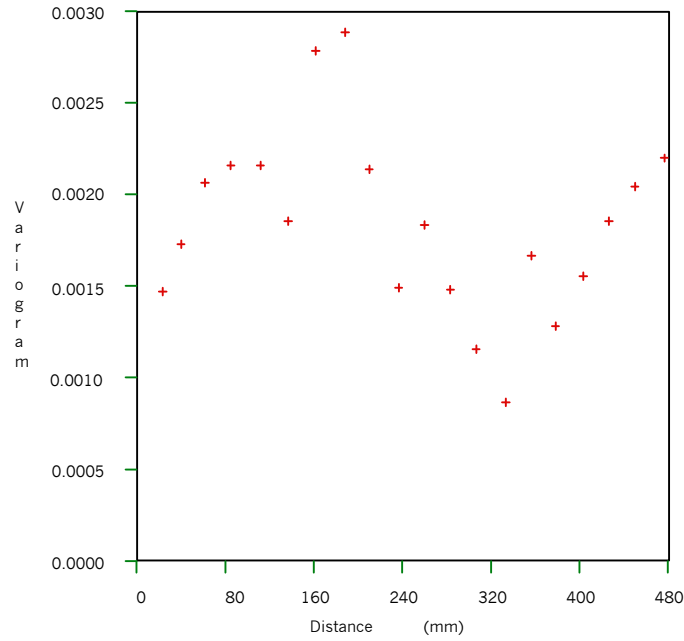


Fig. 8 Semi-variogram of porosity for 10 mm SG slabs.

### 2.3.2 Results from effective diffusivity measurements

About 100 slabs in total were used to determine the effective diffusivity (Fig. 9). The figures in Appendices II and III show, for all experiments, the concentration of iodide that passed through the slab as a function of time. The effective diffusivity,  $D_e$ , was determined using a least square regression technique to fit (3) to the measured data. A blank test was done by placing a PVC slab with silicone rubber on the PVC plate. The result shows that the diffusion through the silicone rubber could be disregarded.

Fig. 9 A view of through-diffusion experiments under performance.

A change in the slope of the concentration versus time was observed in some plots (samples D1 and F7 in Appendix II, and samples D2, D3, F3 and F4 in Appendix III, respectively), although the experimental conditions were unchanged. Similar observations were reported by Skagius (1986), who suggested that an increasing diffusivity might be due to fissure coating material in the slabs. This could not explain, however, a decreasing diffusivity.

Figs. 11 and 12 show the histograms of  $D_e$  for 4 mm and 6 mm  $\ddot{A}$ D slabs. The purpose to measure  $D_e$  values for the two groups is to investigate the effect of sawing on  $D_e$ . The sawing effect on the effective diffusivity is also indicated by a decreasing mean diffusivity with increasing slab thickness.

The measured effective diffusivity data are summarised in Table 4. The semi-variance of the effective diffusivity represented in Fig. 12 are characterised by a similar correlation length as found for porosity, about 30 cm.

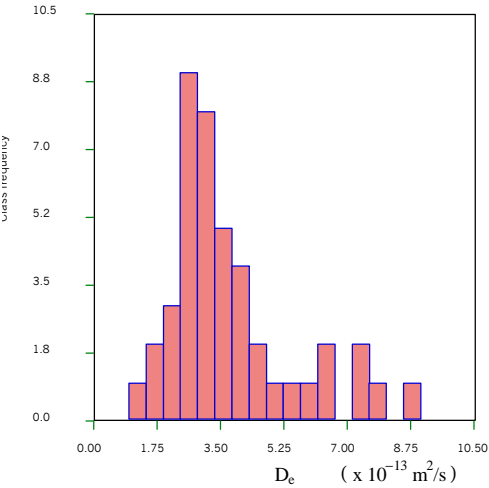


Fig. 10 Histogram of effective diffusivity for 4 mm  $\ddot{A}$ D slabs.

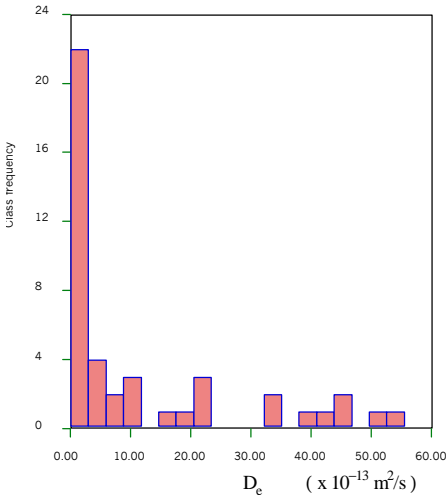


Fig. 11 Histogram of effective diffusivity for 6 mm  $\ddot{A}$ D slabs.

Table 4 Effective diffusivity from through-diffusion experiments

Samples	Mean value $\times 10^{13} \text{ m}^2/\text{s}$	Median value $\times 10^{13} \text{ m}^2/\text{s}$	Variance $\times 10^{26}$	Coefficient of skewness
4 mm $\ddot{A}$ D	4.45	3.64	5.32	+1.77
6 mm $\ddot{A}$ D	12.75	2.77	269.47	+1.42

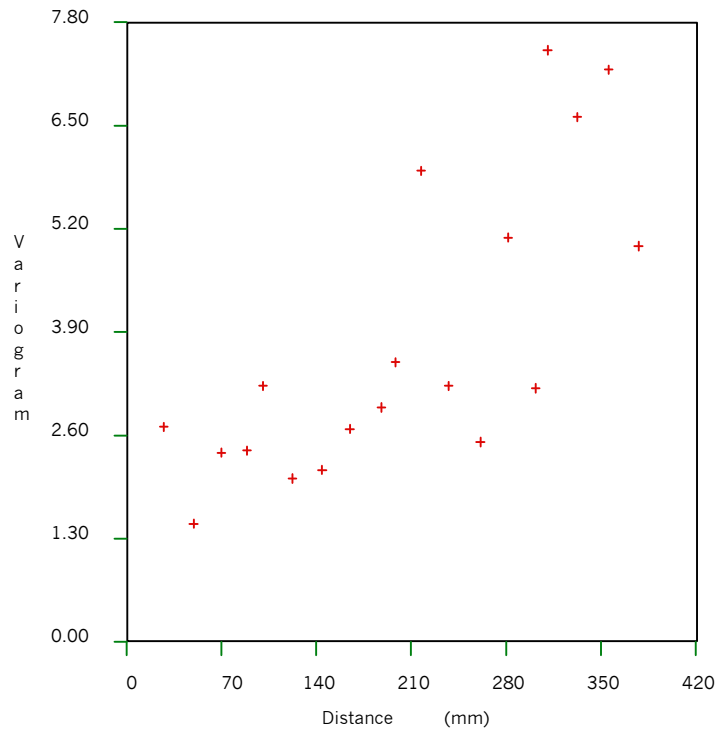


Fig. 12 Semi-variogram of effective diffusivity for 4 mm ÄD slabs.

### 2.3.3 Results from a surface adsorption selectivity experiment

Fig. 13 shows an X-ray mapping of the adsorption of Cs on an ÄD sample surface. Three mineral grains are identified using scanning analyses based on the sodium and iron elements. They are biotite (Bi), plagioclases (Pl) and quartz (Qz). The concentration of Cs is indicated by varying degree of yellow and red. Increasing degree of yellow indicates increasing concentration of Cs. As can be seen, Cs adsorption on the rock surface is strongly selective, with all the adsorption taking place on biotite grains, whereas practically no adsorption was detectable on plagioclases and quartz. The adsorption selectivity is limited not only to specific minerals, but also to different orientations of mineral grains (Hoffstedt, 1997). This fact is reflected by the varying degree of yellow that characterises the two biotite fields in Fig. 13. An important conclusion from these findings is that the variability of the mineral composition and their orientation governs the variability of adsorption.

The exact concentration of Cs could not be determined in X-ray samples due to the lack of standard reference of Cs. If the concentration of each pixel is determined, a statistical structure analysis could be performed and the variability of adsorption on a grain size scale could be evaluated. However, such an approach needs further investigations using digital image analysis of X-ray mapping of Cs adsorption.

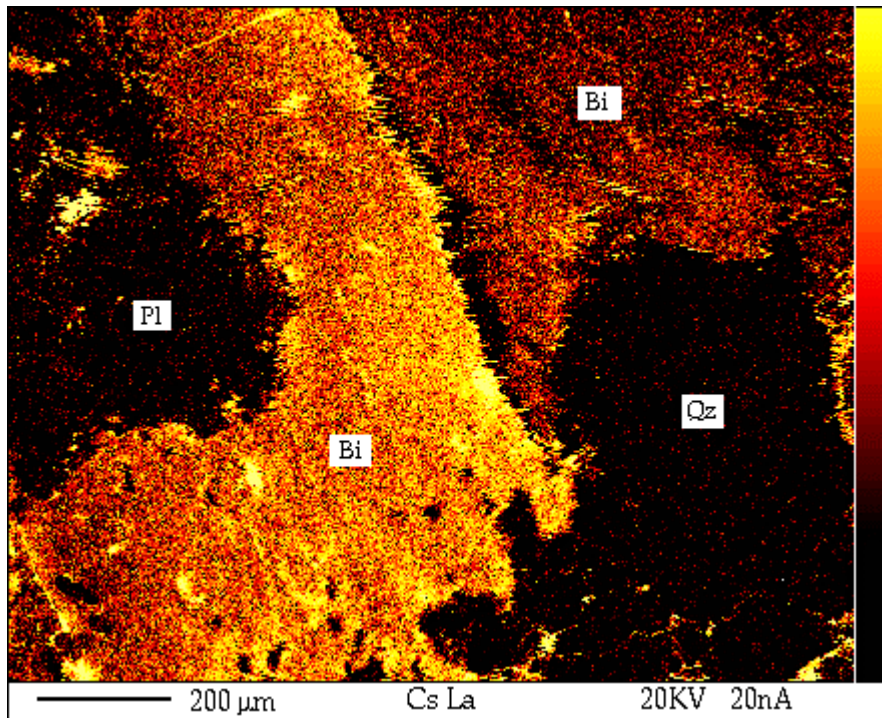


Fig. 13 X-ray mapping of a rock sample surface of ÄD that has been exposed to Cs.

## 2.4 Conclusions

The coefficient of variation of rock porosity,  $CV[\varepsilon]$ , depends on the sample volume. Results from a large number of batch tests, using arbitrary sample sizes of 20x20 mm and varying thickness in the range 6- 15 mm, gave  $CV[\varepsilon] \cdot 10\%$  for both Äspö diorite (ÄD) and Småland granite (SG). Mean porosity is 0.40% for the 15 mm slabs of ÄD (maximal investigated thickness) and 0.36% for the 10 mm slabs of SG (maximal investigated thickness). The porosity decreases slightly with slab thickness, which indicates that there is a small effect of sawing on the porosity.

The distance over which a certain random property exhibits a covariance (the correlation length) does not depend on the sample volume if the property is continuous and stationary for the volume. The semi-variance of the porosity is, for both rock types, characterised by a correlation length of about 30 to 40 cm. The semi-variance for SG is cyclic with the period 34 cm which reflects the spotted nature of the mineral distribution. The cyclic characteristic implies that porosities of the samples separated by 17 cm are generally most dissimilar. Results from samples separated by 34 cm have the highest covariance.

Micro probe analyses indicate that the variability of the mineral composition and their orientation govern the variability of adsorption. Caesium adsorbs predominantly on biotite whereas practically no Cs is adsorbed to plagioclases and quartz.

Results from through-diffusion tests show that the coefficient of variation of the effective diffusivity is about 100% for both rock types and the sampling sizes used in

the study. The correlation length for effective diffusivity is similar to that found for porosity, i.e. about 30 cm. The frequency functions for both porosity and diffusivities are markedly positively skewed, which suggests that log-normal distributions apply as approximations.

## Part B:

### 3 Effect of Sorption Kinetics on Radionuclide Migration

#### 3.1 Introduction

The overall objective of this project is to determine the effect of heterogeneity of geochemical and physical parameters on the migration of radionuclides in fractured rock. As a basis for an adequate interpretation of heterogeneous transport, efforts have been made to improve the process description also for homogeneous cases. A mathematical model describing the migration of radionuclides along single fractures should include the transversal diffusion into the rock matrix as well as sorption processes. Hence, the specific purpose in focus of part B of the current report is to evaluate the relevance of including sorption kinetics (as distinct from equilibrium sorption) and surface diffusion. A particularly important objective is to determine under what conditions the approximation of equilibrium sorption is acceptable.

Several investigations of Cs adsorption on minerals indicate that the equilibration time varies from weeks in laboratory tests with particulate forms of illite and montmorillonite (Comans and Hockley, 1992) up to several years or decades under special conditions for Chernobyl Cs in lake sediments (Meili and Wörman, 1996). Comans *et al.* (1991), Nyffeler *et al.* (1986) and Smith and Comans (1996) discussed the different equilibrium times associated with the readily available binding sites on grain surfaces and less available sites such as frayed edges or in the grain interior (micro fissures of the grain). Skagius (1986) conducted experiments with adsorption and desorption of Cs on crushed granite in different size fractions, the major constituents of which were quartz, feldspar and microcline. In some experiments, the ratio between dissolved and particulate phases of Cs was still changing even after more than one year.

In order to quantify the kinetics of Cs adsorption on granite and to estimate its relevance to radionuclide migration in fractured rock, two experimental approaches are utilized in this study. One approach is to determine the surface adsorption rate by performing batch tests with rock crushed into sufficiently small particles. In this context, sufficiently small particles are those for which the surface available to adsorption is dominated by the external mantle surface. Since there is a certain relationship between the adsorption isotherm (equilibrium state) and the mass transfer rate, a consistent theoretical foundation will be developed for interpretation of the results from these batch tests. In principle, the theory can be used also to generalise the results to intact rock even though such a procedure is not trivial.

Adsorption in intact rock, in general, is influenced both by surface adsorption along the connected inter-granular boundaries and the combined effect of migration in internal micro-fissures of the grains (not inter-connected fissures) and sorption onto solid surfaces. In addition, surface diffusion is another phenomenon affecting the ion mobility in the adsorbed state that can be of significance (Skagius, 1986; Eriksen and Jansson, 1996). Due to these complications the study will also include adsorption experiments with intact rock. The approach is then to evaluate the in-diffusion tests

with intact rock pieces using a model formulation that takes into account both rate limited mass transfer in the rock matrix and surface diffusion. The two approaches are used to determine the limits for adsorption rate for  $^{137}\text{Cs}$  in crystalline rock.

Analytical expressions for the temporal moments of the solute residence time in fractured rock are definite measures of the overall transport process that can be used to understand the importance of adsorption kinetics to the transport. The temporal moments can readily be translated into statistical quantities such as mean and variance of the residence times. Hence, one of the objectives is to derive expressions for the relative error in the variances resulting from the assumption of equilibrium chemistry. As distinct from the variance, the criterion used to evaluate the degree of importance of adsorption kinetics can also be based on the peak concentration. This criterion will be deduced from interpretations of numerical experiments using the simulation package of Wörman and Xu (1996).

### 3.2 Models and Criteria of the Effect of Sorption Kinetics

#### 3.2.1 Models of migration process

The solute transport in a single fracture is represented as a two-dimensional process on a rectangle with open up- and downstream boundaries according to Fig. 14. Radionuclides are allowed to diffuse into the pores of the rock matrix (inter-granular micro fissures) lateral to the main flow direction. The porous matrix extends for a certain distance at which no flux is permitted. The no-flux condition can be motivated either as a symmetry condition with neighbouring fractures in which transport occurs simultaneously or simply by the fact the permeability is higher adjacent to the fracture than in the parent rock. Stress relaxation along a fracture

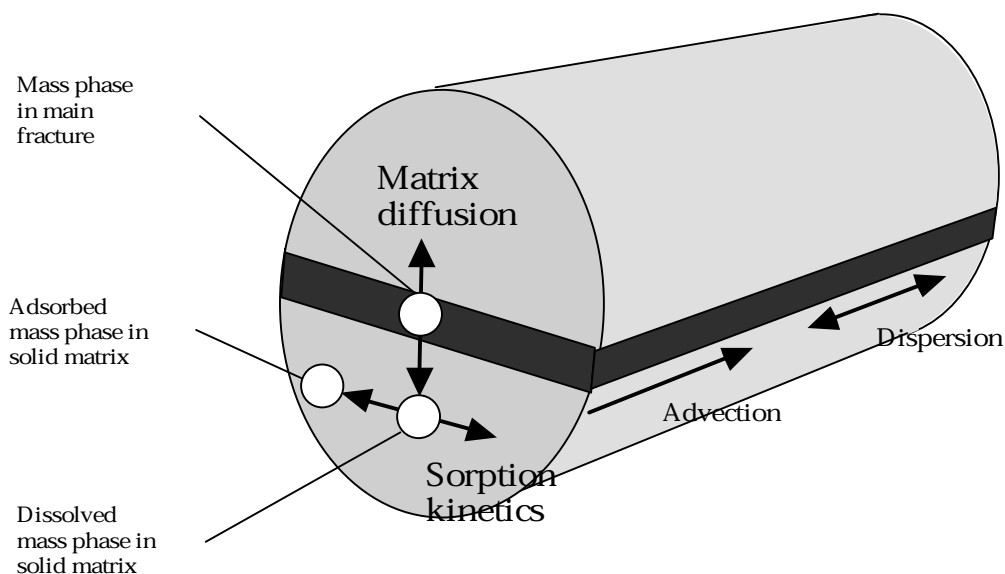


Fig. 14 Schematic illustration of the conceptual model used to analyse the effect of matrix diffusion and adsorption kinetics on radionuclide migration.

causes an opening of the inter-granular micro fissures. Advection in the longitudinal direction does not occur in the rock.

The above aspects of the transport lead to a model concept similar to that of Kunstman *et al.* (1997). However, the current transport formulation incorporates variability in aperture and physical-chemical parameters. The model also includes surface diffusion and non-equilibrium sorption. For incompressible fluids, we may write the depth-averaged form of the A/D equation for the fracture planes as (Wörman and Xu, 1996)

$$\begin{aligned} \frac{\partial c}{\partial t} + u_k \frac{\partial c}{\partial x_k} - \frac{1}{h} \frac{\partial h}{\partial x_k} \left[ (E_{kj} + D_{kj}) \frac{\partial c}{\partial x_j} \right] - \frac{\partial}{\partial x_k} \left[ (E_{kj} + D_{kj}) \frac{\partial c}{\partial x_j} \right] \\ + \gamma c - \frac{2}{h} D_e \frac{\partial c_m}{\partial z} \Big|_{z=0} = 0 \end{aligned} \quad (4)$$

in which  $c$  is concentration of solute per unit volume of water [ $\text{kg}/\text{m}^3$ ],  $c_m$  is dissolved mass per unit volume of water [ $\text{kg}/\text{m}^3$ ],  $D_{kj}$  is molecular (ionic) diffusivity tensor [ $\text{m}^2/\text{s}$ ] in which indices  $k = j = 1, 2$ ,  $u$  is advective velocity [ $\text{m}/\text{s}$ ],  $\gamma$  is rate of radioactive decay [ $1/\text{s}$ ],  $t$  is time [ $\text{s}$ ],  $x_k$  is Cartesian co-ordinate vector,  $h$  is fracture aperture,  $E$  is dispersion coefficient [ $\text{m}^2/\text{s}$ ],  $D_e$  is effective diffusivity which is expressed by  $D_e = \epsilon_t D_p + k_{d1} \rho D_s$  in which pore diffusivity  $D_p = D \delta_D / \tau^2$  [ $\text{m}^2/\text{s}$ ],  $D$  is molecular diffusivity [ $\text{m}^2/\text{s}$ ],  $\epsilon_t$  is porosity of rock matrix available to matrix diffusion,  $\delta_D$  is constrictivity,  $\tau$  is tortuosity,  $D_s$  is surface diffusivity [ $\text{m}^2/\text{s}$ ],  $\rho$  is density of the rock [ $\text{kg}/\text{m}^3$ ] and  $k_{d1}$  is partitioning coefficient which is defined in (5). The variables  $c$ ,  $u$ ,  $E$  and  $D$  in the equation are depth-averaged. An explanation of the diffusivity and adsorption model is provided below.

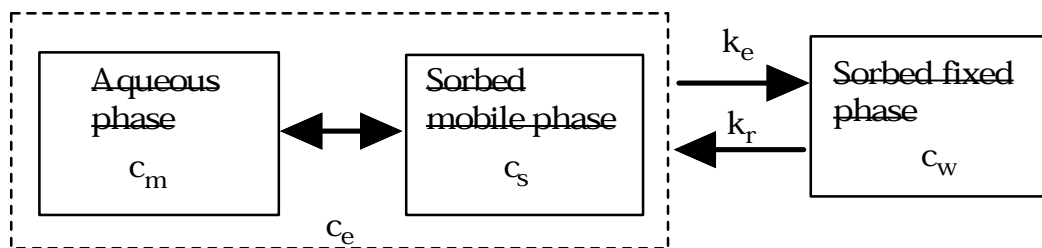


Fig. 15 Schematic representation of the kinetic sorption and surface diffusion model.

As cations, like  $\text{Cs}$ , are adsorbed to mineral surfaces one fraction of the ions takes specific sites on the surface due to complexation or ion exchange and the other fraction is more weakly attracted to the surface by electrostatic interaction. The mobility of the weakly attracted ions is altered compared with the mobility of the free phase in the aqueous solution. The mobility of the ions in this weakly sorbed phase is known as surface diffusion (Skagius, 1986; Eriksen and Jansson, 1996; Ohlsson and Neretnieks, 1997). In addition to the alteration of mobility, the distinction between the aqueous and weakly sorbed (mobile) phases is motivated

also because the determination of the partitioning coefficient for particulate rock generally represents the weakly sorbed phase as being completely sorbed. Experiments with particulate rock are an important method to determine the partition coefficient since equilibrium condition can be achieved also for highly sorbing nuclides.

Diffusion of solutes in the rock matrix is thus dependent on molecular diffusion in pore water and in a weakly sorbed phase. The model adopted in this study is similar to that used for Cs in aquatic sediments by, e. g. Smith and Comans (1996). A distinction is made between the dissolved solute mass per unit volume of water,  $c_m$  [kg/m<sup>3</sup>], the sorbed mobile (aqueous) solute mass per unit solid mass,  $c_s$  [kg/kg], and the solute mass which is “fixed” on solids per unit solid mass,  $c_w$  [kg/kg], (Fig. 15). An instantaneous equilibration between the aqueous and sorbed mobile phase prevails and is defined by the partitioning coefficient

$$k_{d1} = c_s / c_m \quad (5)$$

which has the units [m<sup>3</sup>/ kg]. The diffusive flux of solute in water phase per unit area of the rock medium in units [kg/ m<sup>2</sup> s] is given by

$$F_w = \varepsilon_t D_p \frac{\partial c_m}{\partial z} \quad (6)$$

For solid phase, the flux of solute per unit area due to surface diffusion in units [kg/ m<sup>2</sup> s] is given by

$$F_s = D_s \frac{\partial(c_s \rho)}{\partial z} \quad (7)$$

The mass conservation can thus be formulated in terms of the concentration of mobile phase,  $c_e$  [kg/ m<sup>3</sup>], i.e. the combined aqueous/ exchangeable phase

$$c_e = \varepsilon c_m + \rho c_s \quad (8)$$

For a constant porosity, diffusivity and adsorption in the rock matrix, the mass conservation equations for the mobile and fixed phases can be written

$$\frac{\partial c_e}{\partial t} - \frac{\partial}{\partial z} \left( \varepsilon_t D_p \frac{\partial c_m}{\partial z} + D_s \frac{\partial(c_s \rho)}{\partial z} \right) + \gamma c_e + k_e c_e - k_r c_w \rho = 0 \quad (9)$$

$$\frac{\partial(c_w \rho)}{\partial t} + \gamma c_w \rho + k_r c_w \rho - k_e c_e = 0 \quad (10)$$

in which  $k_r$  and  $k_e$ , are first order transfer rates in units [s<sup>-1</sup>]. If (5) and (8) are substituted into (9) and (10), one obtains after some rearrangements

$$\frac{\partial c_m}{\partial t} - \Omega \frac{\varepsilon_t}{\varepsilon} D_p \frac{\partial^2 c_m}{\partial z^2} + \gamma c_m + k_r \Psi \frac{\rho}{\varepsilon} (K_D c_m - c_w) = 0 \quad (11)$$

$$\frac{\partial c_w}{\partial t} + \gamma c_w - k_r (K_D c_m - c_w) = 0 \quad (12)$$

in which

$$\Omega = \frac{1 + \frac{D_s}{D_p} \frac{\rho}{\varepsilon_t} k_{dl}}{1 + \frac{\rho}{\varepsilon} k_{dl}} \quad (12a)$$

$$\Psi = \frac{1}{1 + \frac{\rho}{\varepsilon} k_{dl}} \quad (12b)$$

and the partitioning coefficient,  $K_D$  [ $\text{m}^3/\text{kg}$ ], is defined as

$$K_D = \left[ \frac{c_w}{c_m} \right]_e = \frac{\varepsilon}{\rho \Psi} \frac{k_e}{k_r} \quad (13)$$

For the special case that the weakly sorbed phase is omitted in the model framework,  $k_{dl} = 0$  which gives  $\Psi = \Omega = 1$ . The definition of  $K_D$  according to (13) still applies.

### 3.2.2 Semi-empirical equation for adsorption kinetics

The equilibration time for the diffusion of Cs (in water) into a cubic piece of rock with a side length of 1 cm is several years. The long equilibration times prohibits reliable estimates of the sorption partition coefficients without careful evaluations also of the time rate of change of the concentration ratio between dissolved and sorbed mass phases. Independent measurement of the partition coefficient for strongly sorbing nuclides is therefore often done on crushed material. Particularly the adsorption isotherm can be determined using crushed rock. A requirement is that the rock particles are small enough for the diffusion into the grains to be negligible. As the particles become larger the inner surface available to sorption through diffusion in micro fissures in the grains will constitute an increasing part of the total adsorbent surface area. Sorption kinetics is then dominated by diffusion related processes in the grains. Section 3.4.1 contains a description of the method used to select the sufficiently small grains that are dominated by their external (mantle) surface area. This selection procedure facilitates a study of surface sorption kinetics that will be used as a reference for the sorption kinetics study with intact rock described in sections 3.3.3 and 3.4.2.

The evaluation of the experiments requires a theoretical basis that combines the kinetic description with an applicable adsorption isotherm. Hence, both the

equilibrium state and the mass transfer rate will be related to the ratio between dissolved phase concentration and the adsorbent surface area. In this purpose, consider a suspension of particulate granite in a solution of a certain adsorbate substance. The concentration ratio of the adsorbed to dissolved solute mass at equilibrium defines the partition coefficient

$$k_d = \left[ \frac{c_a}{c_d} \right]_e \quad (14)$$

in which  $c_a$  is bulk concentration for adsorbed phase of solute [ $\text{kg}/\text{m}^3$ ],  $c_d$  is bulk concentration for dissolved phase of solute [ $\text{kg}/\text{m}^3$ ], the subscript e denotes chemical equilibrium. The partition coefficient  $k_d$  and the partition coefficient  $K_D$ , defined previously in (13), are related according to

$$K_D = \frac{\varepsilon}{\rho} k_d \quad (15)$$

The rate of adsorption of the solute on the particles can be expressed in terms of entities from surface chemistry as (Attkins, 1983). The net adsorption rate is expressed as

$$G \equiv \frac{dc_a}{dt} = G_{ad} - G_{des} \quad (16)$$

in which  $G_{ad}$  is mass rate of adsorption and  $G_{des}$  is mass rate of desorption. Further, one may write

$$G_{ad} = \frac{U}{\sqrt{3}} s \Phi c_d \quad (17)$$

$$G_{des} = a c_a \quad (18)$$

in which  $U$  is squared mean speed of molecules [ $\text{m}^2/\text{s}$ ],  $s$  is sticking probability,  $a$  is rate of departure [ $\text{s}^{-1}$ ] and  $\Phi$  is specific surface area [ $\text{m}^2/\text{m}^3$ ] (solid surface area per unit bulk volume of rock). Eq. (17) is based on the kinetic theory for molecules moving randomly, independently of each other (e.g. Attkins, 1983, pp 860-874, 1003-1030) and rapidly compared to the grains.

The continuing derivation is based on three additional assumptions, of which the first is that the sticking probability  $s = s_0 (1 - c_a/c_{as})$ , the second that the saturation concentration  $c_{as} = \alpha \Phi$ , and the third that the rate of departure  $a = \beta \Phi$ , in which  $s_0$ ,  $\alpha$  and  $\beta$  are constants. Hence, (16) can be written as

$$G = \frac{dc_a}{dt} = k_r (k_d c_d - c_a) \quad (19)$$

in which the kinetic adsorption rate coefficient is defined as

$$k_r = \Phi (\beta + \gamma c_d / (\alpha \Phi)) \quad (20)$$

and the partition coefficient as

$$k_d = \frac{1}{\beta/\gamma + c_d / (\alpha \Phi)} \quad (21)$$

and  $\gamma = [U / (2\sqrt{3})] s_0$ . The constants  $\alpha$ ,  $\beta$  and  $\gamma$  should be determined from regression analysis with the experimental data.

If we assume that  $k_r$  and the total concentration  $c_{tot} = c_a + c_d$  are constant in a batch test, the solution to (19) can be given as

$$c_a = \frac{k_d c_{tot}}{k_d + 1} - \frac{1}{k_d + 1} e^{\ln(k_d c_{tot}) - k_r t (k_d + 1)} \quad (22)$$

The  $k_r$  value can be determined by fitting the analytical solution to the observed data from each individual batch test. To determine the constants in (20) and (21), the linearised forms

$$\frac{k_r}{\Phi} = \beta + \frac{\gamma}{\alpha} \frac{c_d}{\Phi} \quad (23)$$

$$\frac{1}{k_d} = \frac{\beta}{\gamma} + \frac{1}{\alpha} \frac{c_d}{\Phi} \quad (24)$$

is used in a regression analysis (linear in  $\beta$ ,  $\gamma/\alpha$ ,  $\beta/\gamma$  and  $1/\alpha$ ). From several batch tests, the constants in (23) and (24) can be estimated by means of linear regression.

### 3.2.3 Analytical solution to the temporal moments of the breakthrough curves

A usual methodology for deriving analytical solutions to solute transport processes involves Laplace transforms. Even if analytical solution can not be found in closed form, the temporal moments of the solute concentration curve (the breakthrough curve) often can. The temporal moments can, further, be transformed into statistical properties (central moments) like mean residence time, variance and skewness. Even a relatively small number of moments captures the most important characteristics of the solution and a general understanding of the processes. An infinite number of the temporal moments defines the solution exactly. The Laplace transform of a function  $u$  is expressed in the form

$$L[u] = \bar{u} = \int_0^{\infty} u e^{-pt} dt \quad (25)$$

in which  $p$  is an arbitrary real number. Setting  $p = 0$  in (25) yields the zeroth temporal moment of the function  $u$  as

$$m_0 = L[u] \Big|_{p=0} = \int_0^{\infty} u dt \quad (26)$$

If  $u$  is divided by the zeroth moment, the result is in the form of a probability density function,  $f$ , for the time. By repeated differentiation, one can readily show that the temporal moments of  $f$  can be given as

$$m_j = \int_0^{\infty} t^j f dt = (-1)^j \frac{\partial^j L[f]}{\partial p^j} \Big|_{p=0}; \quad j=1,2,\dots \quad (27)$$

If  $u$  is now taken as the concentration,  $c$ ,  $f$  is the probability density function for residence times and (27) gives the temporal moments of the probability density function for the residence time.

For a uniform fracture plane, constant dispersion and negligible radioactive decay, the transport equation for the main fracture can be written as

$$\frac{\partial c}{\partial t} + u \frac{\partial c}{\partial x} - E \frac{\partial^2 c}{\partial x^2} - 2 \frac{D_e'}{h} \frac{\partial c_m}{\partial z} \Big|_{z=0} = 0 \quad (28)$$

Together with the equations for transport in the rock matrix (11) and (12), as well as the boundary and initial conditions, the solution in the form of  $L[c(x,t)]$  is obtained following a similar procedure as that proposed by Maloszewski and Zuber (1990), except for the boundary condition for the porous matrix, which is defined as no-flux (impervious surface) at a distance,  $L$ , from the main fracture plane instead of an infinite extent (Appendix I).

Basic relationships between the residence time  $E[t]$  and the variance  $\sigma^2$  of the residence time distribution and the first two temporal moments can be given as

$$E[t] = \mu = m_1 \quad (29)$$

$$\sigma^2 = m_2 - \mu^2 \quad (30)$$

After several operations, based on (11), (12), (27) and (28) which are accounted for in Appendix I, the residence time and the variance of the residence time associated with a Dirac pulse (cf. (A5) and (A9) in Appendix I for a definition of initial and boundary conditions) become

$$m_1 = E[t] = \frac{x}{u} \left[ 1 + 2 \frac{D_e' L}{\Omega \frac{\epsilon_t}{\epsilon} D_p h} \left( 1 + \Psi \frac{\rho}{\epsilon} K_D \right) \right] \quad (31)$$

$$\sigma^2 = \frac{x}{u} \left[ 2 \left( 1 + 2 \frac{D'_e L}{\Omega \frac{\epsilon_t}{\epsilon} D_p h} \left( 1 + \Psi \frac{\rho}{\epsilon} K_D \right) \right)^2 \frac{E}{u^2} + \frac{4}{3} \left( 1 + \Psi \frac{\rho}{\epsilon} K_D \right)^2 \frac{D'_e L}{\Omega \frac{\epsilon_t}{\epsilon} D_p h} \frac{L^2}{\Omega D_p} + 4 \Psi \frac{\rho}{\epsilon} K_D \frac{D'_e L}{\Omega \frac{\epsilon_t}{\epsilon} D_p h} \frac{1}{k_r} \right] \quad (32)$$

From (31) the one may conclude that the combined effect of matrix diffusion and sorption kinetics can be represented in terms of a retardation factor which is conveniently defined as the second term on the right hand side of (31). As porosity approaches zero ( $D'_e$  approaches zero), the celerity of propagation of the solute pulse approaches the advection velocity; i.e.  $x/E[t] = u$ . As the matrix diffusion approaches infinity the celerity of propagation approaches zero. Further, the spreading of the solute pulse can be related to three terms on the right hand side of (32) which from left to right represent 1) the effect of dispersion in the main fracture, 2) the effect of matrix diffusion and equilibrium sorption and 3) the effect of sorption kinetics. Accordingly, the sorption kinetics does not affect the mean residence time but may have a significant impact on the spreading of the pulse.

### 3.2.4 Effect of adsorption kinetics, dispersion and matrix diffusion on solute migration

As stated, matrix diffusion and sorption onto the solid matrix retard the solute pulse travelling through a fracture in relation to the advection velocity in the fracture. Matrix diffusion and sorption also spread the pulse. Based on (32) the spreading can be quantified as a function of five dimensionless numbers:

$$\Pi_{KD} = \Psi \frac{\rho}{\epsilon} K_D; \Pi_E = \frac{Ek_r}{u^2}; \Pi_{kr} = \frac{L^2 k_r}{\Omega \frac{\epsilon_t}{\epsilon} D_p}; \Pi_x = \frac{x k_r}{u}; \Pi_L = \frac{D'_e L}{\Omega \frac{\epsilon_t}{\epsilon} D_p h}$$

The numbers reflect, in falling order, the equilibrium state of adsorption, relative dispersion, relative reaction kinetics, relative transport distance and ratio of penetration length and fracture aperture. In case surface diffusion is not to be considered,  $\Psi = \Omega = 1$  and  $\Pi_L = (\epsilon L)/h$ . Hence, Eq. (32) is re-written as

$$k_r^2 \sigma^2 = D + M + K = M \left( 1 + \frac{K}{M} \right) \left( 1 + \frac{D}{M \left( \frac{K}{M} + 1 \right)} \right) \quad (33a)$$

in which

$$D = \Pi_x \left( 2 \left( 1 + 2 \Pi_L \left( 1 + \Pi_{KD} \right) \right)^2 \Pi_E \right) \quad (33b)$$

$$M = \frac{4}{3} \Pi_x \left( 1 + \Pi_{KD} \right)^2 \Pi_L \Pi_{kr} \quad (33c)$$

$$K = 4 \Pi_x \Pi_L \Pi_{KD} \quad (33d)$$

Dispersion is not a significant phenomenon if

$$\frac{D}{M \left( \frac{K}{M} + 1 \right)} \ll 1 \quad (34)$$

The effect of adsorption kinetics can be omitted if  $K/M \ll 1$ , i.e.

$$\frac{3 \Pi_{KD}}{(1 + \Pi_{KD})^2 \Pi_{kr}} \ll 1 \quad (35)$$

The relative error of the variances of the residence time distribution resulting from the assumption of equilibrium chemistry ( $k_r \rightarrow \infty$ ) can be expressed as

$$\varepsilon_{\text{var}} = \frac{\sigma_k^2 - \sigma_E^2}{\sigma_E^2} = \frac{4 \Pi_L \Pi_{KD}}{2(1 + 2 \Pi_L (1 + \Pi_{KD}))^2 \Pi_E + \frac{4}{3} (1 + \Pi_{KD})^2 \Pi_L \Pi_{kr}} \quad (36a)$$

in which

$$\sigma_k^2 = (D + M + K)/k_r^2 \quad (36b)$$

$$\sigma_E^2 = (D + M)/k_r^2 \quad (36c)$$

Especially, if  $\Pi_E \approx 0$ , the relative error has the form of

$$\varepsilon_{\text{var}} = \frac{3 \Pi_{KD}}{(1 + \Pi_{KD})^2 \Pi_{kr}} \quad (37)$$

Because (35) and (37) are second order in  $\Pi_{KD}$ , there is a lower and an upper limit in  $\Pi_{KD}$  below and above which sorption kinetics is not important to take into account. In an intermediate range, sorption kinetics can be important.

### 3.2.5 Simulation of the effect of adsorption kinetics

In principle, the concentration distribution can be represented by the infinite series of all its moments (Holley and Jirka, 1986). In practice, even the third moment of the Laplace transform of the transport model is hard to derive and to overview. Hence, to complement the error description (35) - (37) with higher order statistics, numerical experiments were conducted. Simulations were performed to examine the error of

the peak value of the solute pulse resulting from neglecting sorption kinetics. The relative error in the peak value resulting if  $k \rightarrow \infty$  is defined as

$$\varepsilon_{\text{peak}} = \frac{P_k - P_E}{P_E} \quad (38)$$

in which  $P_k$  is peak value of the concentration pulse with account taken to sorption kinetics and  $P_E$  is peak value of concentration pulse with account taken only to equilibrium chemistry. The simulation results are evaluated on the basis of the five dimensionless numbers described in previous sections.

### 3.3 Materials and Experimental Methods

#### 3.3.1 Materials

The adsorption experiments reported here are all conducted with Äspö diorite, both indiffusion experiments and experiments with crushed rock. The dominating minerals are plagioclase, potassium feldspar, quartz and biotite. The average mineral compositions are given in Table 2 (see section 2.2.1).

#### 3.3.2 Method for determining adsorption kinetics on crushed rock particles

Batch tests with crushed rock was partly included in the MSc thesis of Nyberg (1997). The current study include additional experiments as well as a new theoretical basis for the evaluation (section 3.2.2).

The rock was crushed and dry-sieved into three size fractions. Particles larger than 1.198 mm were washed several times with distilled water and dried at 80 °C for 24 hours. The size of the finest fraction was determined using a Galai CIS-1 instrument to be 0.0154 mm. The Galai instrument is based on registration of the interference caused by particles on a laser beam rapidly circulating in a particle suspension. For the other size fractions, the mean diameter was determined through sieving to be 1.198 and 2.397 mm.

A 200 ml batch solution was prepared by adding  $^{137}\text{Cs}$  in dissolved form into synthetic ground water (Allard and Beall, 1979) and mixed with a suspension of crushed granite. Samples of about 1 ml were withdrawn repeatedly from the gently shaken batch solution and immediately separated (by centrifugation) into their dissolved and particulate components. The partition ratio between the particulate and the dissolved phase,  $k_d$ , was obtained by measuring the concentration decrease of the clear water phase. The initial concentration of Cs was  $1.3 \cdot 10^5$  M. The particle concentration was 40 g/l, 60 g/l, 100g/l and 150 g/l for the particle size 0.0154 mm, and for the other two particle sizes the corresponding concentration was 40 g/l. The experiments were performed at room temperature and under oxic conditions because the planned laboratory migration experiments will be performed under the same conditions.

### 3.3.3 Method for determining adsorption kinetics on intact rock

The estimation of adsorption kinetics for intact rock was based on the evaluation of experimental data from the in-diffusion tests using the model described in section 3.2.1. The in-diffusion technique described by Ittner *et al.* (1990) was employed herein. The rock slabs had a size of 2 x 2 x 1 cm and were coated with silicone rubber on all sides except one. The samples were kept in contact with synthetic ground water for about two months for pre-equilibration before they were submerged in the synthetic ground water with <sup>137</sup>Cs as a tracer element. Hence, the Cs ions start to slowly diffuse into the only open side of the rock slab which gives rise to a concentration profile with depth in the rock.

After a contact time of more than 6 months, the slab was taken out from the solution and washed. 0.1 mm thick layers of the slab were successively removed using sand-paper. The trace element was analysed by measuring the radioactivity of the removed material, including the sand-paper. The radioactivity was measured by means of a  $\gamma$ -counter (CG-4000).

The rate of diffusion of <sup>137</sup>Cs through the slab follows the same mathematical framework as outlined in section 3.2.1, particularly (4), (11) and (12). The free water phase (corresponding to the main fracture) is homogenous in the indiffusion experiments whereby the differential terms in space can be neglected in (4). Further, (4) should be averaged over the cross section, A [m<sup>2</sup>], of the rock sample. Hence, for negligible radioactive decay the system becomes

$$\forall \frac{\partial c}{\partial t} - A D_e' \frac{\partial c_m}{\partial z} \Big|_{z=0} = 0 \quad (39)$$

$$\frac{\partial c_m}{\partial t} - \Omega \frac{\epsilon_t}{\epsilon} D_p \frac{\partial^2 c_m}{\partial z^2} + k_r \Psi \frac{\rho}{\epsilon} (K_D c_m - c_w) = 0 \quad (40)$$

$$\frac{\partial c_w}{\partial t} - k_r (K_D c_m - c_w) = 0 \quad (41)$$

in which  $\forall$  is volume of the solution in the free water phase [m<sup>3</sup>].

The boundary and initial conditions applicable to the experimental set-up can be defined as

$$c(x, t = 0) = c_0 \quad (42a)$$

$$\bullet c_m / \bullet z \Big|_{(z=L, t=\infty)} = 0 \quad (42b)$$

$$c_m(z = 0, t = 0) = c(t) \quad (42c)$$

$$\bullet c_w / \bullet z \Big|_{(z=L, t=\infty)} = 0 \quad (42d)$$

$$c_m(z, t=0) = c_w(z, t=0) = 0 \quad (42e)$$

in which L is the limited distance of the porous matrix (L = 1 cm). The boundary conditions (42b) and (42d) can be replaced by arbitrary conditions in the evaluations

since the downward boundary has negligible effect on the transport in the experiments. The system of equations is solved numerically by the central finite difference and the Crank-Nicolsons approximation for time. All the parameters in the equation system are determined independently except for  $D_s$ ,  $k_r$ ,  $K_D$  and  $k_{d1}$ , which are estimated by fitting the solution of the equation system to the measured concentration profile (see section 3.4.2).

The parameter  $K_D$  governs the total concentration in the rock close to the boundary since chemical equilibration with the free water phase is nearly reached in this region. Both the parameters  $k_r$  and the product  $(k_{d1} D_s)$  have similar effect on the shape of the concentration profile; decreasing  $k_r$  or increasing  $(k_{d1} D_s)$  contribute to effectively higher diffusion rates. Consequently, the three parameters have to some extent different influence on the transport process and this will facilitate evaluation of the parameter values. The parameters  $k_{d1}$  and  $D_s$  can not be evaluated independently of each other from the experiments conducted in this study.

### 3.4 Results and Discussions

#### 3.4.1 Results from measurements of adsorption kinetics on crushed rock particles

An important part of the evaluation is to select those grain size fractions in which the surface area of the grains dominate the total area available to sorption. The particle surface area can be defined as the 1) external geometric surface area,  $A_E$ , including surface roughness, 2) physical surface area,  $A_T$ , including the internal surface area,  $A_{IN}$ , of (micro) pores and / or (micro) fissures and external geometric surface area  $A_E$ , and 3) geometric surface area of a sphere with the same diameter as that of the mean particle (surface area of the equivalent sphere),  $A_{ES}$ . Fig. 16 schematically represents the three surface concepts.

The ratio of the internal surface area,  $A_{IN}$ , and the volume of the particles,  $V$ , can be assumed to be constant for a specific type of rock material

$$\frac{A_{IN}}{V} = \text{constant} = c_1 \quad (43)$$

Eq. (43) states that the specific inner surface is independent of size. Further, the

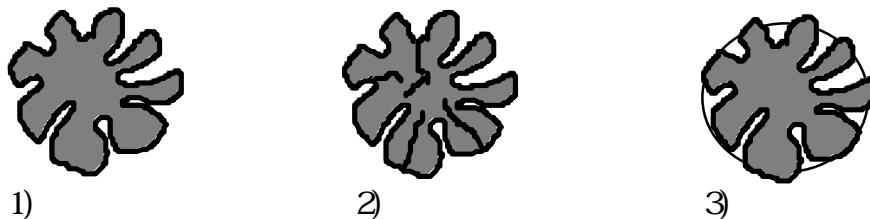


Fig. 16 Definition of particle surface: 1) external geometric surface area, 2) physical surface area, which includes the internal surfaces of (micro) pores and / or (micro) cracks, and 3) geometric surface area of a sphere with the same size as the mean particle.

Table 5 BET surface area data

Mean particle size, $d_{ph}$ mm	BET-surface area $m^2/g$	Geometric surface area $m^2/g$	BET-surface / Geometric surface area, $\lambda_g$
0.0154	$0.97 \pm 0.03$	0.1443	6.7
0.605	$0.13 \pm 0.01$	0.0036	35.4
1.198	$0.11 \pm 0.01$	0.0018	59.3

ratio of the external geometric surface area,  $A_E$ , and the surface area of the equivalent sphere,  $A_{ES}$ , is constant

$$\frac{A_E}{A_{ES}} = \text{constant} = c_2 \quad (44)$$

This implies that the surface roughness factor is independent of size. According to (43) and (44) the total physical surface area can be written as

$$A_T = A_{IN} + A_E = c_1 V + c_2 A_{ES} \quad (45)$$

A surface roughness factor,  $\lambda_g$ , is defined as the ratio between the physical surface area and the surface area of the equivalent sphere which means that (45) becomes

$$\lambda_g = \frac{A_T}{A_{ES}} = c_1 \frac{V}{A_{ES}} + c_2 \quad (46)$$

in which  $V/A_{ES} \propto d_{ph}$  and  $d_{ph}$  is the harmonic mean by volume of the grain diameters. Eq. (46) can thus be replaced by

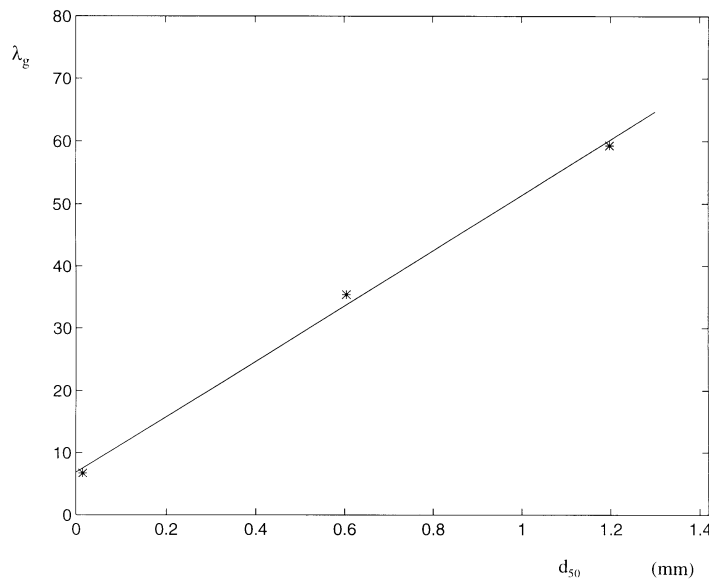


Fig. 17 Particle size,  $d_{ph}$ , versus  $\lambda_g$  according to data (stars) and Eq. (47) (line).

$$\lambda_g = c_3 d_{ph} + c_2 \quad (47)$$

The residual,  $c_2$ , as the diameter approaches zero is the ratio between the external geometric surface area and the surface area of the equivalent sphere. Consequently, if one can find grains such that  $c_2 \gg c_3 d_{ph}$  the surface of these grains will be dominated by the external geometric surface.

The physical surface area of the particle was estimated by nitrogen gas BET (Brunauer, Emmet, and Teller)-surface area using a Micromeritics Flow Sorb II 2300 analyser. Measured BET surface areas data are shown in Table 5. Fig. 17 shows a plot of the particle fraction size versus  $\lambda_g$ . As can be seen, the  $\lambda_g$  value for the smallest particle size 0.0154 mm is about the same as the intercept value  $c_2$  (the value of  $c_2$  is about 7 and similar to those reported by Anbeek, 1992). In other words, the measured surface area for 0.0154 mm particles is dominated by the external geometric surface area. Consequently, only the particles with a size of 0.0154 mm are included in the interpretation of surface sorption kinetics and evaluation according to (23) and (24). The rate coefficient  $k_r$  was obtained by fitting the results from each individual adsorption experiment according to (22) by means of a non-linear regression technique. Fig. 18 shows the concentration of the adsorbed phase,  $C_s$ , versus time according to data obtained from a batch test and fitted theory. As can be seen, there is a certain deviation between data and theory. The reason for the deviation is probably that the surface adsorption kinetics follow slightly more complicated mechanisms than those proposed in section 3.2.2. The assumption of constant  $k_r$  applies only as an approximation.

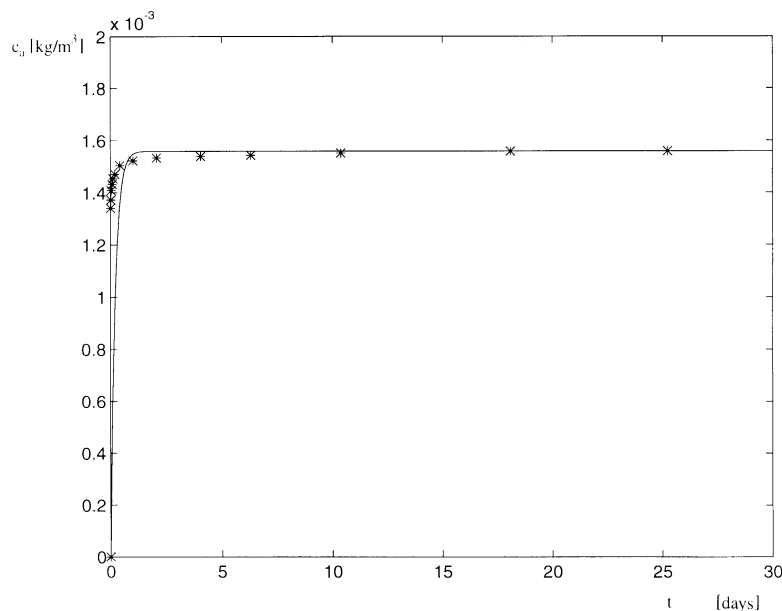


Fig. 18 Concentration,  $c_a$ , for adsorbed phase of Cs versus time from a batch test with a particle concentration of 150 g/l and particle size of 0.0154 mm.

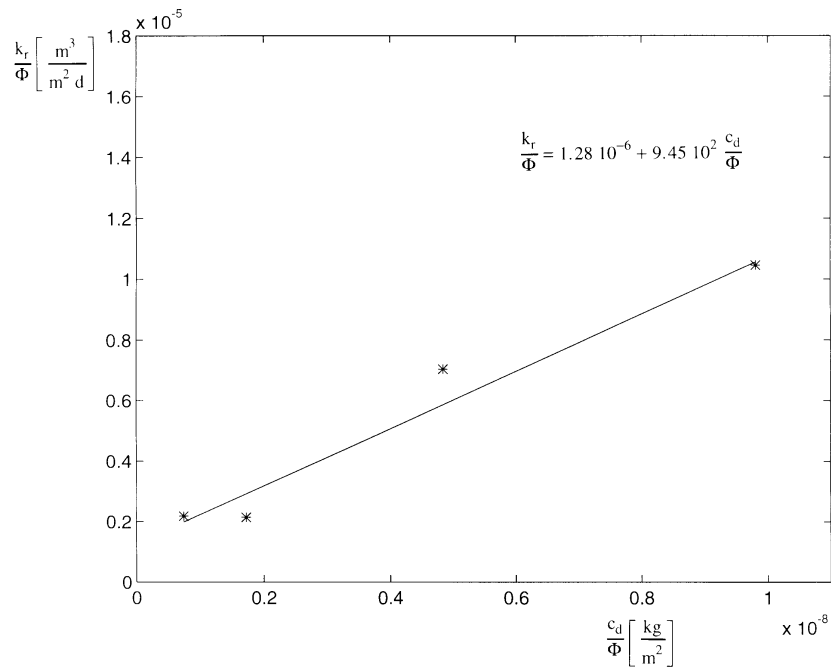


Fig. 19  $k_r/\Phi$  vs.  $c_d/\Phi$  according to experimental results (\*) and theory (solid line).

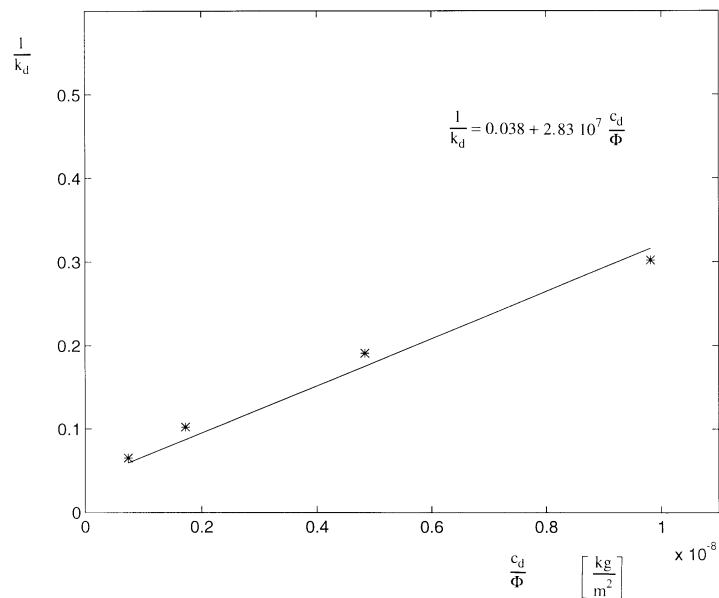


Fig. 20  $1/k_d$  vs.  $c_d/\Phi$  according to experimental results (\*) and theory (solid line).

Results of  $k_r$  from four batch tests are plotted using  $k_r/\Phi$  and  $1/k_d$  versus  $c_d/\Phi$  (Figs. 19 and 20). The constants in (23) and (24) were then determined using an iterative least square regression technique. The non-linear adsorption isotherm, (24), and the associated dependence on the rate coefficient of partial pressure is verified with an acceptable degree of confidence. The non-linearity is, however, a minor problem in most practical cases of interest whereas the dependence of the rate coefficient on the specific inner surface of intact rock is generally a significant problem.

Various values of specific inner surface area for intact rock have been reported in the literature. A conservative estimation of the specific inner surface of the intact rock is about  $20\text{ m}^2/\text{kg}$  (Hakanen and Hölttä, 1992). The specific inner surface of granite coupons measured by Eriksen and Locklund (1989) based on  $\text{N}_2$ -sorption was  $200\text{ m}^2/\text{kg}$ . As a qualitative estimate, the specific inner surface for intact rock is assumed to be  $100\text{ m}^2/\text{kg}$ , i.e.  $270\,000\text{ m}^2/\text{m}^3$  (taking the density as  $2700\text{ kg}/\text{m}^3$ ). Hence, for intact rock the  $c_d/\Phi$  ratio is practically zero and from Fig. 18,  $k_r/\Phi = 1.28\,10^6\text{ m}/\text{d}$ . Since  $\Phi = 270\,000\text{ m}^2/\text{m}^3$ , we have  $k_r = 0.34\text{ d}^{-1}$  or  $4\,10^6\text{ s}^{-1}$ . This value will be used as a reference in the interpretation of the in-diffusion experiments.

### 3.4.2 Results from measurement of adsorption kinetics on intact rock

The purpose of the simulation procedures accounted for in this section is to verify the model (39) - (41) and, particularly, to provide estimates of the rate coefficient  $k_r$ . Because of the complexity of the mathematical frame work and number of parameters, one would expect a comparatively wide range of acceptable solutions. The range of solutions is associated with a certain range of the plausible values of  $k_r$ . Even though a definite verification of the model is not possible, its degree of fit to experimental data is compared with the corresponding fit of two other, simpler, model approaches.

#### *Equilibrium sorption with no surface diffusion*

The results from the in-diffusion experiments were evaluated using three special cases of the same matrix transport model defined by (40) and (41) and schematically shown in Fig. 15. In a traditional equilibrium type model there is no surface diffusion,  $k_{d1} = 0$ , and the partitioning (sorption) between the aqueous (dissolved) and sorbed fixed phases are instantaneous,  $k_r \rightarrow \infty$ . For simplicity, a constant boundary concentration is also assumed for this equilibrium approach,  $\varepsilon c_m(z=0,t) + \rho c_w(z=0,t) = \kappa C_0$  in which  $C_0$  is the constant concentration in the pore water at the boundary and  $\kappa = \varepsilon + K_D \rho$  is the sorption capacity factor. The solution to (40) and (41) for a semi-infinite medium is obtained as (Crank, 1975)

$$\frac{\varepsilon c_m + \rho c_w}{\kappa C_0} = \text{erfc} \left( \frac{z}{2 \sqrt{\frac{\varepsilon_t D_p}{\kappa} t}} \right) \quad (48)$$

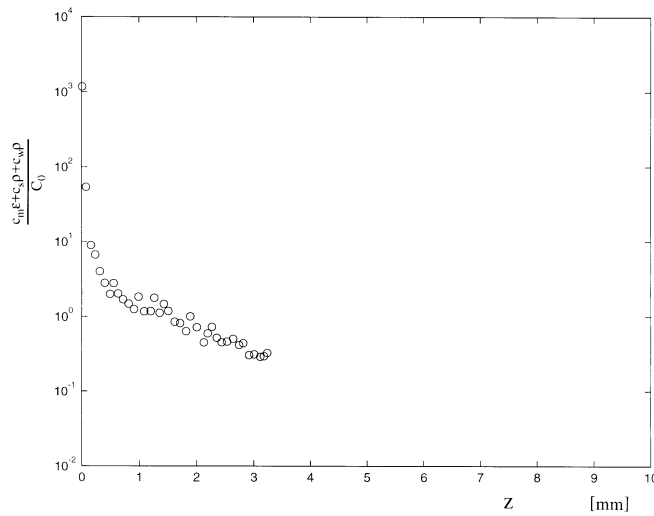


Fig. 21 Concentration profile of  $^{137}\text{Cs}$  in Äspö diorite (sample slab B6 in Fig. 1) as a function of the penetration depth. Diffusion time is 316 days.

in which  $\epsilon c_w + \rho c_m$  is the total concentration in the rock. Several researchers have used this type of model formulation and pointed out that it deviates significantly from results obtained from in-diffusion experiments (Ittner *et al.*, 1990, Idemitsu *et al.*, 1992, Tsukamoto *et al.*, 1993 and Johansson *et al.*, 1998).

### *Surface diffusion model*

In the second special case there is no exchange between the sorbed mobile phase and the sorbed fixed phase,  $k_r$  is taken as 0 in (39) - (40). Eq. (41) can be omitted. Hence, the total concentration in the rock is the sum  $\epsilon c_m + \rho c_s$ . Such a model was used by Skagius (1986) and Eriksen and Jansson (1996). However, prior to evaluation of the experimental results a special problem of adsorption needs to be addressed. At the rock interface towards the aqueous solution, the surface available to sorption is larger than in the interior of the rock. One reason is that the sawing splits both grains and inter-granular connections and, thus, increases the open surface area. Another reason is that the sawing also tends to produce micro fissures between the grains even at a minor depth from the sawing face.

Fig. 21 shows the concentration of Cs as a function of the penetration depth after 316 days in one of the experiments. The concentration of Cs at the first few layers (tens of millimetres) is higher than expected from the data obtained deeper in the rock. The abrupt change in gradient cannot be explained using the model equations (40) and (41) with constant parameters. In the experiment represented in Fig. 21, more than 50% of the total Cs mass was accumulated in the first few layers in this experiment. Due to the limited spatial extension of the anomaly in the concentration profile, an evaluation of the spatial variation in model

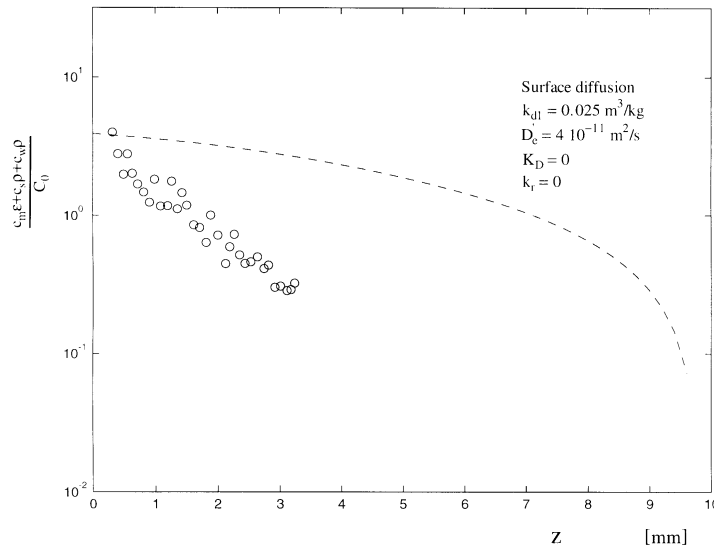


Fig. 22 Concentration profile of  $^{137}\text{Cs}$  in Äspö diorite (sample slab B6 in Fig. 1) and the solution to the surface diffusion model. The ratio  $M_2/M_1 = 5.5$ . Diffusion time is 316 days.

parameters will be difficult and not so valuable. The alternative preferred in this study is to treat the surficial layer as a separate pool of accumulation. As an approximation, the equilibration between the solute masses in the free water phase and the surficial layer is instantaneous, which means that the ratio between  $M_1$  and  $M_2$  is constant. Hence, the initial concentration in the free water phase becomes

$$c(t=0) = \frac{M_0/V}{\left(1 + \frac{M_2}{M_1}\right)} \quad (49)$$

in which  $M_0$  is the total mass of the solute used in the in-diffusion test. Further, the flux into the rock sample is assumed to be governed by the concentration gradient in the interior of the surficial layer independently of the high concentration at the surface. Hence, the conservation equation for solute mass in the free water phase becomes

$$V \frac{\partial c}{\partial t} - \frac{A D_c}{1 + \frac{M_2}{M_1}} \frac{\partial c_m}{\partial z} \Big|_{z=0} = 0 \quad (50)$$

The  $M_2/M_1$  ratio can be determined directly from measurements. The first three data points shown in Fig. 21 are considered parts of the surficial layer which resulted in  $M_2/M_1 = 5.5$ . However, a slightly lower ratio can also be motivated in (50) due to the impact of the solute accumulation in the surficial layer on the flux. Therefore, the  $M_2/M_1$  ratio was evaluated also by curve fitting.

Fig. 22 shows that when the effective and surface diffusivity were chosen according to the values reported by Skagius (1986) or Eriksen and Jansson (1996) the solution to the surface diffusion model did not fit the measured data especially well. The best fit between data and the surface diffusion model was obtained for the parameter values  $D'_e = 1.5 \cdot 10^{12} \text{ m}^2/\text{s}$ ,  $k_{d1} = 0.01 \text{ m}^3/\text{kg}$  and  $K_D = k_r = 0$  (Fig. 23). The  $M_2/M_1$  ratio was then kept at 5.5. The most significant deviation between data and theory is that the data describes a relatively straight line in the log-normal diagrams whereas the model solution has a marked negative curvature (negative second derivative).

The other parameter values were taken from the literature or independent measurement results reported in part A. Molecular diffusivity,  $D$ , in a free aqueous phase for Cs is  $\sim 1 \cdot 10^9 \text{ m}^2/\text{s}$  (Cussler, 1984). The pore diffusivity is thus  $1 \cdot 10^{10} \text{ m}^2/\text{s}$  ( $D_p = D \delta_D / \tau^2$ , where  $\delta_D / \tau^2$  is assumed to be 0.1). Since the porosity associated with space available for transport is about 60% of the total porosity (Johansson *et al.* 1998), the porosity available to transport for this particular slab was 0.0033. The effective diffusivity in the aqueous phase is thus  $D_e = \epsilon_t D_p = 3.3 \cdot 10^{13} \text{ m}^2/\text{s}$  which is in the range found for the  $\ddot{A}D$  in the through-diffusion tests using iodide (cf. Figs. 10 and 11). Rock density,  $\rho$ , was  $2700 \text{ kg}/\text{m}^3$ . The ratio of the solution volume and the area of the rock sample,  $\forall / A$ , was 0.035 m.

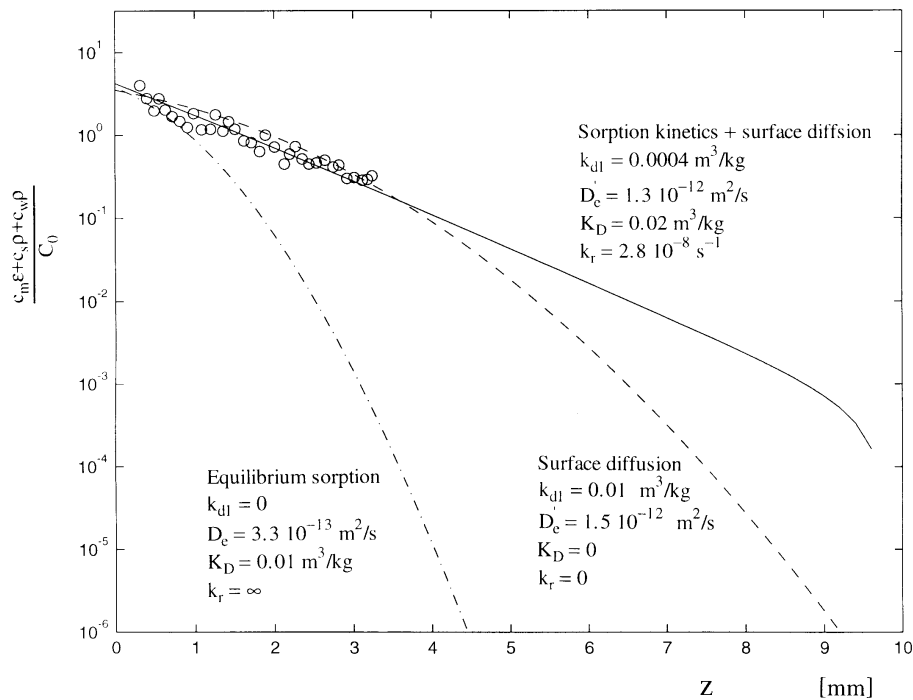


Fig. 23 Concentration profile of  $^{137}\text{Cs}$  in Äspö diorite (sample slab B6 in Fig. 1) and solutions for various model assumptions. The ratio  $M_2/M_1 = 5.5$ . The circles denote the measured data. Diffusion time is 316 days.

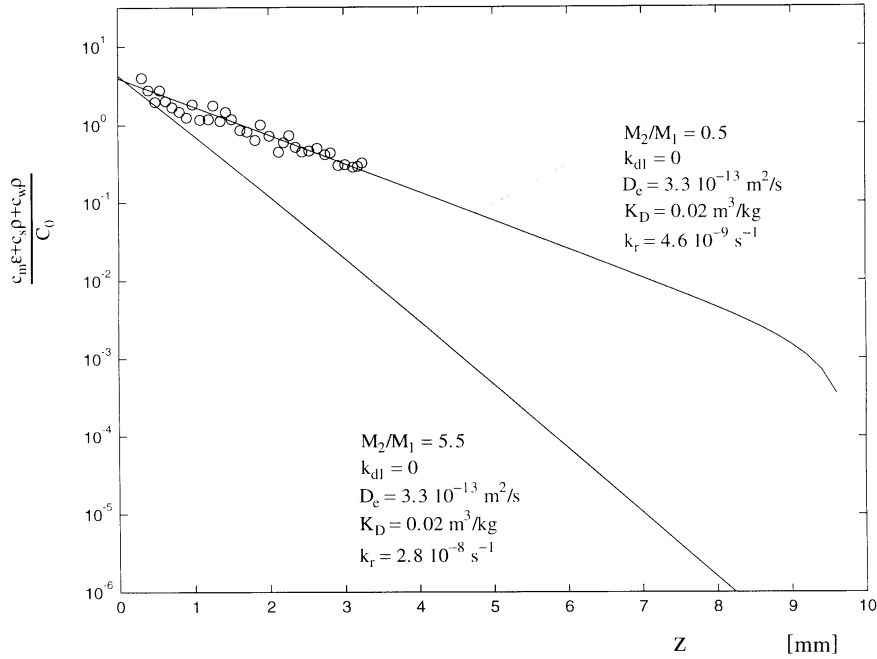


Fig 24 Concentration profile of  $^{137}\text{Cs}$  in Äspö diorite (sample slab B6 in Fig. 1) and solutions for various model assumptions. The ratio  $M_2/M_1 = 0.5$ . The circles denote the measured data. Diffusion time is 316 days.

### *Sorption kinetics and surface diffusion model*

The best fit between data and theory was obtained for the combined surface diffusion and sorption kinetics model ((40) and (41)). Based on an ocular examination of the best fit between theory and data the following optimised parameter values were obtained:  $D_e = 1.3 \cdot 10^{12} \text{ m}^2/\text{s}$ ,  $k_{d1} = 0.0004 \text{ m}^3/\text{kg}$ ,  $K_D = 0.02 \text{ m}^3/\text{kg}$ ,  $k_r = 2.8 \cdot 10^8 \text{ s}^{-1}$  and  $M_2/M_1 = 5.5$  (Fig. 23). Apparently, the introduction of sorption kinetics leads to a better agreement between theory and the data than obtained from previous models. If the  $M_2/M_1$  ratio is lowered to 0.5, a nearly perfect fit is obtained even if the surface diffusion is completely omitted (Fig. 24). Consequently, sorption kinetics appears to be more important than surface diffusion in explaining the data obtained in this study.

However, if the  $M_2/M_1$  ratio is kept at 5.5 and surface diffusion is omitted, an acceptable fit was not possible, as can be seen in Fig. 24. This indicates that an acceptable solution is delimited by the two cases 1)  $M_2/M_1 = 0.5$  and no surface diffusion (Fig. 24) and 2)  $M_2/M_1 = 5.5$  and a combination of surface diffusion and sorption kinetics (Fig. 23). The range of plausible  $k_r$  values depend on the exact  $M_2/M_1$  ratio and surface diffusion, but falls in the range  $4.6 \cdot 10^9 \text{ s}^{-1} < k_r < 2.8 \cdot 10^8 \text{ s}^{-1}$ .

Table 6 Values applicable to the laboratory migration experiments

Parameters	Units	Values	Notes
D	[ m <sup>2</sup> /s ]	1 10 <sup>9</sup>	Cussler (1984)
D <sub>p</sub>	[ m <sup>2</sup> /s ]	1 10 <sup>10</sup>	
D <sub>s</sub>	[ m <sup>2</sup> /s ]	1.3 10 <sup>12</sup>	This study
u	[ m/s ]	7.9 10 <sup>6</sup>	
L	[ m ]	0.05	
ε <sub>t</sub>	[ % ]	0.23	This study
K <sub>D</sub>	[ m <sup>3</sup> /kg]	0.02	This study
k <sub>d1</sub>	[ m <sup>3</sup> /kg]	0.0004	This study
h	[ m ]	0.001	
k <sub>r</sub>	[ s <sup>-1</sup> ]	2.8 10 <sup>8</sup>	This study

The adsorption rate obtained is 2 or 3 orders of magnitude smaller than that obtained from the crushed rock particles. The probable explanation is that the kinetics evaluated from the in-diffusion experiments is primarily due to rate-limited transport in micro-fissures (non-conducting/dead end similar to that in Cunningham *et al.*, 1997) but also surface sorption kinetics. Since only about 60% of the pore volume is available to through transport (are conducting), the pore space available to such rate-limited transport is significant.

### 3.4.3 Effect of adsorption kinetics on migration of radionuclides in fractures

The analysis of the relative importance of the different transport mechanisms on migration of Cs in fractured granite is based on the criteria presented in section 3.2.4. A laboratory migration experiment that is planned to be conducted in a later phase of the project is chosen as a reference case of the analysis. Table 6 shows the relevant parameter values. The diffusivities, adsorption rate and partition coefficient values for Cs were estimated from intact Äspö diorite as described in section 3.4.3. The sorption rate was taken as the highest plausible value obtained for intact rock which consequently provides a safe estimate of the effect of sorption kinetics (the effect is slightly underestimated). The porosity value for Äspö diorite was taken from the investigation presented in Part A of this report. As mentioned, the porosity available for transport, ε<sub>t</sub>, is about 60% of the total porosity. The dispersion coefficient, E, for flow between two parallel plates with infinite width can be expressed as

$$E = \frac{u^2 h^2}{210D} \quad (51)$$

Substitution of the value of E and values given in Table 6 gives E/D = 3.8 10<sup>-5</sup>, which suggests that molecular diffusion dominates over shear dispersion. Furthermore, (34) suggests that the effect on the spreading of a solute pulse due to dispersion is much smaller than that of matrix diffusion and can thus be neglected in this case.

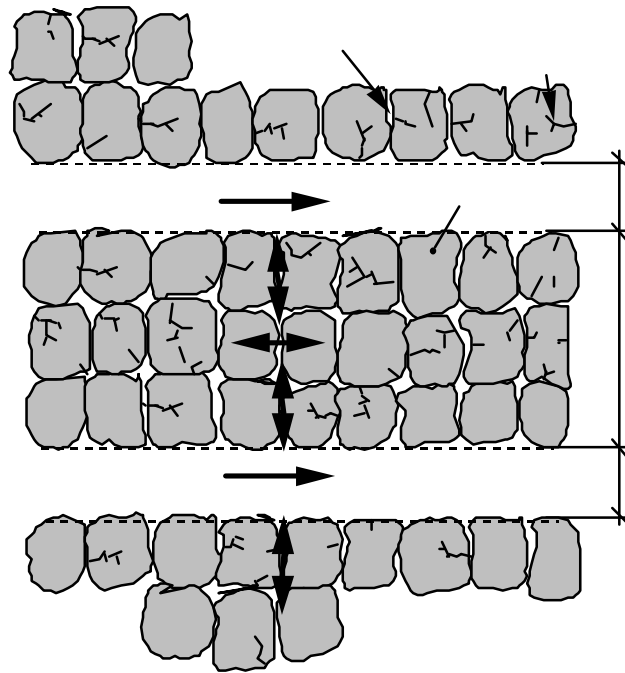


Fig. 25 Definition of the boundary of the model framework used to analyse the effect of matrix diffusion and adsorption kinetics on radionuclide migration.

If we insert the values in Table 6 in (36) and take  $E = D = 10^{-9} \text{ m}^2/\text{s}$  and  $\rho = 2700 \text{ kg/m}^3$ , the relative error of the variance of the residence time resulting from omitting the kinetics will be less than 1 % (for Cs and  $\text{ÄD}$ ). If  $L$  is decreased to 0.005 m, the error is about 10%. As mentioned before,  $L$  is defined as a limited distance of the matrix diffusion or as a symmetry plane between two parallel fractures in which transport occurs simultaneously as shown schematically in Fig. 25. The limited extension of the matrix diffusion can be due to the fact that the porosity of the rock is higher along the fracture because of the stress relaxation in this zone. The stress relaxation also generally causes several fracture planes with a spacing between individual fractures in the range of millimetres or more.

Fig. 26 shows a contour plot of the relative error in the variance of the solute pulse as a function of  $\Pi_{kr}$  and  $\Pi_{KD}$ . For a certain value of the normalised partitioning coefficient,  $\Pi_{KD} \approx 1$ , the maximum error occurs. The importance of adsorption decreases for both smaller and larger  $\Pi_{KD}$ -values which is consistent with (37). The cross corresponds to the 10% error obtained for Cs and  $\text{ÄD}$ .

The developed numerical simulation package (Wörman and Xu, 1986) was used to study the error of the peak concentration due to a Dirac pulse travelling in a fracture resulting from omitting sorption kinetics. The geometry of the problem is outlined in Fig. 14 and surface diffusion was omitted ( $D_s = k_{d1} = 0$ ). The other parameters are taken according to Table 6. The result is presented in terms of the five dimensionless numbers presented in section 3.2.4 and the individual variables are varied in a number of different ways. Fig. 27 shows the simulation results in terms of  $c(x,t)$  caused by a Dirac pulse defined at the upstream boundary

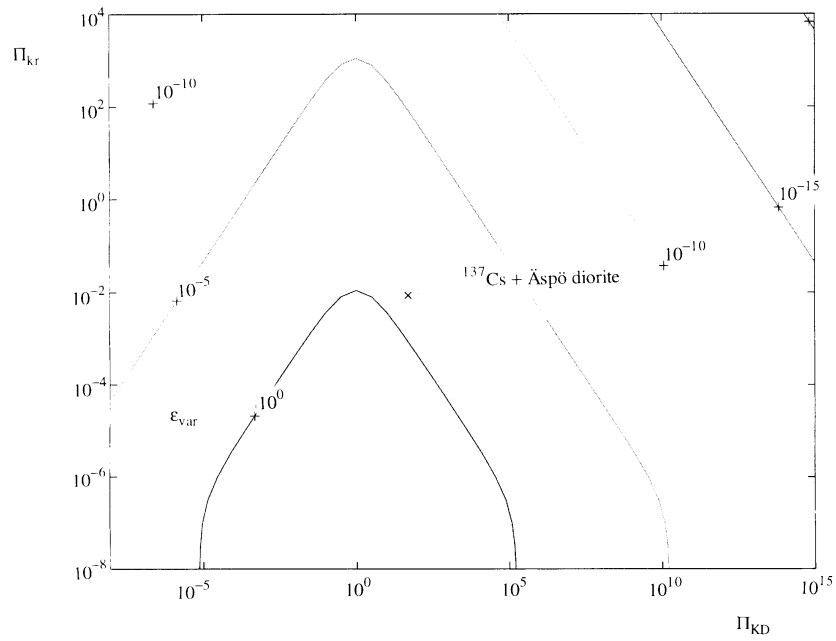


Fig. 26 Isopleth diagram of the relative error,  $\epsilon_{\text{var}}$ , as a function of  $\Pi_{\text{KD}}$  and  $\Pi_{\text{kr}}$ , with  $\Pi_{\text{L}} = 5.4$ , and  $\Pi_{\text{E}} = 5.6 \cdot 10^7$ .

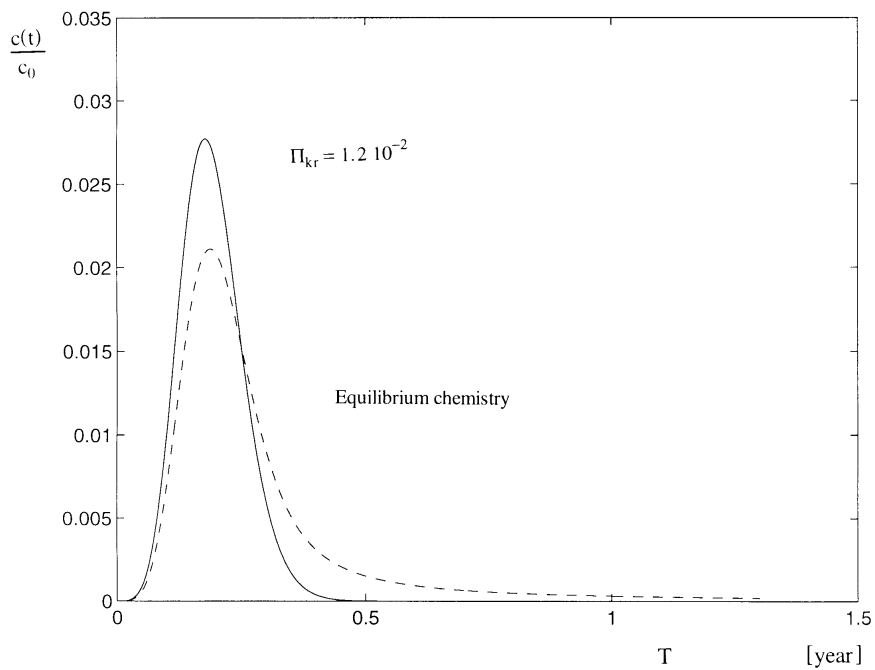


Fig. 27 Breakthrough curve for  $\Pi_x = 3.5 \cdot 10^3$ ,  $\Pi_{\text{KD}} = 1.4 \cdot 10^4$ ,  $\Pi_{\text{L}} = 2 \cdot 10^2$ , and  $\Pi_{\text{E}} = 4.5 \cdot 10^7$  due to a Dirac pulse of Cs defined at the upstream boundary.

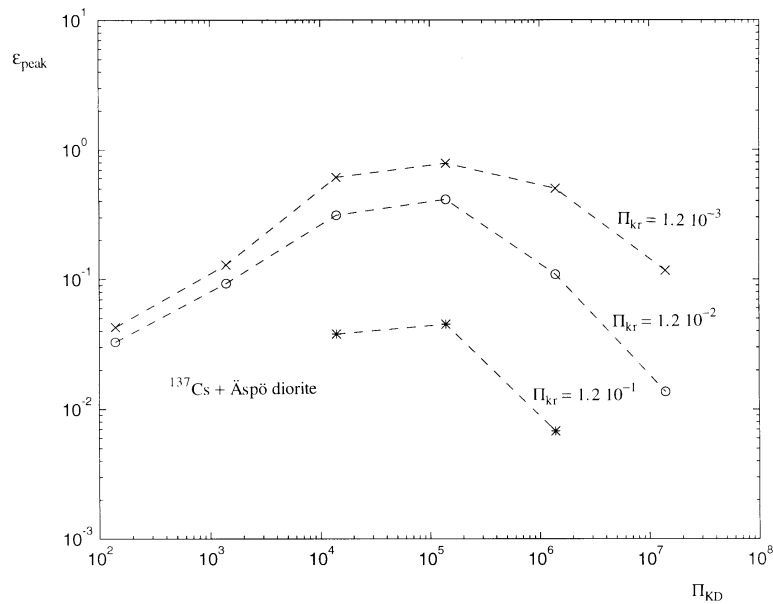


Fig. 28 Relative error in the peak value of a solute pulse resulting from omitting adsorption kinetics as a function of  $\Pi_{KD}$  and  $\Pi_{kr}$ . The values of  $\Pi_x$ ,  $\Pi_L$  and  $\Pi_E$  are constants ( $\Pi_x = 3.5 \cdot 10^7$ ,  $\Pi_L = 0.02$  and  $\Pi_E = 4.5 \cdot 10^7$ ).

and a semi-infinite domain (in the downstream direction) for different  $\Pi_{kr}$ -values, whereas the other parameters are constants.

The kinetics of the adsorption process during the uptake phase can be interpreted as a decrease in the effective partition coefficient. In contrast, adsorption kinetics during the release phase can be interpreted as a net increase of the partition coefficient. These conditions are manifested in terms of a higher peak value and lower tail values for the case of kinetic sorption in comparison to the case of equilibrium sorption. For the specific simulation results shown in Fig. 27, adsorption kinetics increases the height of the peak in the breakthrough by as much as 31% compared with the equilibrium case (a much higher  $\Pi_{kr}$ -value). Consequently, the kinetic case has a lower mass retention at maximum but a more prolonged retardation effect than for the equilibrium case. The effect of adsorption kinetics for  $^{137}\text{Cs}$  on Äspö diorite depends on the value of  $L$  that has been more or less arbitrarily chosen in this study.

Fig. 28 shows the relative error in the peak concentration,  $\varepsilon_{\text{peak}}$ , resulting if kinetics is omitted as a function of  $\Pi_{KD}$  and  $\Pi_{kr}$ , while the other three dimensionless numbers are kept as constants. Similarly as for the error in variance, the error in the peak concentration is negligible when the  $\Pi_{KD}$ -value is sufficiently low or high. In other words, adsorption kinetics has no effect on non-sorbing or extremely strongly sorbing nuclides. If the  $\Pi_{kr}$ -isopleth for Cs and ÄD is taken as a reference, a relative error less than 10% is obtained for  $\rho/\varepsilon K_D < \sim 2.5 \cdot 10^3 \text{ m}^3/\text{kg}$  (weakly sorbing nuclides) or  $\rho/\varepsilon K_D > \sim 2.5 \cdot 10^6 \text{ m}^3/\text{kg}$  (strongly sorbing).

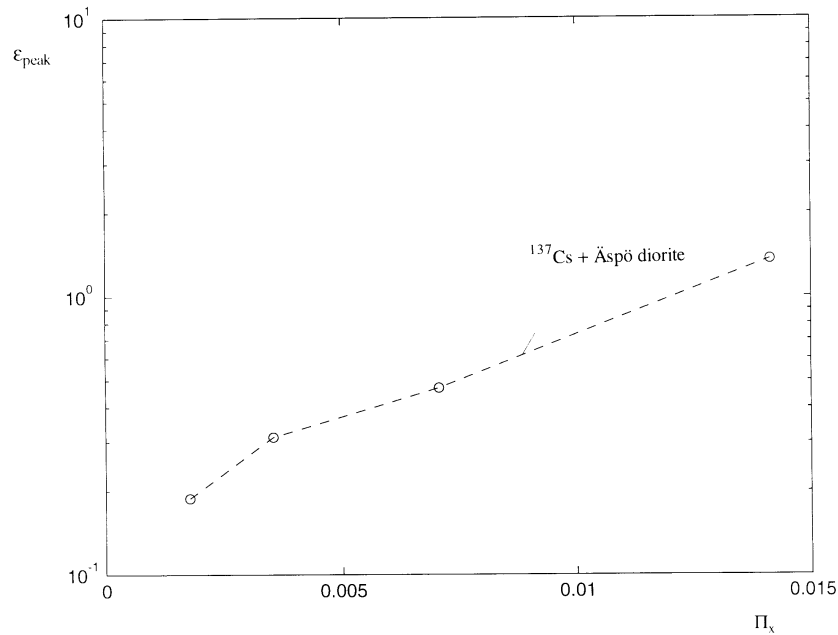


Fig. 29 Error resulting from disregarding adsorption kinetics as a function of  $\Pi_x$ . Constants are  $\Pi_{kr} = 1.2 \cdot 10^2$ ,  $\Pi_{KD} = 14000$ ,  $\Pi_L = 0.02$ , and  $\Pi_E = 4.5 \cdot 10^7$ .

The two error functions, defined for the variance and the peak, are similar. However,  $\epsilon_{\text{peak}}$  is also a function of  $\Pi_x$ . The mathematical reason for this is that  $\epsilon_{\text{peak}}$  depends also on higher-order statistics in addition to the second order temporal moment in the residence time probability function (i.e. the variance). The higher-order statistics are non-linear in  $x/u$ , which implies that  $x$  cannot be eliminated in an error definition in the form of (36). Fig. 29 shows how the error resulting from omitting sorption kinetics,  $\epsilon_{\text{peak}}$ , increases significantly with  $\Pi_x$ . As a reference, the  $\Pi_{kr}$ -isopleth represented in the figure is that for Cs and ÄD.

From the figure, the relative error of the peak value for  $\Pi_x = 0.014$  is  $\sim 136\%$ . If  $u$  is taken according to table 6,  $k_r$  is that obtained for Cs and ÄD, the distance corresponding to  $\Pi_x = 0.014$  is  $\sim 3.8$  m. For a distance plausible in a performance assessment (PA) analysis, the error will be much larger than 136%.

### 3.5 Conclusions

Matrix diffusion of sorptive nuclides in crystalline rock is affected both by diffusion in the free aqueous phase and by surface diffusion in a weakly sorbed state. Further, the sorption process is affected by rate-limited transport that probably occurs in micro fissures in the mineral grains, referred to as sorption kinetics. About 40% of the total porosity consists of pore volumes not active in matrix diffusion (dead-end pores). Matrix diffusion occurs predominantly along inter-granular boundaries.

A mathematical framework ((4), (11) and (12)) is developed in which both surface diffusion and sorption kinetics is included. Two experimental/theoretical approaches were used to estimate the rate of adsorption, one that is focused on the surface sorption kinetics for  $^{137}\text{Cs}$  on crushed rock (grains) and one that is focused on the effective sorption kinetics for  $^{137}\text{Cs}$  in intact rock. Grains for which the external surface area dominates the total area available to sorption could be selected by theoretically deriving and empirically studying the relationship, (47), between surface roughness factor and particle size. These sufficiently small grains could be used to study surface sorption kinetics.

The adsorption rate obtained for crushed rock (surface sorption) is 2 or 3 orders of magnitude higher than that obtained for intact rock. The probable explanation is that the sorption rate evaluated from the in-diffusion experiments is primarily due to the rate-limited transport in micro-fissures. The sorption rate coefficient was evaluated by fitting the theory to experimental data obtained from in-diffusion experiments using  $^{137}\text{Cs}$ . Due to uncertainties in this fitting procedure, the coefficient has an uncertainty by a factor of  $\sim 10$ . Accordingly, the adsorption rate of Cs estimated from one in-diffusion test with a slab of Äspö diorite appears to be in the range  $4.6 \cdot 10^9 \text{ s}^{-1} < k_r < 2.8 \cdot 10^8 \text{ s}^{-1}$ .

The adsorption kinetics affects the transport of radionuclides in fractured rock as a decrease of the effective partition coefficient during the uptake phase. In contrast, adsorption kinetics during the release phase can be interpreted as a net increase of the partition coefficient. If the sorption process is sufficiently slow, the sorption equilibrium state is never a limitation to the pulse propagation (cf. Fig. 28).

Analytical solutions for the first two temporal moments of the solute residence time were derived from the developed transport model (i.e. (31) and (32)). The propagation velocity of a solute pulse in a fracture can be written in terms of the advection velocity and a retardation factor that is a function of matrix diffusion, sorption and surface diffusion. For the analysed case (cf. section 3.2.3) only the second temporal moment depends on sorption kinetics.

Analytical criteria for the importance of different mechanisms to the migration of radionuclides were obtained from the temporal moments ((36) and (37)). The equations contain five dimensionless numbers, which describe the influence of the equilibrium state of sorption, dispersion, penetration length in the matrix, sorption kinetics and transport distance. The dimensionless numbers facilitate a generalisation of numerical simulation results and a simpler presentation of conditions for which adsorption kinetics is an essential factor.

The analytical criteria and the numerical simulation results show that adsorption kinetics has a negligible effect on the transport of sufficiently weakly adsorbing ( $\rho/\varepsilon K_D < \sim 2.5 \cdot 10^3 \text{ m}^3/\text{kg}$ ) or strongly adsorbing ( $\rho/\varepsilon K_D > \sim 2.5 \cdot 10^6 \text{ m}^3/\text{kg}$ ) nuclides. The effect on the peak value of a solute pulse in a fracture increases, however, significantly with transport distance. For conditions typical to a PA analysis (assuming Cs and ÄD), the relative error of the peak value can be several hundred percents or more. Hence, the adsorption kinetics can be an important factor in the

interpretation of migration experiments in fractured rock, depending on experimental conditions such as the kind of nuclides, the kinetic adsorption rates, the type of rocks (mineralogy) and the scale of the experimental set-up as well as the flow rates.

#### 4 General Conclusions

This study provides basic statistics of geochemical and physical transport parameters for Äspö diorite and Småland granite through a large number of measurements of porosity, effective diffusivity and adsorption characteristics in the scale of a drill core (20 cm in diameter and 50 cm in length). Semi-variograms show that both porosity and effective diffusivity can be represented by a correlation length of 30 to 40 cm. The coefficient of variations for rock pieces with a size of  $\sim 4 \cdot 10^6 \text{ m}^3$  are, for both rock types, about 10% for porosity and 100% for effective diffusivity.

Adsorption kinetics can be an essential factor for the interpretation of radionuclide migration in fractured rock, especially for intermediately sorbing nuclides and at long transport distances. The methods developed in this study provide a possibility to estimate the effects of adsorption kinetics in intact rock. By deducing basic data of the adsorption kinetics of  $^{137}\text{Cs}$  in crystalline rock, both on mineral surfaces and for intact rock, definite conclusions on the effect of adsorption kinetics could be established.

Analytical solutions show that four dimensionless numbers describes the relative error of the variance of the probability density function for the residence time resulting from omitting sorption kinetics. These numbers represent the relative importance of the equilibrium state of sorption, dispersion, penetration length and reaction kinetics in matrix diffusion.

Numerical experiments show that the relative error in the peak value of a breakthrough curve increases markedly with transport distance. Sorption kinetics seems to be a highly important factor in the interpretation of field scale experiments and for PA analyses.

#### 5 Acknowledgements

The present project was initiated by Dr. Björn Dverstorp, Swedish Nuclear Power Inspectorate, SKI. He provided many fruitful discussions during the whole course of the project. Dr. Björn Dverstorp, Dr. Bo Strömberg (SKI) and MSc Christina Lilja (SKI) contributed with valuable comments on the manuscript of the report.

Several persons at the Department of Earth Sciences at Uppsala University contributed to parts in the project. Dr. Sadoon Morad guided us in the mineral composition analysis. MSc Andreas Nyberg conducted many of the analyses of surface adsorption kinetics with crushed particles. MSc Matilda Hoffstedt conducted the surface adsorption selectivity experiment.

Complementary porosity measurements were made by MSc Marja Siitari-Kauppi at the Laboratory of Radiochemistry, the University of Helsinki, using the  $^{14}\text{C}$ -PMMA method.

## 6 References

- Adams, E. E., and Baptista, A. M. (1986). Ocean dispersion modeling. In 'Encyclopedia of Fluid Mechanics. Vol. 6. Complex Flow Phenomena and Modeling'. (Ed. N. P. Cheremisinoff), pp. 865-95. (Gulf: Houston.)
- Allard, B. and Beall, G. W. (1979). Adsorption of Americium on geologic media. *J. Environ. Sci. Health*, 6, 507.
- Anbeek, C., (1992). Surface roughness of minerals and implications for dissolution studies. *Geochemica et Cosmochimica Acta* . Vol. 56, pp. 1461-1469.
- ASCE (1990). Review of Geostatistics in Geohydrology. I: Basic Concepts. *Journal of Hydraulic Engineering*. Vol. 116 No. 5.
- Attkins, P. W. (1983). Physical Chemistry, 2<sup>th</sup> ed., *Oxford University Press*. New York.
- Comans, R. N. J. and Hockley, D. E. (1992). Kinetics of cesium sorption on illite. *Geochemica et Cosmochimica Acta*, Vol. 56, pp. 1157-1164.
- Comans, R. N. J., Haller, M. and Preter, P. D. (1991). Sorption of cesium on illite: Non-equilibrium behaviour and reversibility. *Geochemica et Cosmochimica Acta*, Vol. 55, pp. 433-440.
- Crank, J. (1975). The mathematics of diffusion, 2<sup>nd</sup> ed., *Oxford University Press*, New York.
- Cunningham, J. A., Werth, C. J., Reinhard, M. and Roberts, P. V. (1997). Effects of grain-scale mass transfer on the transport of volatile organics through sediments 1. Model development. *Water resources research*, Vol. 33, No. 12, pp. 2713-2726.
- Cussler, E. L. (1984). Diffusion: Mass transfer in fluid system. *Cambridge University Press*, New York.
- Eriksen, T. E. and Locklund, B. (1989). Radionuclide sorption on crushed and intact granitic rock -- Volume and surface effect. *SKB TR 89-25*.
- Eriksen, T. E. and Jansson, M. (1996). Diffusion of I, Cs<sup>+</sup> and Sr<sup>2+</sup> in compacted bentonite – Anion exclusion and surface diffusion. *SKB TR 96-16*.
- Hakanen, M. and Hölttä, P. (1992). Review of adsorption and diffusion parameters for TVO-92. *Report YJT-92-14*.

- Hoffstedt, M. (1997). Adsorption of Cs on mineral surface: A study of adsorption capacity of phyllosilicates. Nov. 1997. *Master thesis. Department of Earth Sciences, Uppsala University.*
- Holley, E. R. and Jirka, G. H. (1986). Mixing in rivers. Technical Rep. E-86-11, US Army Engineer Waterways Experiment Station, Vicksburg, Miss.
- Idemitsu, K., Furuya, H., Hara, T., Inagaki, Y. (1992). Migration of cesium, strontium and cobalt in water-saturated inada granite. *J. Nucl. Sci. Technol.* Vol. 29, pp. 454-460.
- Isaaks, E. H. and Srivastava, R. M. (1989). Applied geostatistics. *Oxford University Press*, New York.
- Ittner, T., Torstenfelt, B., Allard, B. (1990). Diffusion of strontium, iodine and cesium in granitic rock. *Radiochim. Acta.* Vol. 49, pp. 101-106
- Johansson, H., Byegård, J., Skarnemark, G. and Skålberg, M., 1997. Matrix diffusion of some alkali- and alkaline earth-metals in granitic rock., *Scientific Basis for Nuclear Waste Management XX*, edited by W.J. Gray and I.R. Tray, Mat. Res. Soc. Symp. Proc. Vol. 465, pp. 871-878
- Johansson, H., Siitari-Kauppi, M. Skålberg, M. and Tullborg, E. L. (1998). Diffusion pathways in crystalline rock- Examples from Äspö-diorite and fine-grained granite (*Submitted*).
- Kunstman, H., Kinzelbach, W., Marschall, P. and Li, G. (1997). Joint inversion of tracer tests using reversed flow fields. *Journal of Contaminant Hydrology.* Vol. 26, Nos. 1-4 pp. 215-226
- Maloszewski, P. and Zuber, A. (1990). Mathematical modeling of tracer behaviour in short-term experiments in fissured rocks. *Water Resources Res.* Vol. 26, No. 7, pp. 1517-1528
- Meili, M. and Wörman, A. (1996). Desorption and diffusion of episodic pollutants in sediments: a 3-phase model applied to Chernobyl <sup>137</sup>Cs. *Appl. Geochem.* Vol. 11, pp. 311-316
- Nyffeler, U. P., Santschi, P. H. and Li, Y-H. (1986). The relevance of scavenging kinetics to modelling of sediment-water interactions in natural waters. *Limnol. Oceanogr.* Vol. 31, No. 2, pp. 277-292
- Nyberg, A., (1997). Adsorption av cesium på krossad granit (in Swedish). *Master thesis. Department of Earth Sciences, Uppsala University.*
- Ohlsson, Y. And Neretnieks, I. (1997). Diffusion data in granite Recommended values. *SKB TR 97-20.*

- Skagius, A.-C. K. (1986). Diffusion of dissolved species in matrix of some Swedish crystalline rock. *Ph.D Thesis. Dept. Chemical Engineering, Royal Institute of Technology, Stockholm, Sweden.*
- Skagius, A.-C. K. and Neretnieks, I. (1986). Porosities and diffusivities of some non-sorbing species in crystalline rocks. *Water Resources Res.* Vol. 22, No. 3, pp. 389-398
- Siitari-Kauppi, M. (1997). Investigation of porosity with  $^{14}\text{C}$ -PMMA method based on samples from Äspö (*Manuscript*).
- Smith, J. T. and Comans, R. N. J. (1996). Modelling the diffusive transport and remobilisation of  $^{137}\text{Cs}$  in sediments: The effect of sorption kinetics and reversibility. *Geochemica et Cosmochimica Acta*, Vol. 60, pp. 995-1004.
- Tsukamoto, M., Ohe, T. (1993). Effects of biotite distribution on cesium diffusion in granite, *Chemical geology*, Vol. 107, pp. 29-46
- Wörman, A. and Xu, S. (1996). Simulation of radio nuclide migration in crystalline rock under influence of matrix diffusion and adsorption kinetics: Code development and pre-assessment of migration experiment. *SKI Report 96:22. Swedish Nuclear Power Inspectorate, Stockholm.*
- Wörman, A. and Xu, S. (1998). Variation of the dispersion coefficient with the aspect ratio of a rectangular flow section (*Under review*).

## Appendix I Solution to the first two temporal moments of the probability density function for the residence time

For a uniform fracture plane, constant dispersion and negligible radioactive decay, the transport equation system, (4) – (6), takes the form of

$$\frac{\partial c}{\partial t} + u \frac{\partial c}{\partial x} - E \frac{\partial^2 c}{\partial x^2} - 2 \frac{D_e'}{h} \frac{\partial c_m}{\partial z} \Big|_{z=0} = 0 \quad (28)$$

$$\frac{\partial c_m}{\partial t} - \Omega \frac{\epsilon_t}{\epsilon} D_p \frac{\partial^2 c_m}{\partial z^2} + k_r \Psi \frac{\rho}{\epsilon} (K_D c_m - c_w) = 0 \quad (40)$$

$$\frac{\partial c_w}{\partial t} - k_r (K_D c_m - c_w) = 0 \quad (41)$$

Based on (40) and (41), (40) can also be written as

$$\frac{\partial c_m}{\partial t} - \Omega \frac{\epsilon_t}{\epsilon} D_p \frac{\partial^2 c_m}{\partial z^2} + \Psi \frac{\rho}{\epsilon} \frac{\partial c_w}{\partial t} = 0 \quad (A1)$$

Applying the Laplace transforms, (25), to (28), (A1) and (41) yields

$$p \bar{c} + u \frac{\partial \bar{c}}{\partial x} - E \frac{\partial^2 \bar{c}}{\partial x^2} - 2 \frac{D_e'}{h} \frac{\partial \bar{c}_m}{\partial z} \Big|_{z=0} = 0 \quad (A2)$$

$$p \bar{c}_m - \Omega \frac{\epsilon_t}{\epsilon} D_p \frac{\partial^2 \bar{c}_m}{\partial z^2} + \Psi \frac{\rho}{\epsilon} p \bar{c}_w = 0 \quad (A3)$$

$$p \bar{c}_w - k_r (K_D \bar{c}_m - \bar{c}_w) = 0 \quad (A4)$$

in which the initial condition has been taken as

$$c_m(z, t=0) = c(x, t=0) = c_w(z, t=0) = 0 \quad (A5)$$

By substituting (A4) in (A3) one obtains

$$\bar{c}_m \left( p + \Psi \frac{\rho}{\epsilon} p \frac{k_r K_D}{p + k_r} \right) - \Omega \frac{\epsilon_t}{\epsilon} D_p \frac{\partial^2 \bar{c}_m}{\partial z^2} = 0 \quad (A6)$$

A general solution to (A6) is

$$\bar{c}_m = A \exp(\alpha z) + B \exp(-\alpha z) \quad (A7)$$

in which

$$\alpha = \sqrt{\frac{p(p + k_f) + \Psi \frac{\rho}{\varepsilon} p k_f K_D}{\Omega \frac{\varepsilon_t}{\varepsilon} D_p (p + k_f)}} \quad (\text{A 8})$$

A and B are determined by means of the boundary conditions

$$c_m(z=0, t) = c(x, t) \quad (\text{A 9a})$$

$$\frac{dc_m}{dz} \Big|_{z=L} = 0 \quad (\text{A 9b})$$

$$c(x=0, t) = \frac{M}{Q} \delta(t) \quad (\text{A 9c})$$

$$c(x=\infty, t) = 0 \quad (\text{A 9d})$$

Hence, the constants in (A 7) can be determined from

$$\bar{c}_m \Big|_{z=0} = A + B = \bar{c} \quad (\text{A 10})$$

$$\frac{d\bar{c}_m}{dz} \Big|_{z=L} = 0 = A \alpha \exp(\alpha L) - B \alpha \exp(-\alpha L) \quad (\text{A 11})$$

Solving (A 10) and (A 11) for A and B, we obtain the solution to (A 6) as

$$\bar{c}_m = \bar{c} \left( 1 - \frac{1}{1 + \exp(-2 \alpha L)} \right) \exp(\alpha z) + \bar{c} \frac{1}{1 + \exp(-2 \alpha L)} \exp(-\alpha z) \quad (\text{A 12})$$

The flux at the fracture wall ( $z = 0$ ) is then

$$\frac{dc_m}{dz} \Big|_{z=0} = \bar{c} \alpha \left( 1 - \frac{2}{1 + \exp(-2 \alpha L)} \right) \quad (\text{A 13})$$

Substituting (A 13) in (A 2) gives

$$\frac{\partial^2 \bar{c}}{\partial x^2} - \frac{u}{E} \frac{\partial \bar{c}}{\partial x} - \left[ \frac{p}{E} - \frac{2 D_e'}{E h} \alpha \left( 1 - \frac{2}{1 + \exp(-2 \alpha L)} \right) \right] \bar{c} = 0 \quad (\text{A 14})$$

A general solution to (A 14) is

$$\bar{c} = C_1 \exp(r_1 x) + C_2 \exp(r_2 x) \quad (\text{A 15})$$

By applying the boundary conditions, (A9c) and (A9d), one obtains

$$\bar{c} = \frac{M}{Q} \exp \left[ \frac{ux}{2E} - \frac{ux}{2E} \sqrt{1 + \frac{4E}{u^2} \left( \frac{p}{E} - \frac{2D_e'}{h} \alpha \left( 1 - \frac{2}{1 + \exp(-2\alpha L)} \right) \right)} \right] \quad (\text{A16})$$

To simplify the presentation, the following substitution is proposed

$$g_2 = \frac{ux}{2E} - \frac{ux}{2E} \sqrt{1 + \frac{4E}{u^2} \left( \frac{p}{E} - \frac{2D_e'}{h} \alpha \left( 1 - \frac{2}{1 + \exp(-2\alpha L)} \right) \right)} \quad (\text{A17})$$

The probability density function is then obtained by the use of (26) and (27) as

$$f = \frac{\bar{c}}{\bar{c}|_{p=0}} = \frac{\exp(g_2)}{\exp(g_2|_{p=0})} \quad (\text{A18})$$

The first moment can be written as

$$m_1 = -\frac{df}{dp} \Big|_{p=0} = -\frac{dg_2}{dp} \frac{\exp(g_2)}{\exp(g_2|_{p=0})} \Big|_{p=0} = -\frac{dg_2}{dp} \Big|_{p=0} \quad (\text{A19})$$

which yields

$$m_1 = E[t] = \frac{x}{u} \left[ 1 + 2 \frac{D_e' L}{\Omega \frac{\epsilon_t}{\epsilon} D_p h} \left( 1 + \Psi \frac{\rho}{\epsilon} K_D \right) \right] \quad (31)$$

Similarly, the second moment can be written as

$$m_2 = \frac{d^2 f}{dp^2} \Big|_{p=0} = \frac{d^2 g_2}{dp^2} \frac{\exp(g_2)}{\exp(g_2|_{p=0})} \Big|_{p=0} + \left( \frac{dg_2}{dp} \right)^2 \frac{\exp(g_2)}{\exp(g_2|_{p=0})} \Big|_{p=0} = \frac{d^2 g_2}{dp^2} \Big|_{p=0} + \left( \frac{dg_2}{dp} \right)^2 \Big|_{p=0} \quad (\text{A20})$$

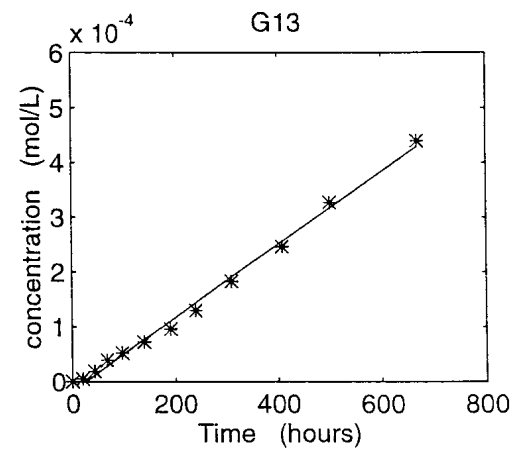
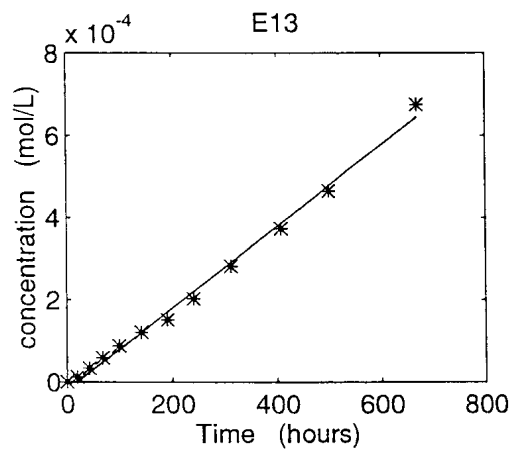
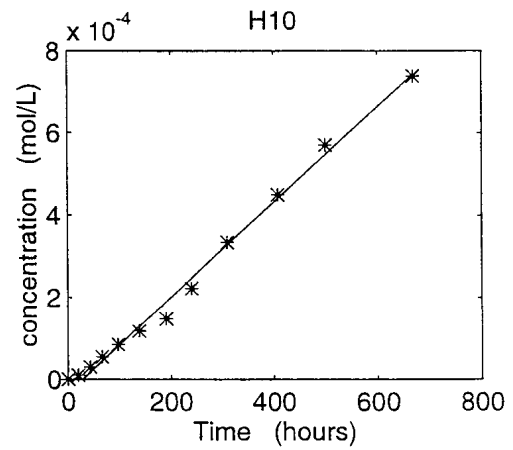
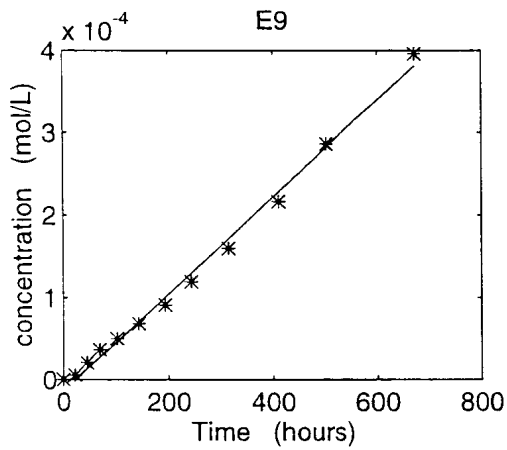
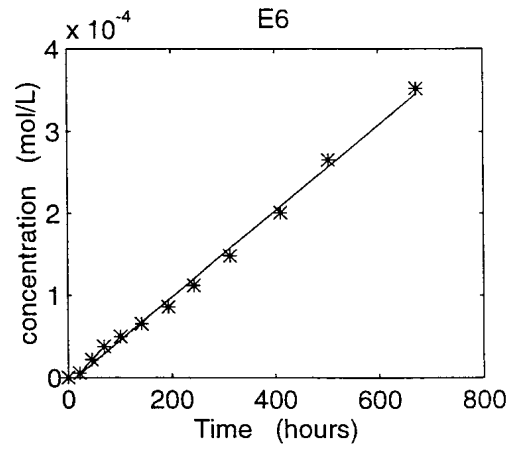
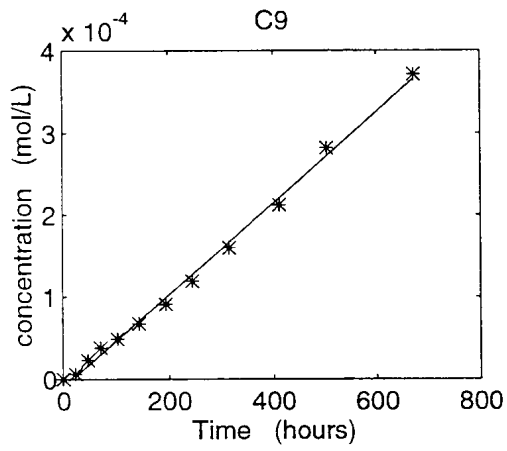
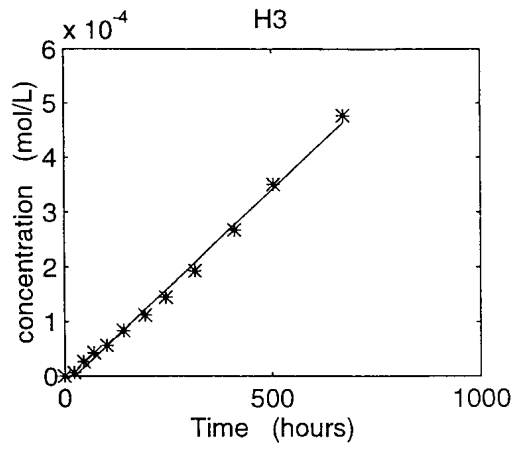
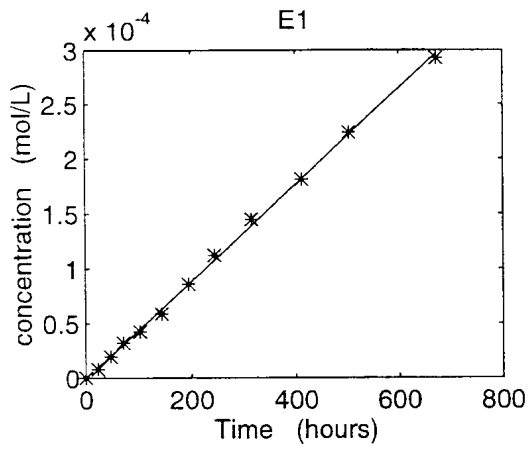
The variance of the residence time is given by

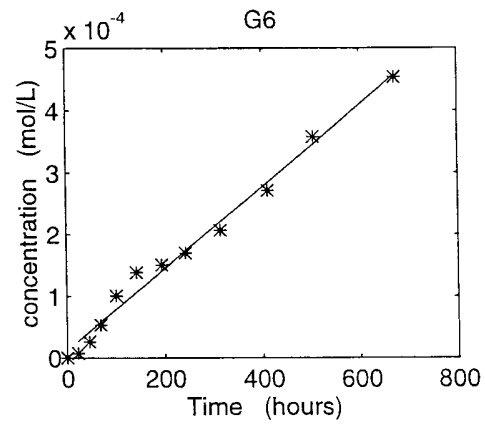
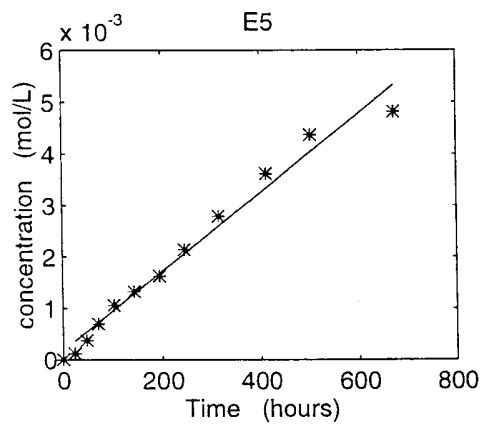
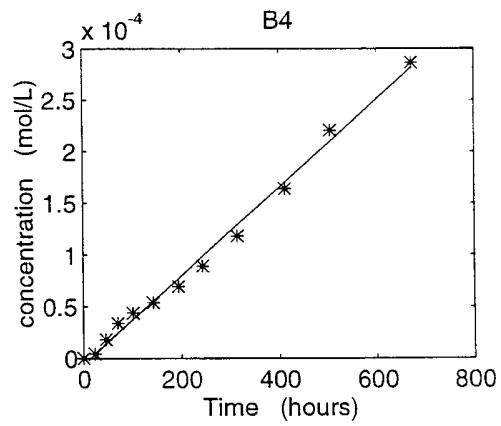
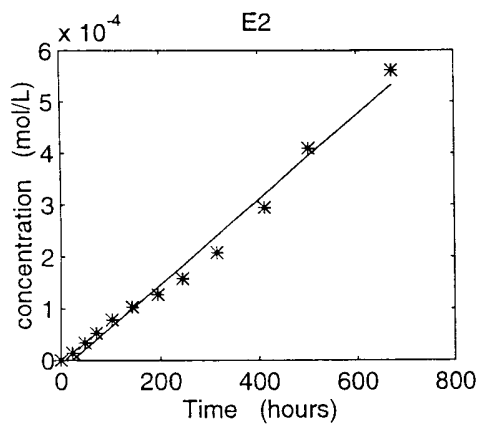
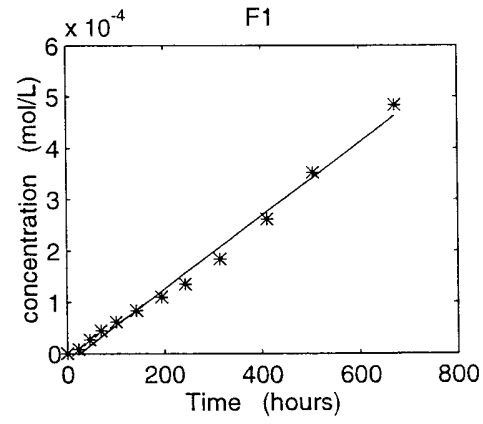
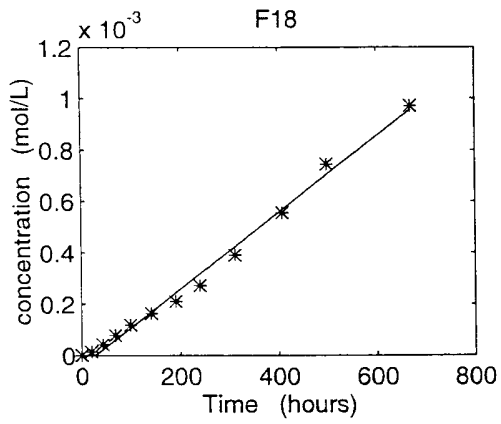
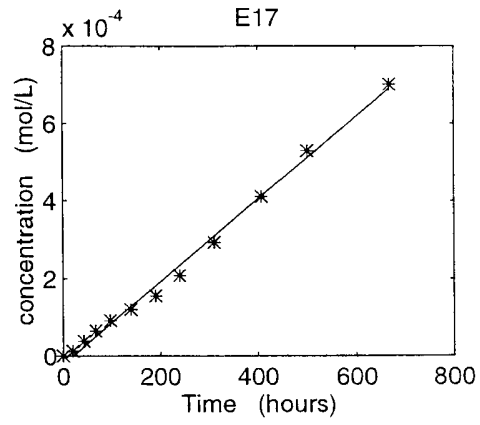
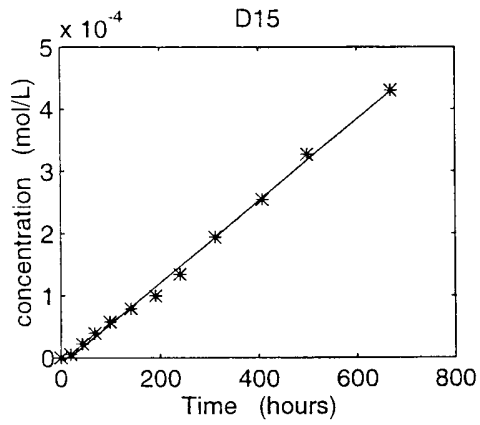
$$\sigma^2 = m_2 - (m_1)^2 = \frac{d^2 g_2}{dp^2} \Big|_{p=0} \quad (\text{A21})$$

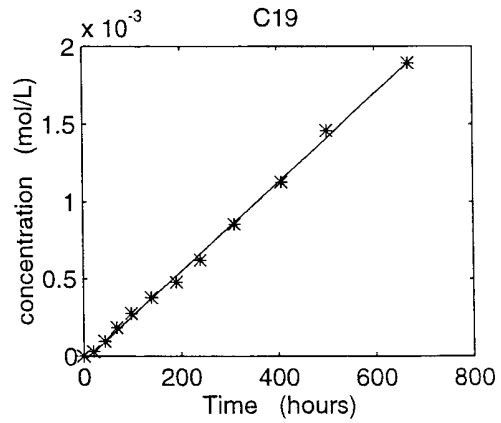
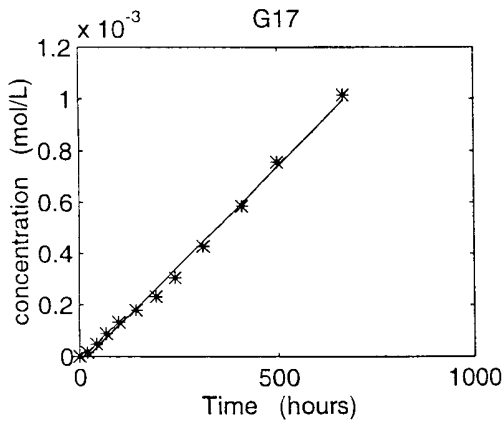
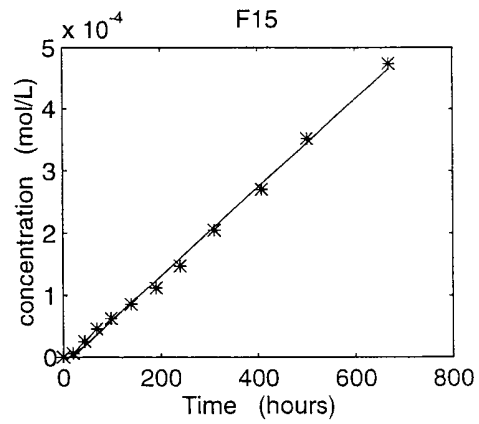
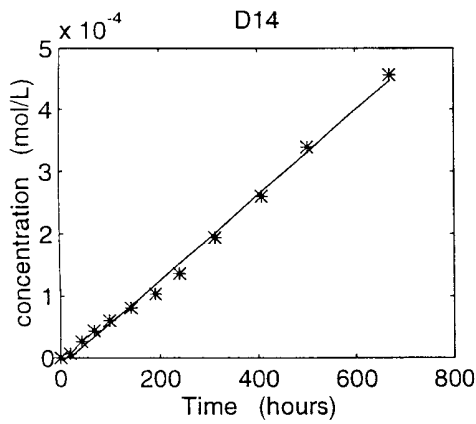
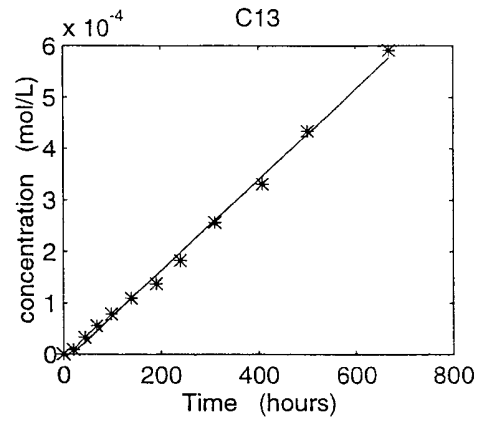
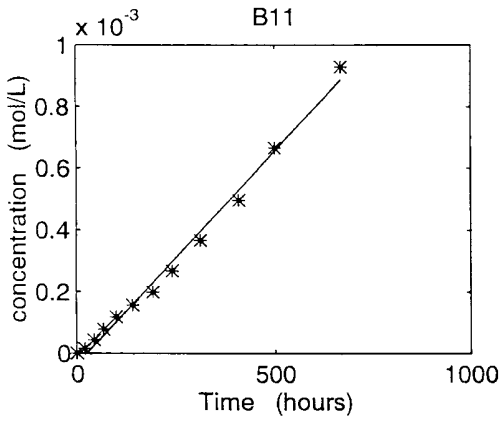
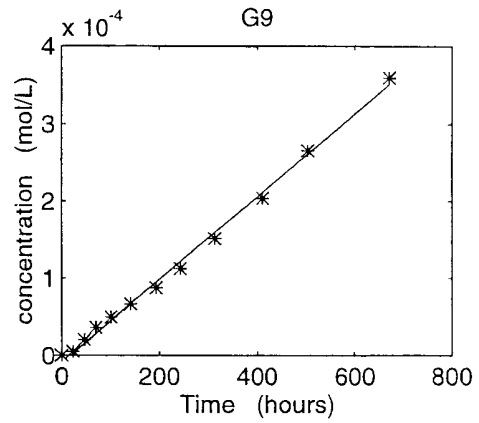
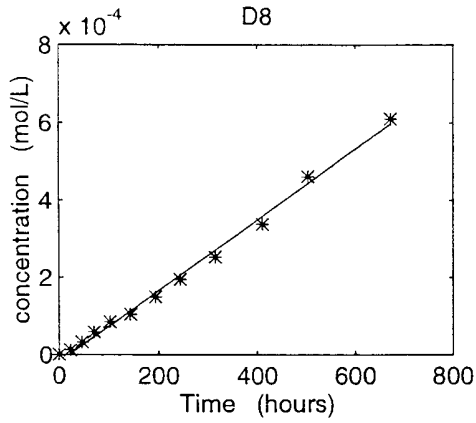
A repeated derivation of  $g_2$  finally leads to the expression for the variance of the residence time

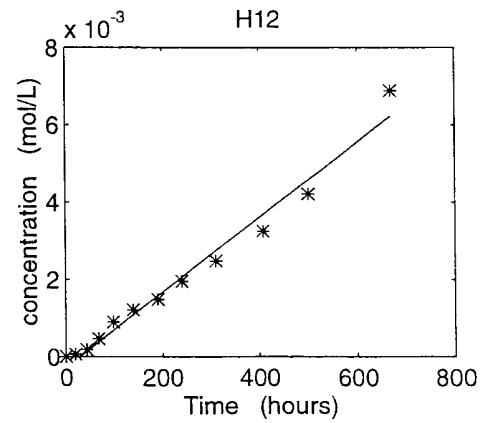
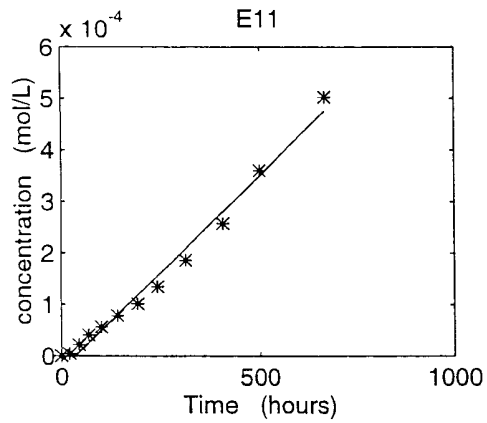
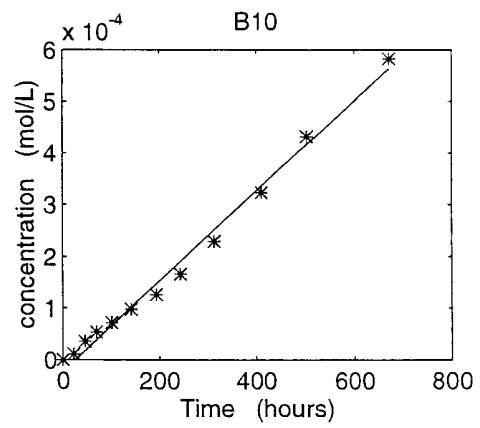
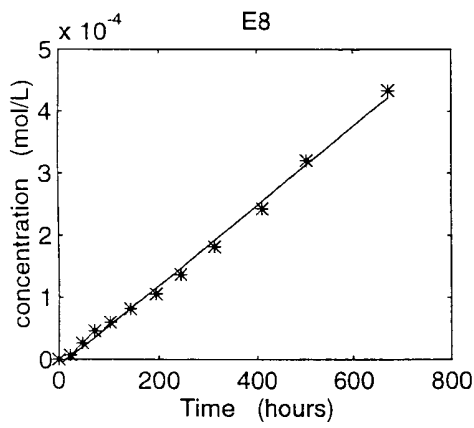
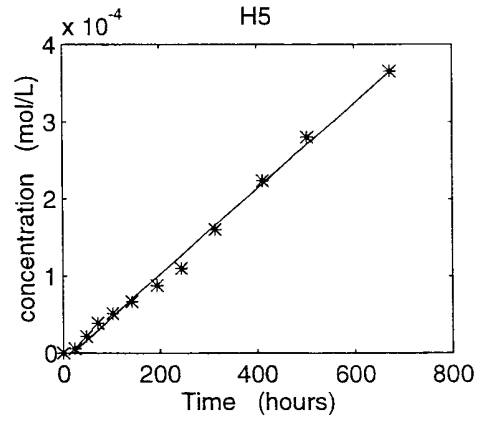
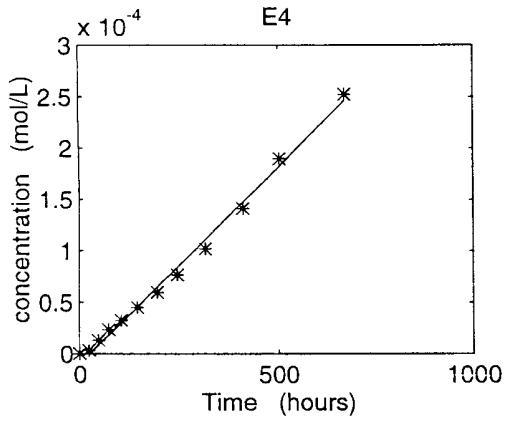
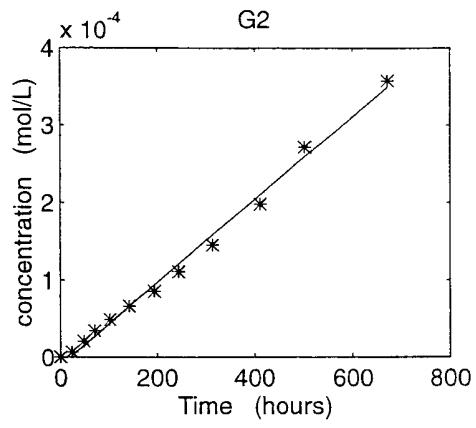
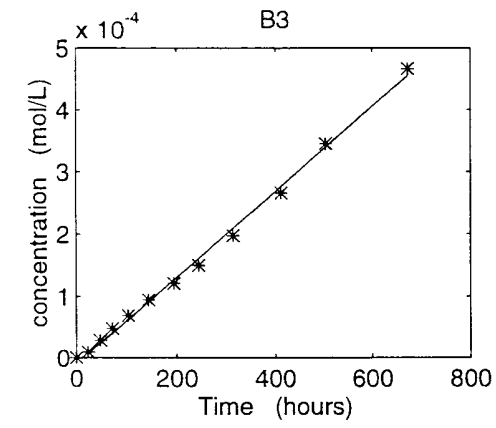
$$\sigma^2 = \frac{x}{u} \left[ 2 \left( 1 + 2 \frac{D_e' L}{\Omega \frac{\varepsilon_t}{\varepsilon} D_p h} \left( 1 + \Psi \frac{\rho}{\varepsilon} K_D \right) \right)^2 \frac{E}{u^2} + \right. \\ \left. + \frac{4}{3} \left( 1 + \Psi \frac{\rho}{\varepsilon} K_D \right)^2 \frac{D_e' L}{\Omega \frac{\varepsilon_t}{\varepsilon} D_p h} \frac{L^2}{\Omega D_p} + 4 \Psi \frac{\rho}{\varepsilon} K_D \frac{D_e' L}{\Omega \frac{\varepsilon_t}{\varepsilon} D_p h} \frac{1}{k_r} \right] \quad (32)$$

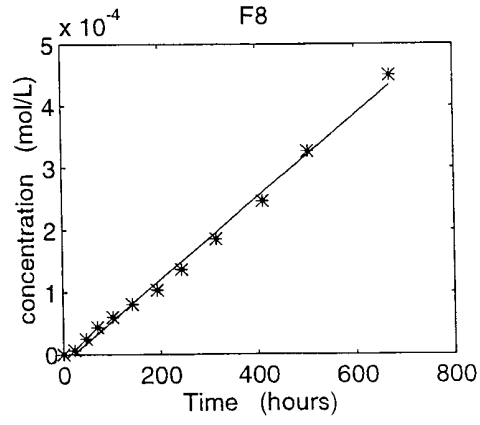
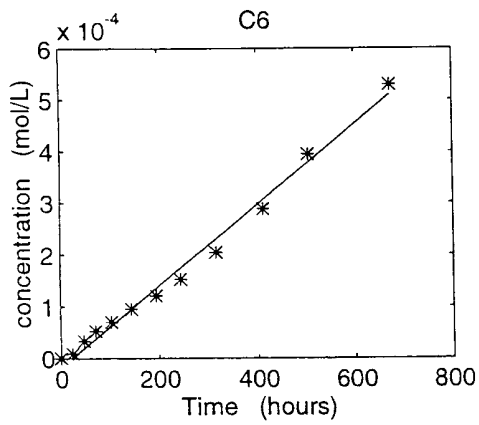
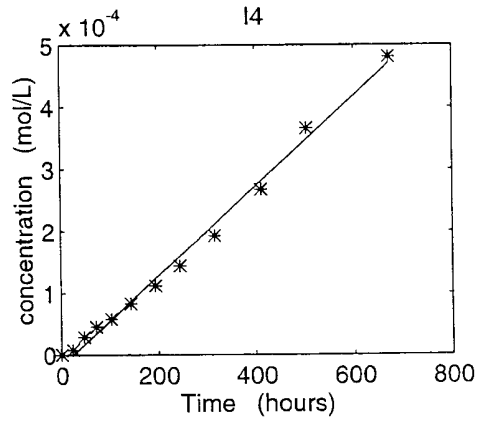
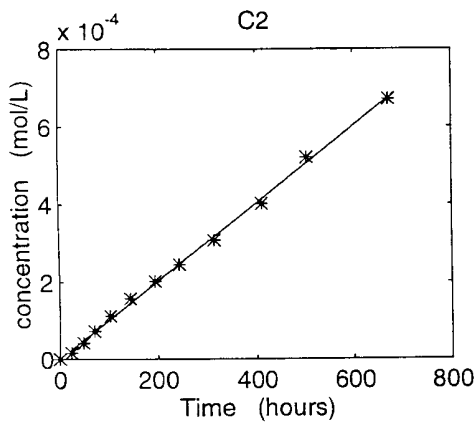
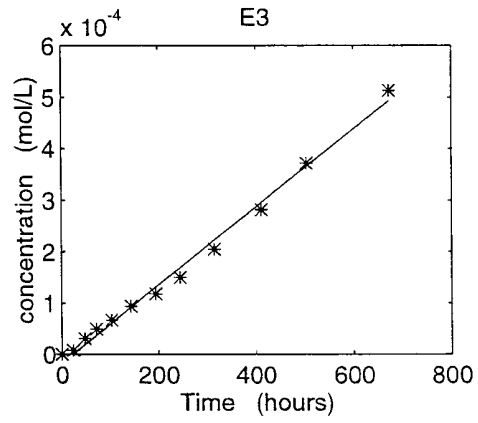
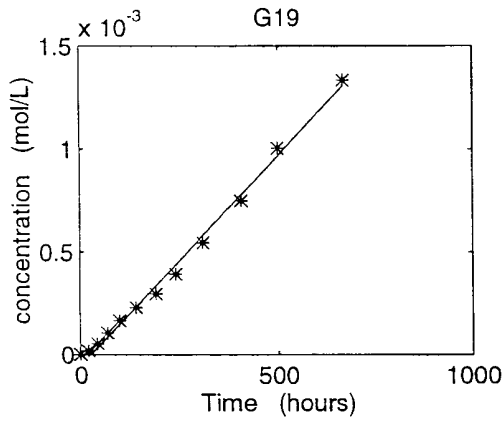
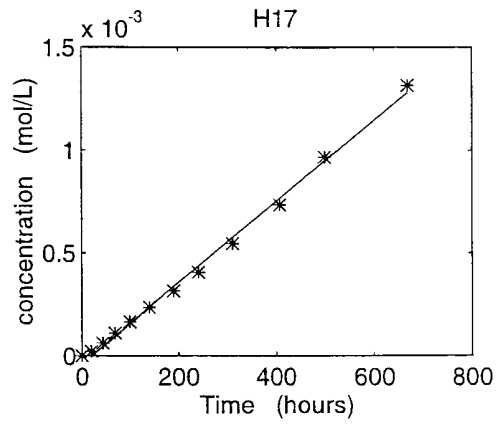
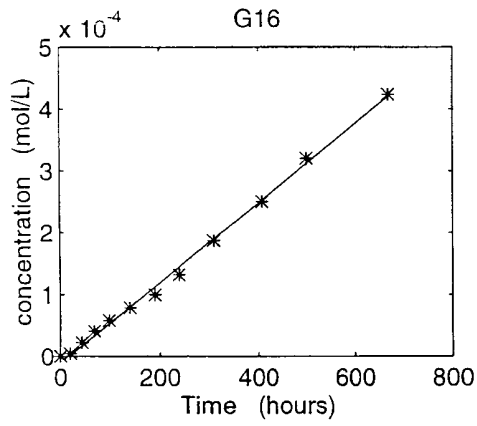
## Appendix II Diffusivity data from 4 mm $\text{AD}$ slabs

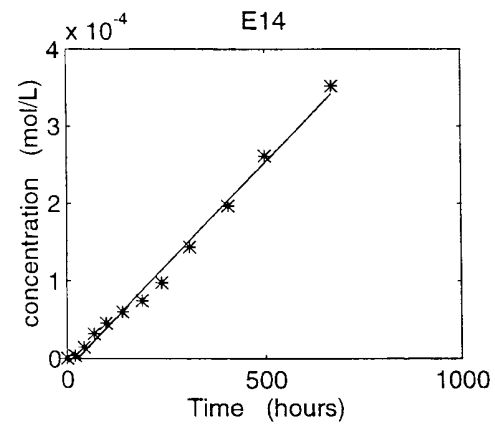
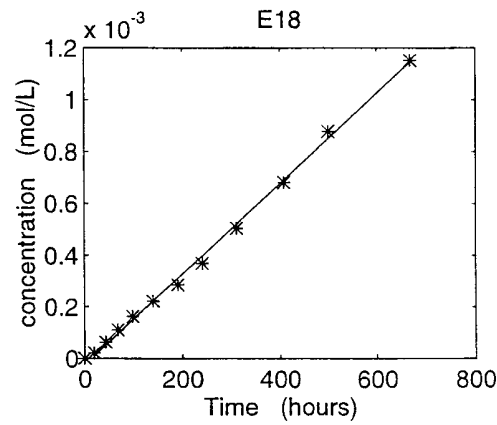
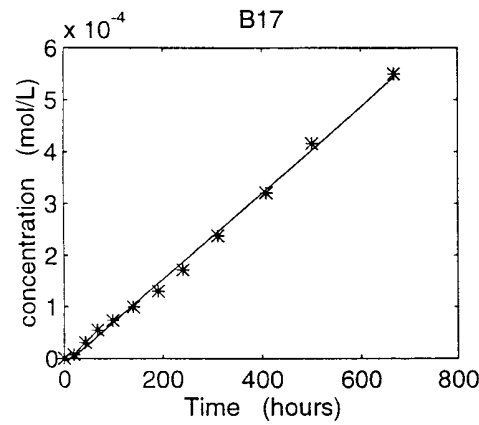
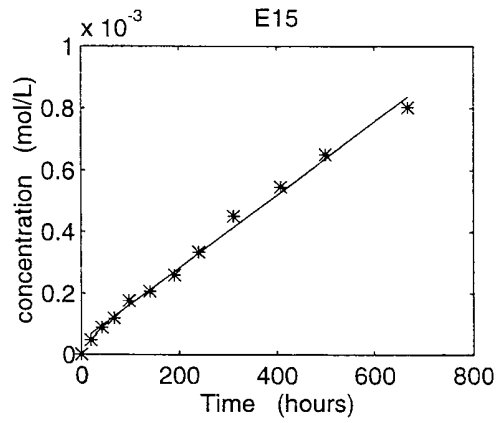
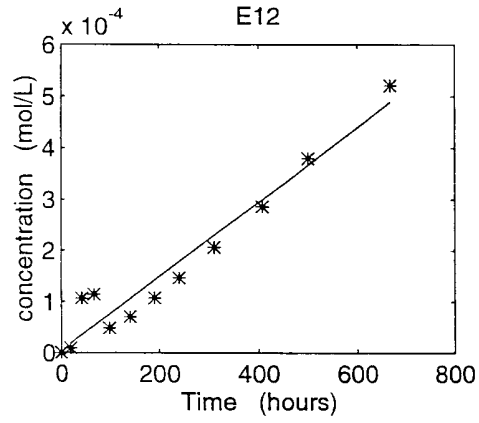
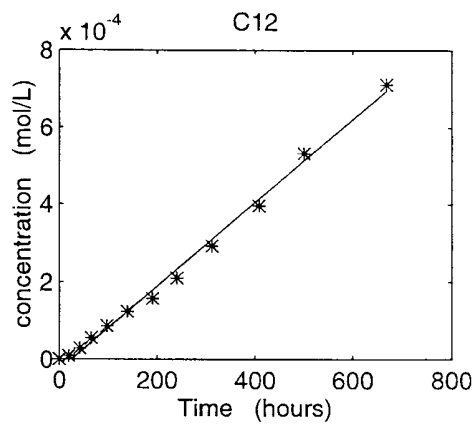
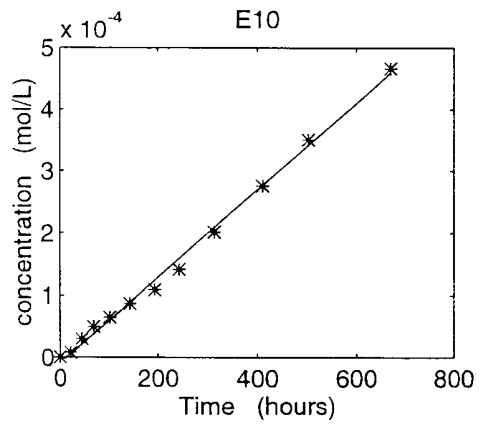


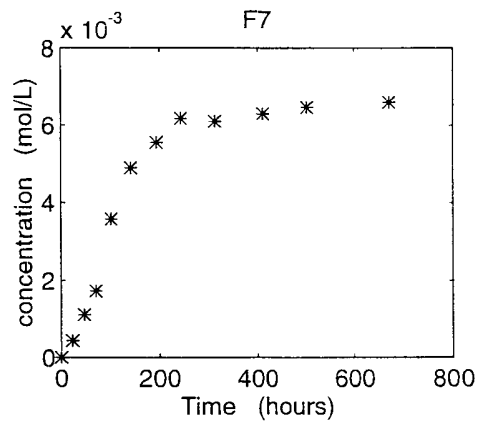
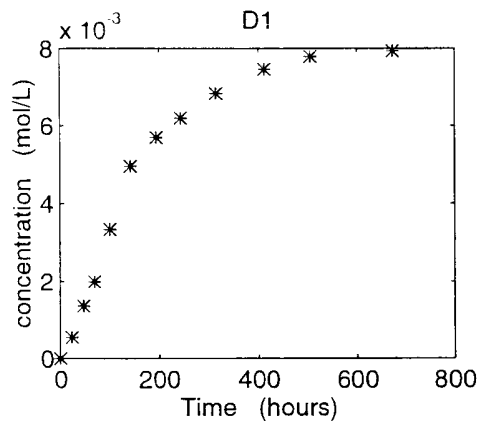




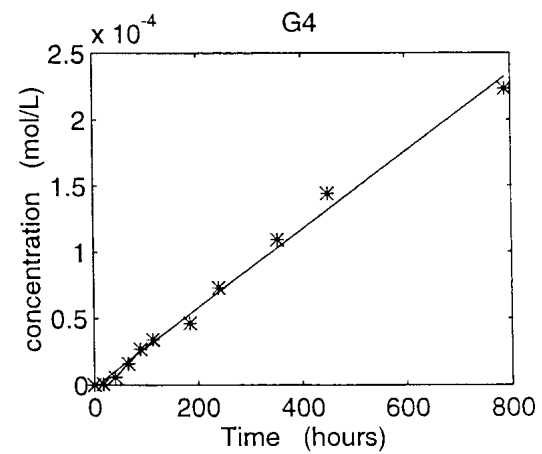
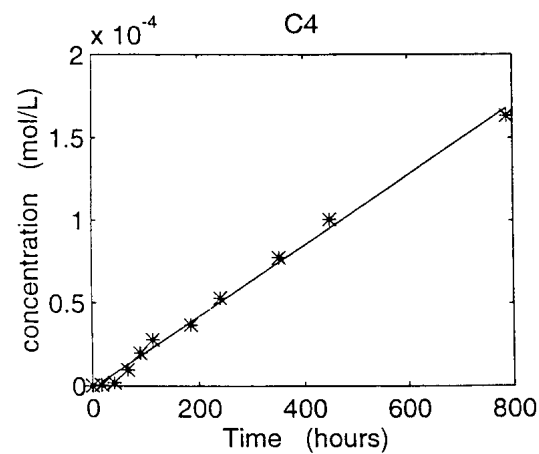
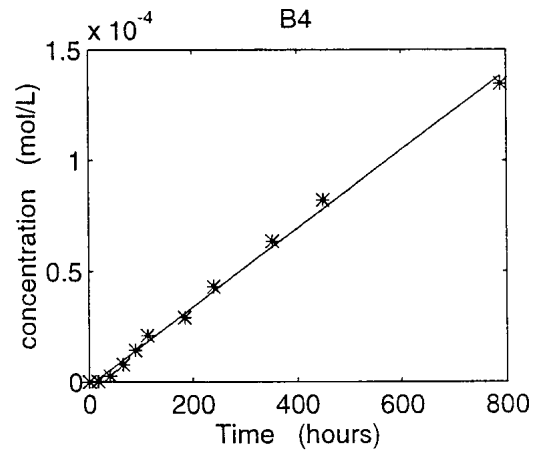
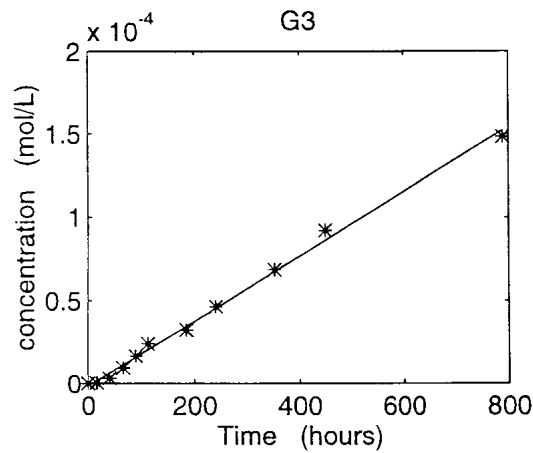
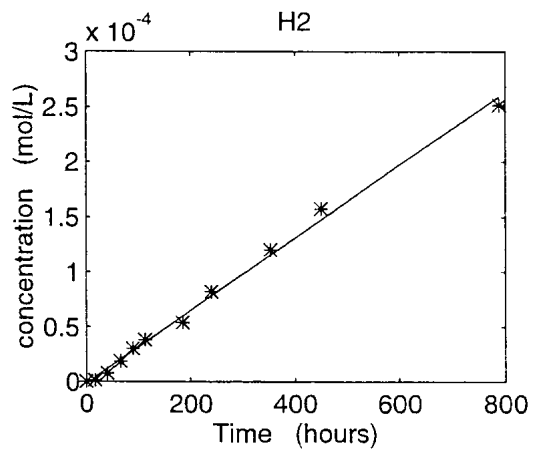
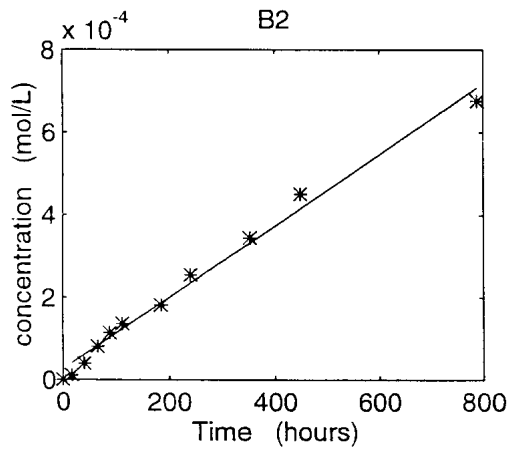
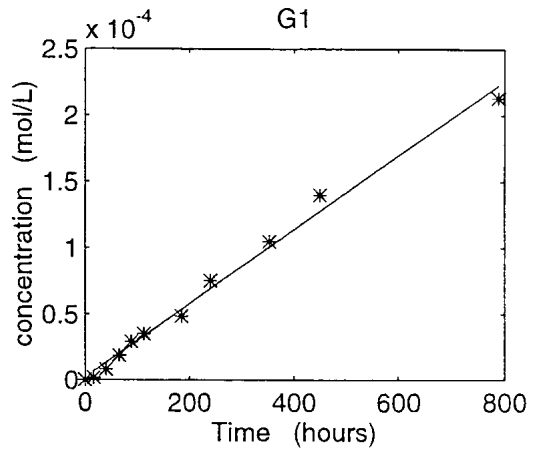
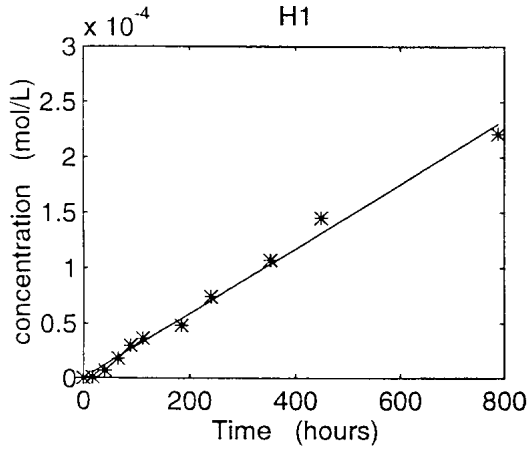


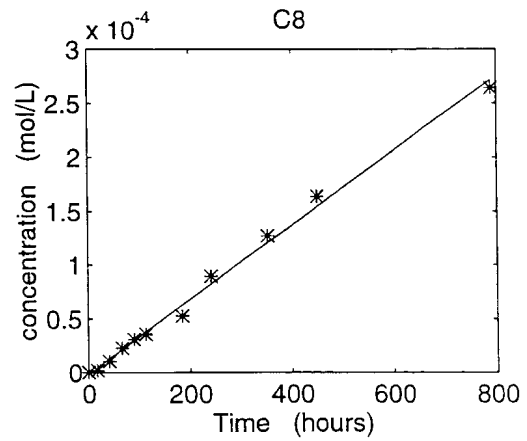
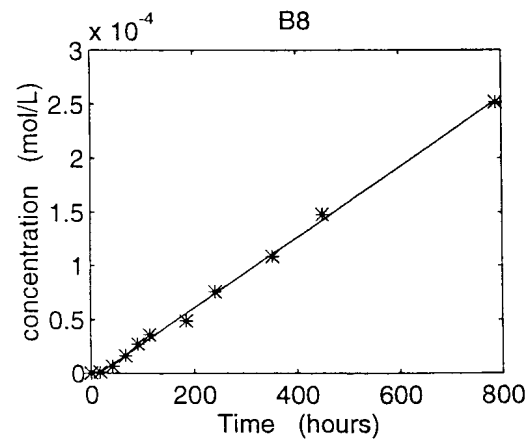
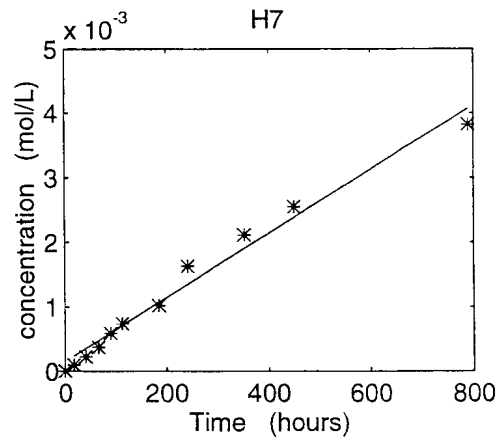
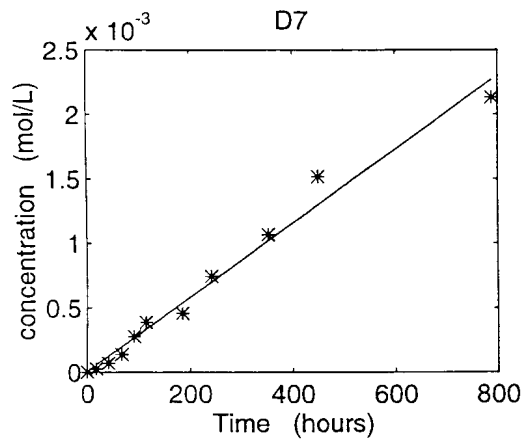
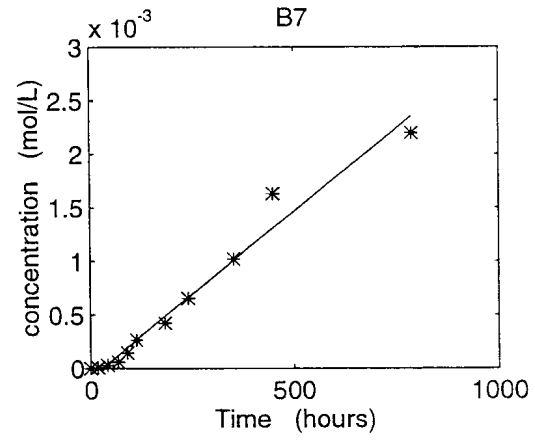
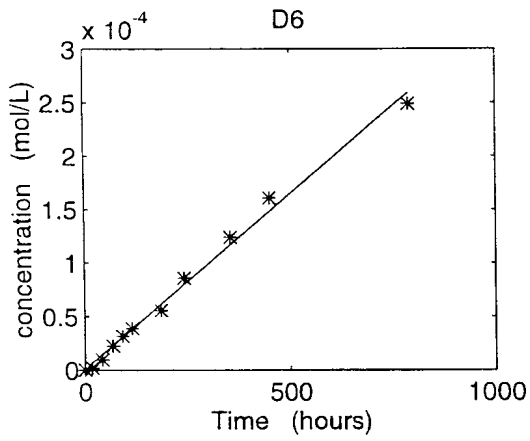
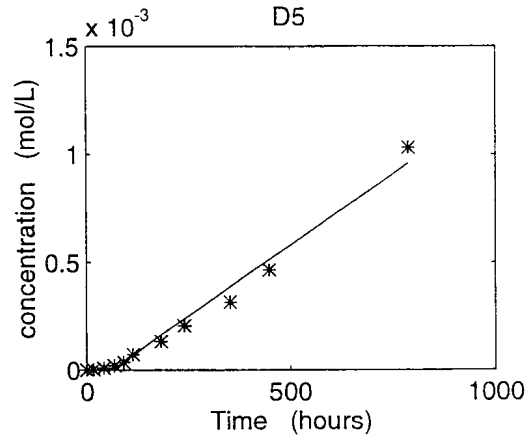
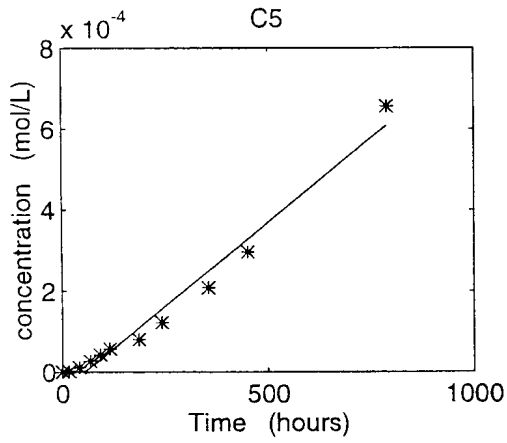


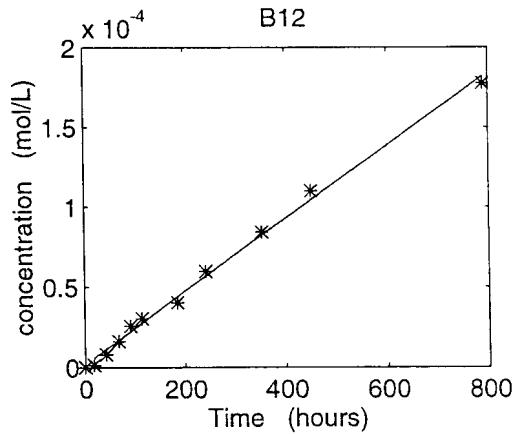
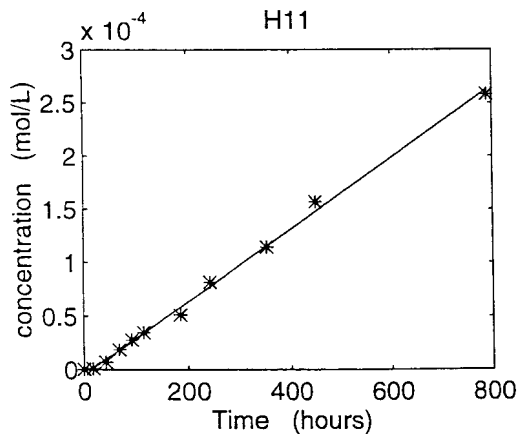
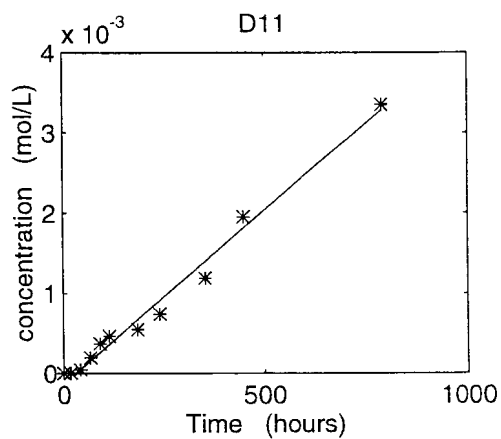
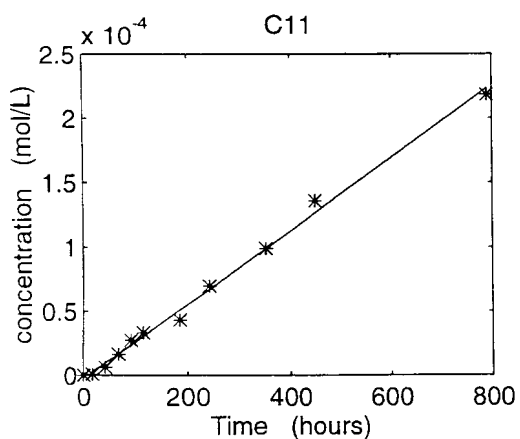
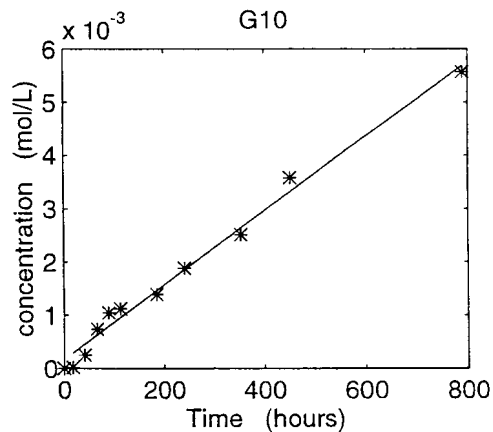
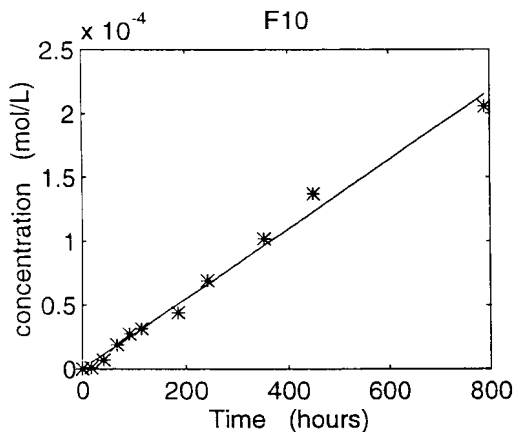
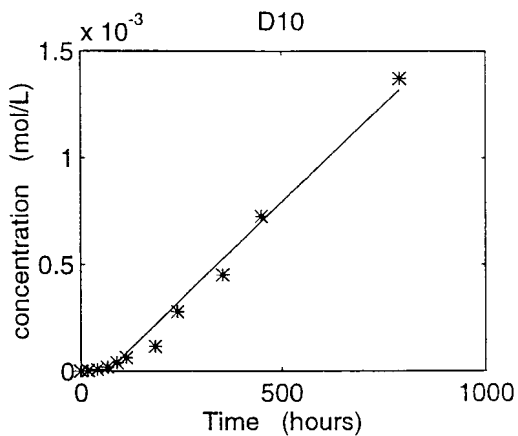
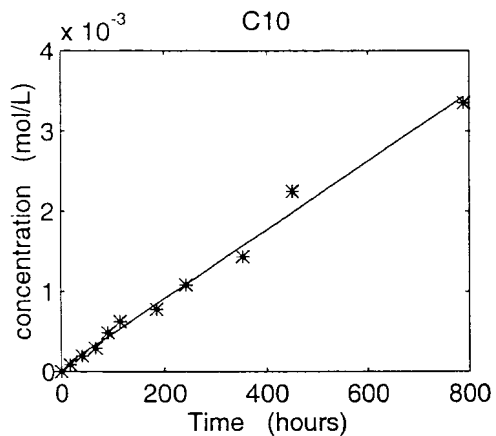


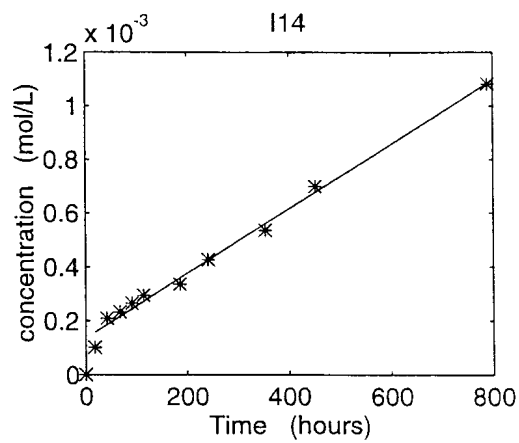
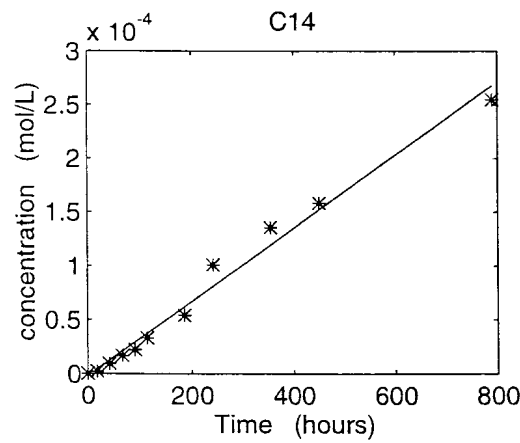
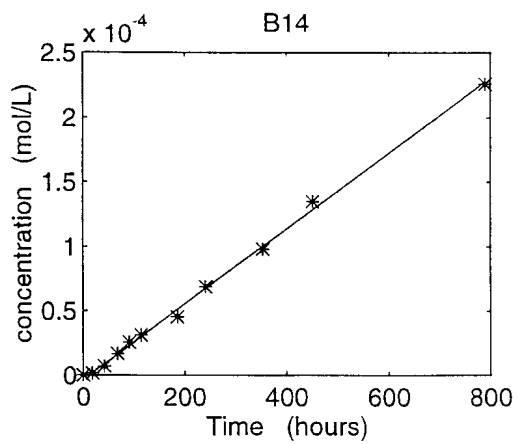
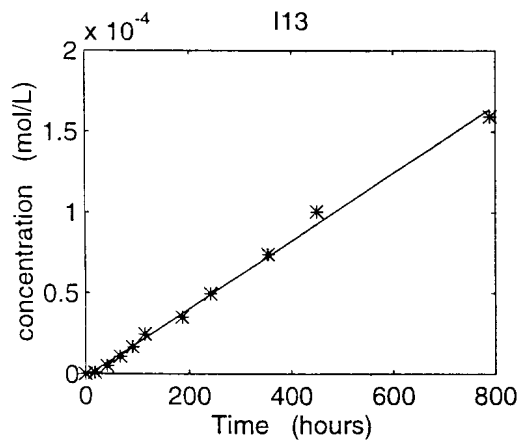
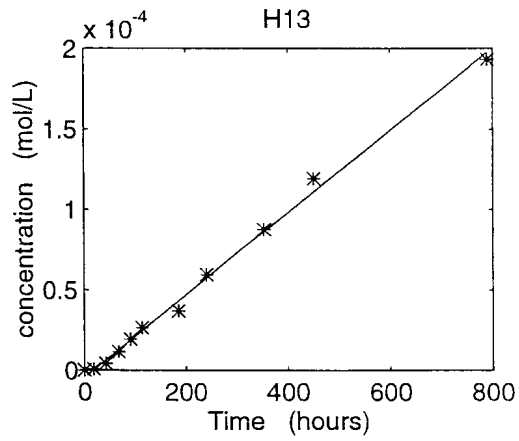
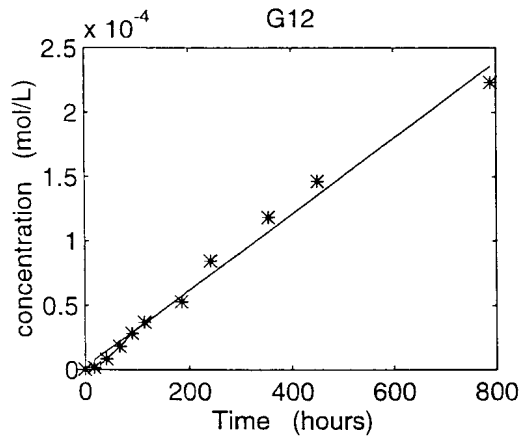
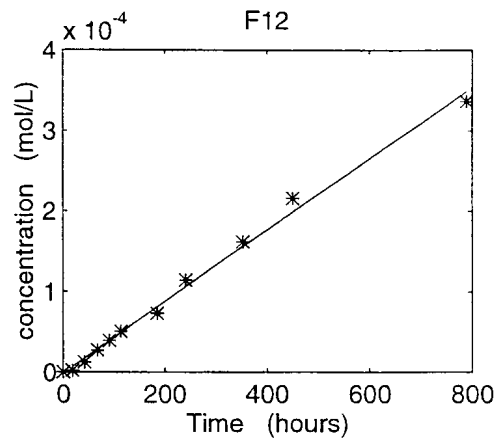
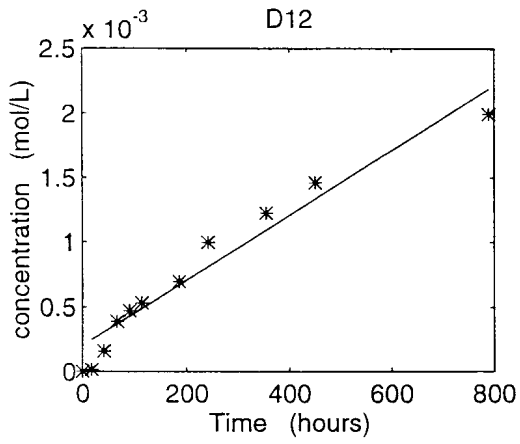


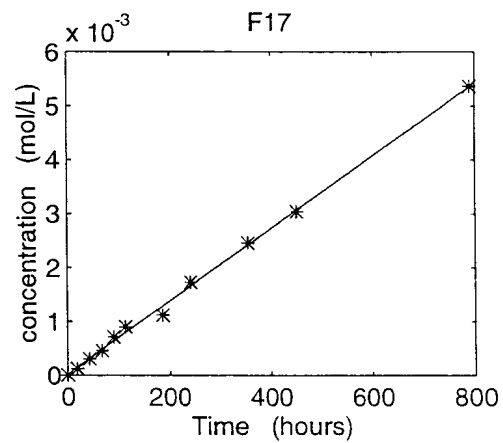
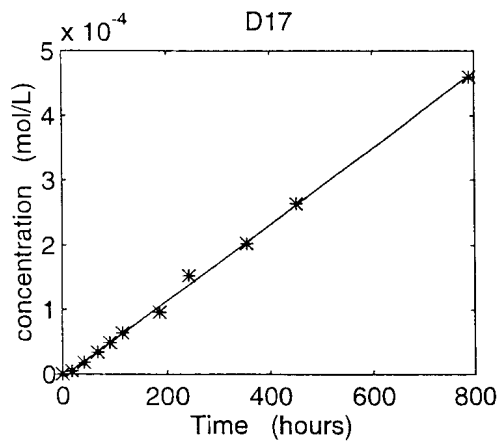
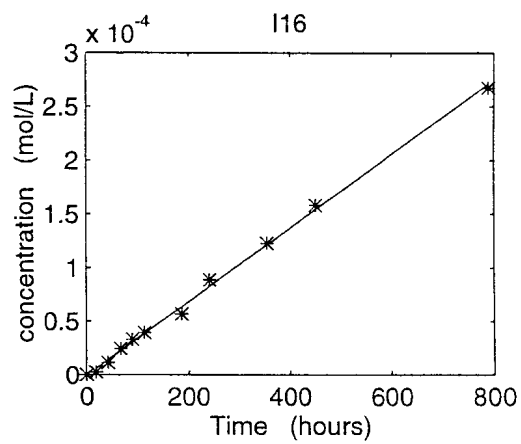
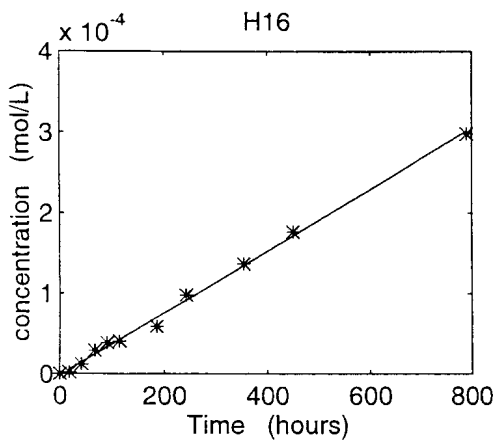
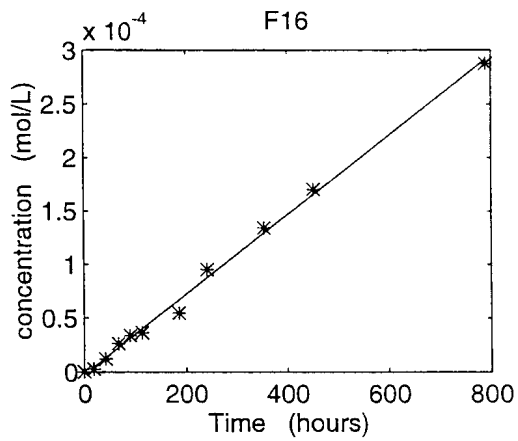
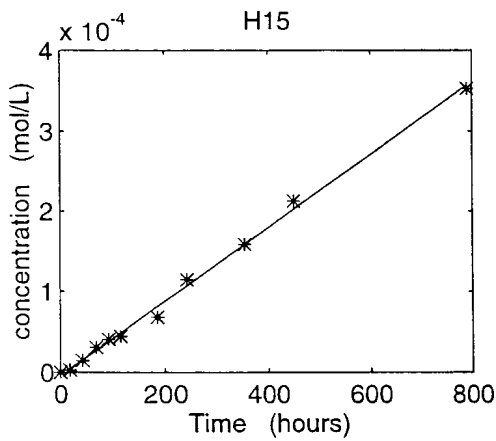
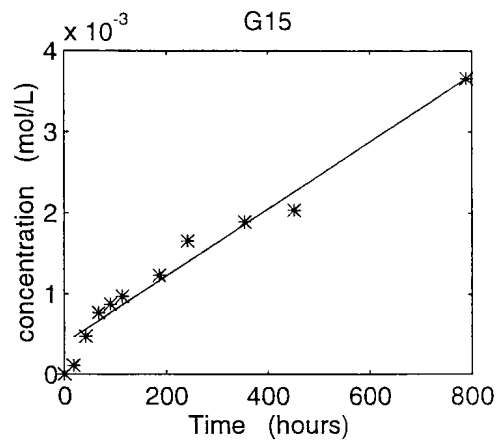
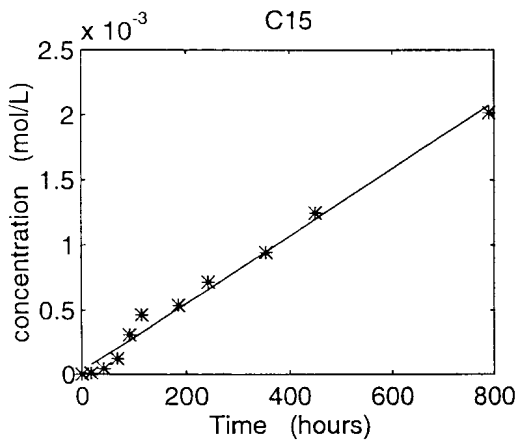
### Appendix III Measured diffusivity data from 6 mm AD slabs

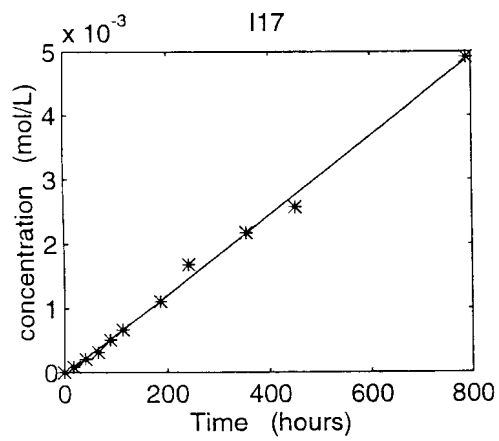
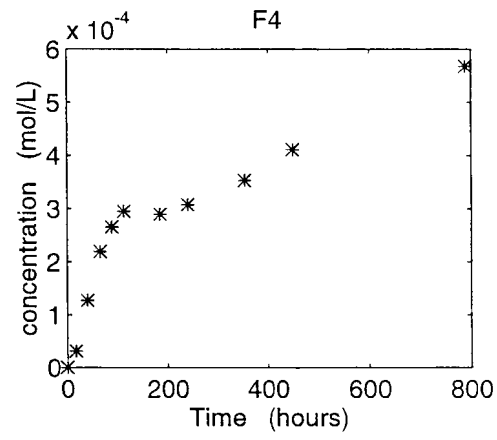
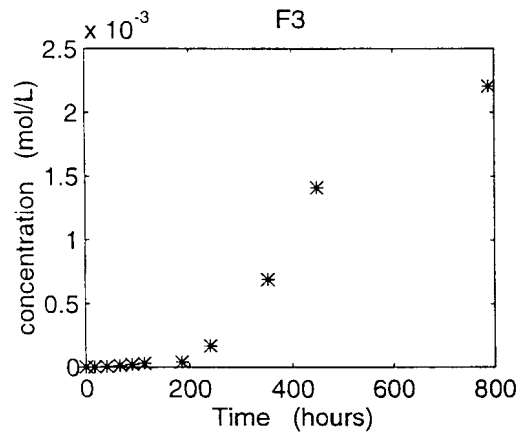
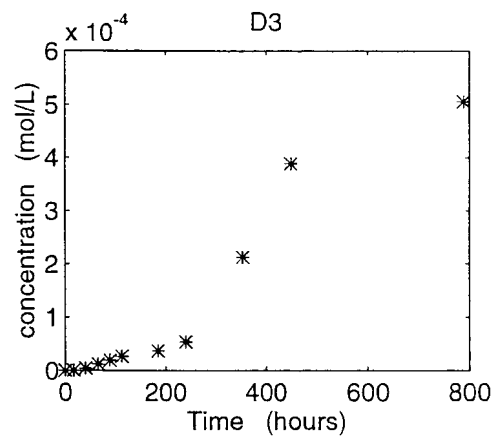
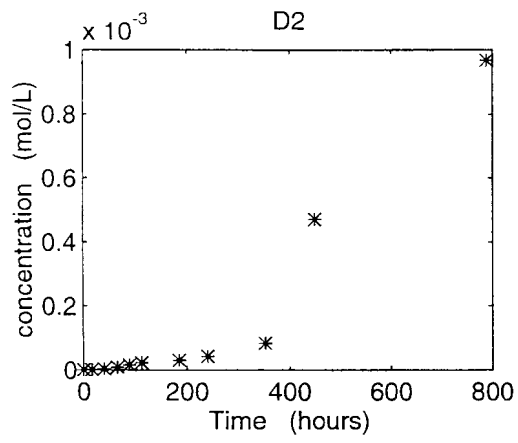












## Appendix IV Notation

a	rate of departure, [s <sup>-1</sup> ]
A <sub>E</sub>	total external geometric surface area, [m <sup>2</sup> ]
A <sub>ES</sub>	geometric surface of a sphere with the same size as that of the mean particle, [m <sup>2</sup> ]
A <sub>IN</sub>	internal surface area, [m <sup>2</sup> ]
A <sub>T</sub>	physical surface area, [m <sup>2</sup> ]
b(x <sub>i</sub> )	parameter values at point x <sub>i</sub>
b(x <sub>i</sub> +   w  )	parameter values separated from point x <sub>i</sub> by the vector w
c	concentration in main fracture defined as mass/ activity per unit volume of water), [kg/m <sup>3</sup> ]
C <sub>0</sub>	constant concentration in the pore water, [kg/m <sup>3</sup> ]
C <sub>1</sub>	solute concentration on inlet side in Eq. (2), [kg/m <sup>3</sup> ]
C <sub>2</sub>	solute concentration on outlet side in Eq. (2), [kg/m <sup>3</sup> ]
c <sub>1</sub> , c <sub>2</sub> , c <sub>3</sub>	constants in Eqs. (43), (44) and (47)
c <sub>a</sub>	concentration defined as adsorbed solute mass per unit bulk volume of medium, [kg/m <sup>3</sup> ]
c <sub>d</sub>	concentration defined as dissolved solute mass per unit volume of medium, [kg/m <sup>3</sup> ]
c <sub>e</sub>	concentration of mobile phase of solute, [kg/m <sup>3</sup> ]
c <sub>m</sub>	concentration defined as dissolved solute mass per unit volume of water, [kg/m <sup>3</sup> ]
c <sub>s</sub>	concentration defined as adsorbed mobile solute mass per unit solid mass, [kg/kg]
c <sub>tot</sub>	= c <sub>a</sub> + c <sub>d</sub> , [kg/m <sup>3</sup> ]
c <sub>w</sub>	concentration defined as adsorbed (fixed) solute mass per unit solid mass, [kg/kg]
D	Non-dimensional dispersion term in Eq. (33), [-]
D	molecular (ionic) diffusivity, [m <sup>2</sup> /s]
D <sub>e</sub>	effective diffusivity, [m <sup>2</sup> /s], D <sub>e</sub> = ε <sub>t</sub> D <sub>p</sub>
D' <sub>e</sub>	effective diffusivity with account taken to surface diffusion, D' <sub>e</sub> = ε <sub>t</sub> D <sub>p</sub> + k <sub>d1</sub> ρ D <sub>s</sub> , [m <sup>2</sup> /s]
D <sub>kj</sub>	molecular (ionic) diffusivity tensor, [m <sup>2</sup> /s]
D <sub>p</sub>	pore diffusivity, D <sub>p</sub> = Dδ <sub>D</sub> /τ <sup>2</sup> , [m <sup>2</sup> /s]
D <sub>s</sub>	surface diffusivity, [m <sup>2</sup> /s]
d <sub>ph</sub>	the harmonic mean by volume of the grain diameters, [m]
E	dispersion coefficient, [m <sup>2</sup> /s]
E[t]	expected value of t, [s]
f	probability density function for residence time
G <sub>ad</sub>	adsorption rate, [kg/m <sup>3</sup> s]
G <sub>des</sub>	desorption rate, [kg/m <sup>3</sup> s]
h	fracture aperture, [m]
i, j, k	indices
K	Non-dimensional matrix diffusion term in Eq. (33)
k <sub>d</sub>	partition coefficient, k <sub>d</sub> = c <sub>a</sub> /c <sub>d</sub> , [-]
k <sub>d1</sub>	partition coefficient, k <sub>d1</sub> = c <sub>s</sub> /c <sub>m</sub> , [m <sup>3</sup> /kg]

$K_D$	partition coefficient, $K_D = c_w / c_m$ , [ $m^3 / kg$ ]
$k_r$	adsorption rate coefficient [ $s^{-1}$ ]
$L$	extension of rock matrix, [m]
$M$	Non-dimensional matrix diffusion term in Eq.(33)
$M$	total injected solute mass, [kg]
$M_0$	total solute mass, [kg]
$M_1$	solute mass in the free water, [kg]
$M_2$	solute mass in the surficial layer, [kg]
$m_0$	zeroth temporal moment
$m_1$	first temporal moment
$n$	number of observation pairs
$p$	Laplace transform variable
$P_E$	peak value of concentration distribution with equilibrium chemistry
$P_k$	peak value of concentration distribution with kinetics
$Q$	total amount of diffusing substance in, [ $kg / m^2$ ]
$r(w)$	semi-variogram
$s$	sticking probability
$s_0$	constant
$u$	advective velocity, [m/s]
$U$	squared mean speed of molecules, [ $m^2 / s$ ]
$ w $	lag distance, [m]
$x$	Cartesian co-ordinate, [m]
$x_k$	Cartesian co-ordinate vector
$\alpha, \beta, \gamma$	constants in Eqs. (20), (21), (23) and (24)
$\delta$	Dirac delta function
$\delta_D$	constrictivity
$\varepsilon$	porosity of rock
$\varepsilon_{peak}$	relative error in the peak value resulting from the assumption of equilibrium chemistry
$\varepsilon_{var}$	relative error in the variance resulting from the assumption of equilibrium chemistry
$\varepsilon_t$	porosity available for transport
$\kappa$	sorption capacity factor [-]
$\Phi$	specific surface (solid surface area per unit bulk volume of rock), [ $m^{-1}$ ]
$\gamma$	rate of radioactive decay, [ $s^{-1}$ ]
$\lambda_g$	surface roughness factor
$\Pi_E$	relative dispersion
$\Pi_{KD}$	equilibrium state of adsorption
$\Pi_{kr}$	relative reaction kinetics in matrix diffusion
$\Pi_L$	ratio of penetration length and fracture
$\Pi_x$	relative transport distance
$\rho$	density of the rock, [ $kg / m^3$ ]
$\sigma^2$	variance of residence time, [ $s^2$ ]
$\sigma_E^2$	variance of residence time resulting from the assumption of equilibrium chemistry, [ $s^2$ ]
$\sigma_k^2$	variance of residence time resulting from the assumption of kinetic adsorption, [ $s^2$ ]
$\tau$	tortuosity